ArcticNet 2011
Expedition of the CCGS *Amundsen*

Data Report – Leg 2A (ArcticNet/IORVL)
11-25 August, 2011

Principle Investigators :
Dr. David G. Barber
Dr. Tim Papakyriakou
Dr. Simon Prinsenberg

Report prepared by :
Matthew G. Asplin and Randall Scharien

ArcticNet
ᐅᑭᐅᖅᑕᖅᑐᒥᒃ ᑐᑭᓯᓂᐊᖅᑎᑦᑕ

Table of Contents

Executive Summary

This document represents the data report for datasets collected by researchers based at the Centre for Earth Observation Science (CEOS), University of Manitoba, under the Sea Ice research component of the ArcticNet Network for 2011. Our group is actively involved in research that revolves around improving our understanding of ocean-sea ice-atmosphere dynamic and thermodynamic coupling, as well as how this coupling impacts the ecology of the sea ice, and the waters immediately beneath. We employ a large ensemble of ship-based sensors, and physical sampling equipment that collect sensor-based atmospheric, oceanic and sea ice data. Our data collection efforts are driven by many interlinked objectives. Objectives relevant to our partnership with Imperial Oil Research Ventures Limited (IORVL), and corresponding data collection during 2011 are as follows:

1) **Ocean:** Describe the nature of currents, salinity, temperature, and associated physical variables in the southern Beaufort Sea, and over the IORVL exploration block (Ajurak).
2) **Sea Ice:** Describe the aerial concentration, type, growth history, strength and periodicity of sea ice in the southern Beaufort Sea, and over Ajurak.
3) **Atmosphere:** Describe the magnitude and variability of key meteorological variables over the ocean and relative to adjacent land stations.
4) **Coupling:** Provide data on the key coupling mechanisms across the OSA (has this been defined yet?) interface with a particular emphasis on fluxes of mass, energy and momentum.

Field research and data collection activities relevant to these objectives were conducted from the Canadian Coast Guard Ship *Amundsen* (hereafter referred to as "CCGS *Amundsen"*), a research icebreaker, From 11 August to 25 August 2011, our group conducted a variety of sampling activities in the Southern Beaufort Sea including, but not limited to: aerial ice thickness surveys passive and active microwave scanning of sea ice.

Our comprehenisve research program also included *in situ* observations of interesting scientific phenomenom representative of the changing Arctic sea ice regime. The most prominent was new record minimum low summer sea ice extent set on 09 September 2011. Furthermore, several fragments of ice islands were observed during the cruise.

ArcticNet 2011 Data Use Policy

All data described in the document hereafter was collected during the 2011 ArcticNet / IORVL partnership field season. The Centre for Earth Observation Science shall make all datasets available upon request to IORVL, pending resolution of quality-assurance related issues. Telemetry from ice beacons deployed during the 2011 field season is expected to continue into 2012, and updates to these datasets will be made available to IORVL at a later date.

All other data access requests shall be addressed to Dr. David Barber at the Centre for Earth Observation Science, University of Manitoba (dbarber@cc.umanitoba.ca). CEOS retains exclusive rights to all data collected during the field season. Field members have first rights to the data for a period of 2 years, followed by non-field participants. Please reference use of any material in this report as follows:

Section 3.3. Ocean Surface Roughness, *in* Asplin M.G., and Scharien, R. (Eds.) *CEOS-TEC-2012-01-25. 144pp.*

Acknowledgements

First and foremost, we would like to acknowledge the support and expertise of the hardworking crew of the Research Icebreaker CCGS *Amundsen*. Our sincere gratitude is extended to Captain Marc Thibault. His patience and expertise was invaluable to the 2011 partnership field season.

We also would like to acknowledge Imperial Oil Resources Ventures Ltd. (IORVL) for providing funding for the 2011 ArcticNet Cruise, and for CEOS operations and equipment.

We are indebted to Keith Levesque, ArcticNet's Shipbased Research Coordinator, for his tireless efforts, dedication and investment in the preparation of this very challenging 2011 expedition. From community consultations, to research licensing, to planning workshops, to ship mobilization, crew changes, security clearances and the numerous needs of dozens of demanding research groups rotating onboard the ship, a colossal amount of work is involved in the preparation of such an expedition.

We would also like to thank Martin Fortier, Executive Director of ArcticNet, for his dedication to ArcticNet, and in particular for the support and energy that he extended toward the planning and implementation of the 2011 field season. Last but not least, we would also to acknowledge his contributions to the field season overview in this data report (section 1.1).

The authors would like to thank Canadian Coast Guard Helicopter pilot Robert Pelletier and Engineer Eddy Perron for their assistance during the survey. In particular CCG pilot Bob Pelletier is thanked for the smooth flying at low altitude even in tasking weather conditions. The work was supported by the Program of Energy and Development and through ArcticNet and IORVL

Several government agencies contributed to the success of the 2011 ArcticNet / IORVL partnership field season in the Southern Beaufort Sea. These include the Natural Sciences and Engineering Council (NSERC), the Canada Research Chairs Program (CRC), the Networks of Centres of Excellence Program (NCE), Northern Scientific Training Program (NSTP), Department of Indian and Northern Affairs Canada (INAC), the Canadian Ice Service (CIS), the Canadian Space Agency (RADARSAT-1, RADARSAT-2), the European Space Agency (ESA), the National Aeronautics and Space Administration (NASA), Environment Canada (EC), the Meteorological Service of Canada (MSC), the Department of Fisheries and Oceans (DFO), and the Canadian Coast Guard Service (CCGS).

Thanks go to Pritichhanda Nayak for her invaluable assistance preparing this report.

Title page credit: Randall Scharien

List of Tables

List of Figures

SECTION ONE: INTRODUCTION

1.1 Preface

The dramatic change in sea ice affects all physical, biological and geochemical processes operating across the ocean-sea ice-atmosphere (OSA) interface. It also affects how industry must plan and prepare for exploration and development projects involving oil and gas and associated transportation of resources to southern markets. Knowledge of the key meteorological, oceanographic (met-ocean) and sea ice variables is important both for engineering and operation considerations as well as for environmental impact studies required by these projects. This project brought together a number of ArcticNet physical scientists to collect data on key met-ocean and sea ice variables and to provide these to our Oil and Gas industry partners (OGIP).

The Beaufort Sea/Mackenzie Shelf region of the Arctic Ocean has witnessed major changes in recent years, with decreasing sea ice cover and major shifts in sea-ice dynamics. Although major inshore research activities were conducted in the 70's and 80's in large part due to the Oil & Gas interest in the regions, much less is known about the offshore region of the Mackenzie Shelf, shelf slope and Beaufort Sea.

Since 2002, ArcticNet has been conducting extensive multidisciplinary research programs in the area. In addition to an annual fall sampling program, ArcticNet researchers have led two major international overwintering research programs conducted onboard the CGGS *Amundsen* in 2003-2004 (CASES program) and in 2007-2008 (CFL program). A marine observatory of a minimum of 5 oceanographic annual moorings (from 5 to 17 moorings) has been deployed and retrieved annually in the area by ArcticNet researchers.

Recent interest in the Beaufort Sea has resulted in major bids from industry on offshore exploration licenses (EL) located in the 50 – 1500 m depth range of the shelf and shelf break. Of particular relevance to the 2009 expedition is EL446 (called Ajurak) awarded to Imperial Oil in 2007 (see Figure 1).

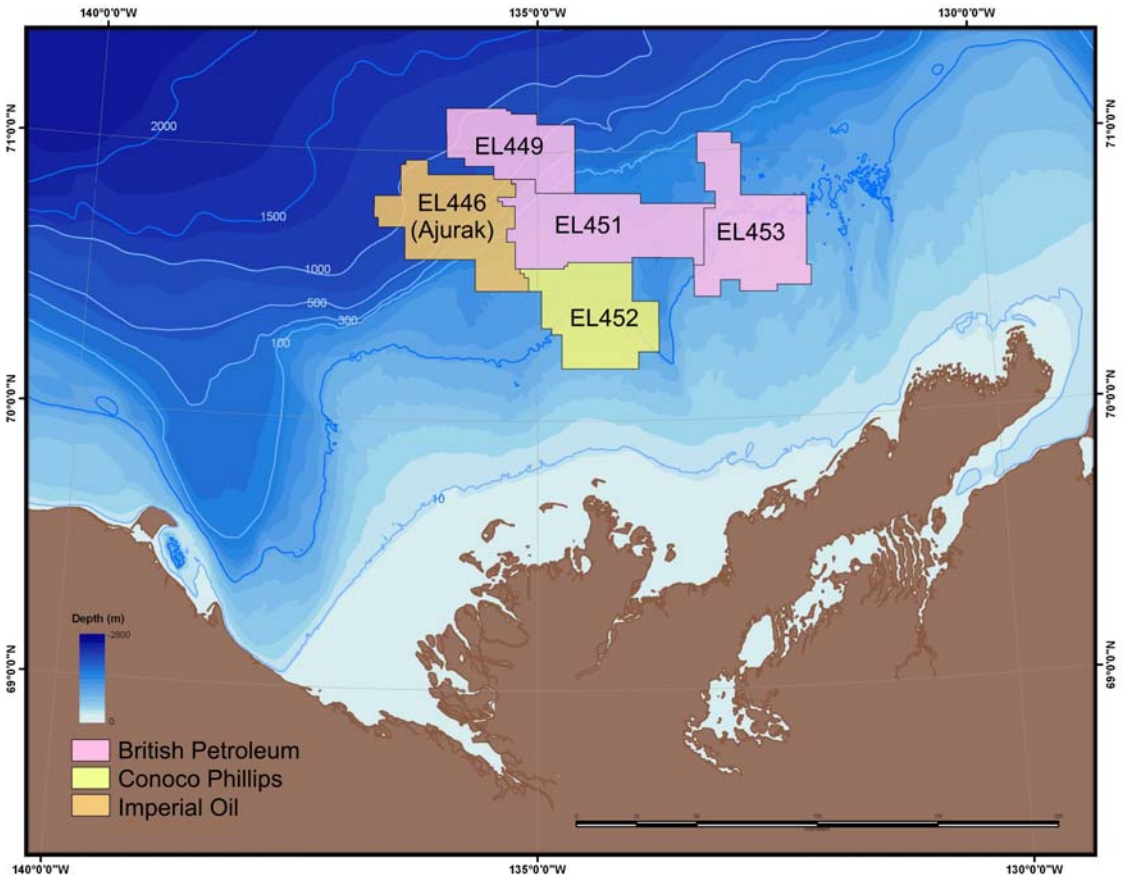

Figure 1. *Map of offshore Exploration Licenses (EL) awarded by the Department of Indian and Northern Affairs in 2007 and 2008 (modified from image courtesy of GSC).*

During the summer of 2011, the CCGS *Amundsen* provided the platform for research conducted under ArcticNet, and the ongoing partnership between ArcticNet and Imperial Oil Resource Ventures Ltd (IORVL) (herein the "Partnership"). This partnership not only forms an important link between industrial and scientific initiatives, but also has extended the duration of valuable data collection and sampling activities in the Western Arctic from two months to five months.

The Partnership has been established as the result of the concurrent need for resources and research within the offshore Northern Oil and Gas lease regions. Under the agreement, IORVL will provide operating and logistic financial support for the CCGS *Amundsen,* and will allow for the consolidation of environmental and risk-assessment research efforts. Active ArcticNet sampling programs, such as ice geophysics and dynamics, ice distribution and thickness and bottom mapping, are of particular interest to IORVL for the reasoning and development of potential future offshore drilling platforms in the Southern Beaufort Sea.

The objective of the partnership is to provide sea ice and met-ocean data relating to data required for development of an ice management system by IORVL (and

BP) for their operations in the southern Beaufort Sea. The 2011 field program focused on instrumenting a selection of Potentially Unmanageable Ice Features (PUIFs) with an ice tethered buoy, distributed sampling throughout two 50 km by 50 km areas and distribution of on ice beacons to track and validate using satellite remote sensing.

The goals set for the 2011 field season were as follows :

1. Contribute to the science required to develop an ice management system for IORVL operations in the southern Beaufort Sea (SBS).

2. Collect data on the 3-D morphology of ice features representing the icescape of the SBS.

3. Collect data on the oceanic and atmospheric forcing of these ice features at a range of space and time scales.

4. Collect data required to understand the engineering forces of these ice features on IOL operations.

This data report is intended to describe and summarize datasets collected by the scientific team based at the Centre for Earth Observation Science, University of Manitoba for field activities conducted between 11 – 25 August 2011.

1.2 The Sea Ice Team

The Principle Investigators of the sea ice team are:

David Barber, CRC, Professor, Director of CEOS, Associate Dean of Research
Centre for Earth Observation Science
University of Manitoba
Winnipeg, MB, Canada, R3T 2N2
dbarber@cc.umanitoba.ca
1-204-474-6981

Tim Papakyriakou, Associate Professor
Centre for Earth Observation Science
University of Manitoba
Winnipeg, MB, Canada,R3T 2N2
papakyri@cc.umanitoba.ca
1-204-474-8513

Simon Prinsenberg,
Coastal Ocean Science,
Bedford Institute of Oceanography
Fisheries and Ocean Canada,
1 Challenger Drive; P.O. Box 1006
Dartmouth, N.S., Canada, B2Y 4A2.
(902) 426 5928 Fax: (902) 426 6927
Simon.Prinsenberg@dfo-mpo.gc.ca

The sea ice team is comprised of multi-disciplinary research associates, technicians, and graduate students who are based at CEOS, University of Manitoba. These individuals were dedicated to one (or more) of the eight disciplinary MetOcean teams: Ocean and Sea Ice Optics, Surface Roughness, Helicopter Electromagnetic Induction Surveys (HEMI), Remote Sensing, Sea Ice Physics, Micrometeorology, and Synoptic Meteorology.Team members were tasked with sampling activities, based upon sampling priorities established for each leg of the cruise. Individuals assigned to each of these sub-disciplines are listed in section 2.2.

1.3 Data Report Outline

Section 1 provides a brief introduction to the partnership between CEOS and IORVL, and sets the context for the report.

Section 2 summarizes the mobilization, crew changes, transit, and science activities of the CCGS *Amundsen*'s 2011 field season as conducted.

Sections 3, 4 and 5 present a detailed summary of ocean, sea ice, and meteorology datasets respectively. Datasets are organized into instrument-specific sub-sections and include descriptions of instrumentation, data collection methodology, and data files. Datasets that involved continuous sampling (e.g. basic meteorological data) are inventoried by date range, and site-specific datasets are inventoried in tabular format.

Section 6 provides information on other available datasets, such as navigation and science logs. A summary of available Synthetic Aperture Radar (SAR) products is also provided as guidance for ordering of imagery.

Appendix A contains the science activities log, including information on stations, positions, sampling activities, and observed weather and ice conditions (as monitored by the watch officer).

Dates are presented in international format (07 July 2011).

Times are presented are UTC (HH:MM:SS) unless otherwise noted as local standard time (LST).

Geographic positions within the dataset may be record in either degrees, decimal-minutes (DD°MM.MMM'), or decimal-degrees (DD.DDDDD°). Although decimal-degree format is highly preferred (mapping, analysis, etc), geographic positions in this report will appear as recorded in the field.

SECTION TWO: CRUISE SUMMARY

2.1 Introduction

Leg 2A began in Kugluktuk on 11 August, coinciding with a crew change. From 11 to 25 August, the Vessel travelled in the Beaufort Sea, carrying out sea ice related scientific sampling operations, including helicopter EMI surveys, on ice buoy and beacon deployments, measurements of physical and chemical properties of multiyear ice floes, and the collection of atmospheric and ocean forcing on sea ice floe data. Additional studies on the engineering forces of sea ice and the identification of ice floes in radar imagery were conducted by IOL personnel. Leg 2A ends on 25 August with a science and crew change in Sachs Harbour.

Six stations were visited during Leg 2A (Figure 2 and Table 1).

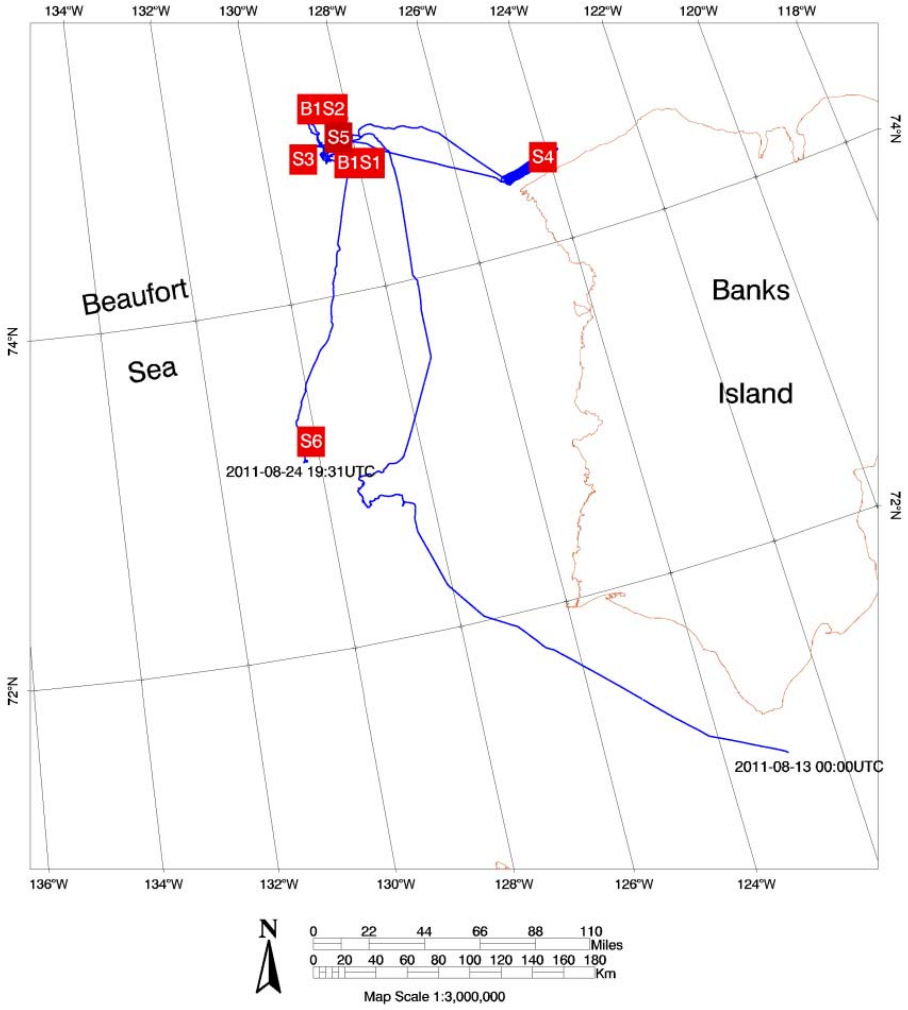

Figure 2. *Map of ArcticNet Leg* 2A *ship track from 2011-08-13 00:00 UTC to 2011-08-24 19:31 UTC, and general site locations.*

From 11-13 August the Amundsen vessel travelled from Kugluktuk to the planned first station for ice sampling operations. Unfavourable ice conditions at the planned Box-1 Site-1 (B1S1) – the ice was rotten and fragmented and not conducive to mooring or sampling – resulted in a transit further north, to approximately 74°52'N/128°13'W, and the commencement of full sampling at B1S1, a giant, MYI floe, on 14 August at 14:34LT. After successful ice sampling operations at B1S1, an ice-breaking management operation to break through the same floe was conducted (16 August 19:30-20:30LT), followed by a short transit N, station keeping, then arrival at the targeted Box-1 Site-2 (B1S2) station, a vast MYI floe with smoothly weathered hummocks, on 17 August 10:30LT. Full sampling was conducted at B1S2 from 17 August 10:30LT to 18 August 19:30LT, after which ice-breaking management operations were conducted and followed by station keeping until 06:50LT on 19 August.

Table 1. ActicNet Leg 2A *sites. Dates and times are in Local (Ship) time (UTC-6h).*

Site	Start (mm.dd hh:mm)	Stop (mm.dd hh:mm)
B1S1	08.14 14:34	08.16 19:05
B1S2	08.17 10:30	08.18 19:30
S3	08.19 18:00	08.20 19:00
S4	08.21 06:00	08.22 19:00
S5	08.23 06:30	08.23 21:08
S6	08.24 08:51	08.24 19:45

On 19 August, the operational decision to cancel the on-ice operations component of Leg 2A was made in the interest of safety. Helicopter and skippy-boat (i.e. secondary sampling) operations to sample sea ice were continued, as were ship-based operations including scatterometer (EM) scanning, atmospheric sampling, bottom profiling, and Rosette deployments. Site 3 (S3 - the 'B1' designation was dropped from site names here forth) comprised these sampling components, as well as ice-breaking management operations, in the MYI floes at approximately 74°45'N/128°30'W. There were several pieces of ice islands in the vicinity; one was visited by helicopter and a beacon deployed.

Strong easterly winds forecast for the region and the potential for high seas resulted in the repositioning of the *Amundsen* vessel from the ice, to a near-shore open water position to the North of Banks Island from 21 August 06:00LT to 22 August 19:00LT. This was declared Site 4 (S4), though science operations were limited in scope during this period.

The vessel returned to the ice at approximately 05:50 LT on 23 August, with compaction and redistribution of the ice evident and likely due to the passing storm. Science operations in Site 5 (S5), located approximately

74°50'N/128°15'W, commenced at 06:30LT on 23 August with scatterometer (EM) scans from the side of the ship, and continued until 21:08LT, though activities were limited by the presence of dense fog. The vessel then transited S to a position within the ice, Site 6 (S6), located at approximately 73°06'N/130°15'W and nearby the Leg 2A termination point at Sachs Harbour. S6 sampling, including Rosette deployments, skippy-boat sampling, and ice-breaking management activities, took place from 08:51LT to 19:45LT on August 24.

2.2 Science Berths and Personnel

CEOS personnel were assigned to the following sub-disciplines during 2011.

Table 2: Sea Ice Berth Allocations by Sub-Discipline

	LEG 1	LEG 2A	LEG 2B	LEG 2C	LEG 3A	LEG 3B
PRIORITY →	TRANSIT	BEAUFORT	BEAUFORT	BEAUFORT	BEAUFORT	TRANSIT
Chief Scientist	N/A	David Barber	N/A	N/A	N/A	N/A
Sea Ice Physical Sampling	x	Julien Barber	x	x	x	
	x	Kerri Warner	x	x		
	x		x	x		
Meteorology	Bruce Johnson	Bruce Johnson	Meredith Pind	Meredith Pind	Chris Stammers	Chris Stammers
	Lauren Candlish	Lauren Candlish	x	x	x	x
	x		x	x	x	x
Surface Roughness	x	Jack Landy	x	X	x	X
	x	Megan Shields	x	X	X	X
Sea Ice Dynamics	x	David Babb	x	X	X	X
	x	Jeremy Barber	x	X	X	X
	x		x	X	X	X
Remote Sensing	x	Randall Scharien	x	X	X	X
	x	Dustin Isleifson	x	X	X	X
	x	Alex Komarov	x	X	X	X
HEMI / SEMI	x	Klaus Hochheim	x	X	X	X
	x	Simon Prinsenberg	X	x	X	X
	x		X	X	X	X
Under-ice Sampling	x	Greg McCullough	X	X	X	X
	x	Geoff Gunn	X	X	X	X

*Note: David Barber was chief scientist on Leg 2A and participated in science activities when his schedule permitted.

SECTION THREE: OCEAN DATA

3.1 Under-Ice Physical Observations

3.1.1 Introduction

The goal of the under-ice observations component of the Multi-year Ice Study was to characterize ocean currents immediately under the ice at each study site. Our primary tool was a z-cell Aquadopp acoustic Doppler current profiler (ADCP) which was deployed under the ice. At intervals during each current profiler deployment, we recorded vertical water column profiles of salinity, temperature and photosynthetically active irradiance (PAR). Our local under-ice observations were supplemented by numerous CTD and PAR profiles made by colleagues working on the same ice floe, continuous current profiles recorded using the *Amundsen*'s RDI ADCP and periodic salinity, temperature and current profiles using the ship's rosette-mounted multi-parameter sensors and RDI ADCP.

3.1.2 Methods

The z-cell Aquadopp was mounted in 4" dia., 1/8" thickness aluminum pipe with extensions to a maximum of 8 m. A 10 m communications cable and a 1/8" wire rope safety line were attached to the Aquadopp and threaded through to the opposite end of the pipe. The safety line was attached to the upper end of the aluminum pipe, which was itself kept safe from falling through the ice by inserting two short lengths of 1" steel pipe through the aluminum pipe and perpendicular to each other. The pipe was inserted through an 8" dia. augur hole to place the Aquadopp in water about 0.5 m below the bottom of the ice facing downwards. The 4" vertical aluminum pipe was supported on the upper ice surface by two short lengths of 1" steel pipe (Figure 3). Slush around the pipe in the augured holes kept the aluminum pipe from tilting, vibrating or otherwise moving due to currents below the ice. The Aquadopp was deployed at 7.15 and 4.57 m depth at B1S1 and B1S2 respectively; that is, roughly 0.5 m below the bottom ice surface in each case.

After installation of the Aquadopp through the ice, the communications cable was connected to a laptop kept in an adjacent Action Packer box (Figure 3). Both Aquadopp and laptop were powered by ac inverted from a 12 V battery in the box. The Aquadopp was run in online mode to allow inspection of the initial current profile records before leaving and at each visit to the site. Aquadopp settings for each deployment are shown in Table 3. In brief, the instrument was set to record current velocities at 1 min. intervals, in 2 m bins from 0–60 m depth below the instrument. Each 1 min. observation stored the mean of the previous 30 sec. of recorded velocity and ancillary data. Pressure and temperature at the instrument head were recorded during every observation. Salinity (for the purpose of estimated velocity of sound) was set at 30.5 based on typical local observational data at 0–60 m depth. Aquadopp settings were the same for all deployments except that the profile interval was reduced from 1 min. at B1S1 and B1S2 to 40 sec. at the Skippy boat stations S4 C1 to C3 and S5 C1 and C2.

A 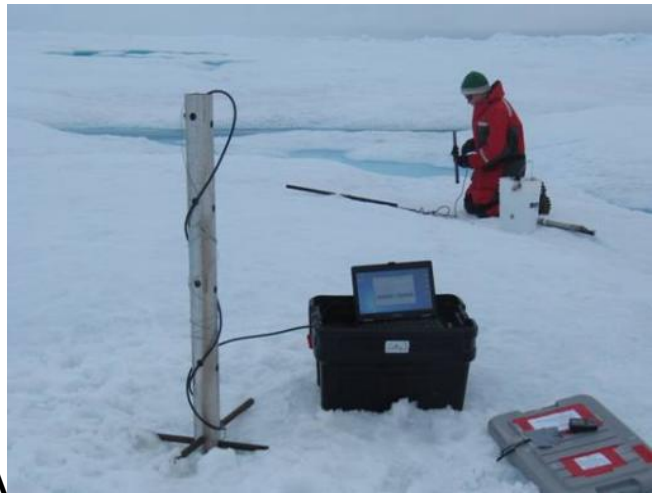 B 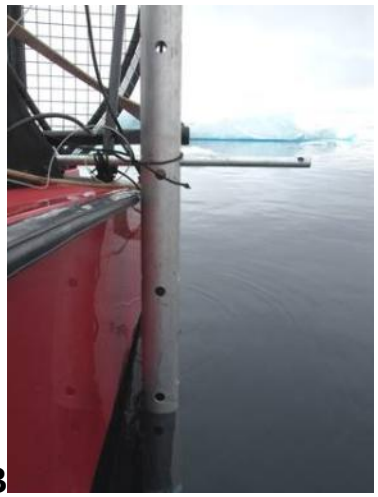

Figure 3. *A) Current profiler deployment at B1S2C. The profiler was mounted approximately 0.5 m below the ice, at the bottom of a length of aluminum pipe. GPS is mounted on laptop container near the instrument. At B1S2 only, a CTD-Tu was moored nearby (upper right) at 1.5 m below the ice. B) Current profiler deployment from Skippy boat.*

Ice thickness, snow thickness and freeboard were recorded at each site. Over the duration of each Aquadopp deployment, a Garmin etrex Vista Cx GPS was used to geographic coordinates at 10 sec. intervals at the instrument site. During each deployment, an Idronaut Ocean Seven 304 was used one or more times to record conductivity-temperature-depth probe (CTD) profiles to depths ranging from 70–130 m via 2 in. augur holes within a few metres of the Aquadopp site. CTD recording frequency was 6 Hz; the instrument was lowered at roughly 0.5 m/sec. PAR profiles were recorded simultaneously using an Alec MDS-MkV/L PAR sensor mounted on the rope 0.9 m above the Idronaut sensors. At one site, B1S2, a CTD and PAR sensor were deployed under the ice (PAR 0.5 m below ice; CTD 1.5 m below ice) throughout the Aquadopp deployment period.

Subsequent to the cessation of on-ice activities, the Aquadopp was deployed from the Skippy boat at two stations, S4 and S5. At these stations, the instrument was mounted in a 2 m section of aluminum pipe and suspended off the side of the boat, while the boat was parked stationary on the windward side of a selected ice floe. The instrument was deployed at 0.9 m depth at all Skippy boat sites. In these cases, observations were recorded at 40 sec. intervals for roughly 20 min. (in one case, for only 12 min.; Table 2.1). A single CTD and PAR profile was recorded immediately after each such boat-mounted Aquadopp deployment. As with through-ice deployments, geographic coordinates were recorded at 10 sec. intervals throughout the deployment period.

Supplementary continuous current profiles were recorded adjacent to each Aquadopp site using the *Amundsen*'s RDI ADCP and periodic salinity, temperature and current profiles using the ship's rosette-mounted multi-parameter sensors and RDI ADCP (Yves Gratton, PI).

All instrument clocks were set to UTC. Observations recorded in field books are MDT unless otherwise noted. All geographic coordinates use datum WGS84.

3.1.3 Data and Data Visualizations

All data, including site photographs and copies of field notes, are stored digitally. Start and end times of each Aquadopp deployment are reported in Table 3. The Aquadopp was deployed at 7.15 and 4.57 m depth at B1S1 and B1S2 respectively; that is, roughly 0.5 m below the bottom ice surface in each case. At Skippy boat sites S4 and S5, it was deployed at 0.9 m depth. GPS tracks recorded during each deployment are shown in Figures 4 and 5. Two representative CTD records are shown in Figures 6. Ice and current velocity time series at B1S1 and B2S2 are shown in Figures 7 and 8. Please be aware that these figures are prepared from initial data returns prior to quality assessment.

Datefiles are found in the database at :

\OCEAN\ Aquadopp(binary)\quality-checked_data

Table 3. Aquadopp settings and other information for each deployment. Note that two files were recorded at each of stations B1S1 and B1S2 due to instrument resets during inspections. Time of first and last measurements are reported as day hour:minute.

	B1S1		B1S2		S4			S5	
File name root	B1S1_01	B1S1B06	B1S2A-01	B1S2B-01	B1S4C101	B1S4C201	B1S4C301	B1S5C101	B1S5C201
Number of measurements	684	338	777	342	39	33	36	37	19
Number of checksum errors	0	0	0	0	0	0	0	0	0
Time of first measurement	16 04:10	16 16:01	18 02:49	18 16:10	20 20:36	20 21:46	20 22:28	23 19:56	23 20:41
Time of last measurement	16 15:33	16 21:38	18 15:45	18 21:51	20 21:01	20 22:08	20 22:52	23 20:20	23 20:53
User setup									
Profile interval	60 sec	60 sec	60 sec	60 sec	40 sec	40 sec	40 sec	40 sec	40 sec
Number of cells	30	30	30	30	30	30	30	30	30
Cell size	200 cm	200 cm	200 cm	200 cm	200 cm	200 cm	200 cm	200 cm	200 cm
Average interval	30 sec	30 sec	30 sec	30 sec	30 sec	30 sec	30 sec	30 sec	30 sec
Measurement load	50%	50%	50%	50%	50%	50%	50%	50%	50%
Transmit pulse length	2.00 m	2.00 m	2.00 m	2.00 m	2.00 m	2.00 m	2.00 m	2.00 m	2.00 m
Blanking distance	0.50 m	0.50 m	0.50 m	0.50 m	0.50 m	0.50 m	0.50 m	0.50 m	0.50 m
Z-cell - Cell size	100 cm	100 cm	100 cm	100 cm	100 cm	100 cm	100 cm	100 cm	100 cm
Z-cell - Blanking distance	1.01 m	1.01 m	1.01 m	1.01 m	1.01 m	1.01 m	1.01 m	1.01 m	1.01 m
Z-cell - Powerlevel	HIGH-	HIGH-	HIGH-	HIGH-	HIGH-	HIGH-	HIGH-	HIGH-	HIGH-
Compass update rate	1 sec	1 sec	1 sec	1 sec	1 sec	1 sec	1 sec	1 sec	1 sec
Power output	DISABLED	DISABLED	DISABLED	DISABLED	DISABLED	DISABLED	DISABLED	DISABLED	DISABLED
Powerlevel	HIGH	HIGH	HIGH	HIGH	HIGH	HIGH	HIGH	HIGH	HIGH
Coordinate system	ENU	ENU	ENU	ENU	ENU	ENU	ENU	ENU	ENU
Sound speed	MEASURED	MEASURED	MEASURED	MEASURED	MEASURED	MEASURED	MEASURED	MEASURED	MEASURED
Salinity	30.5 ppt	30.5 ppt	30.5 ppt	30.5 ppt	30.5 ppt	30.5 ppt	30.5 ppt	30.5 ppt	30.5 ppt
Distance between pings	74.45 m	74.45 m	74.45 m	74.45 m	74.45 m	74.45 m	74.45 m	74.45 m	74.45 m
Number of beams	3	3	3	3	3	3	3	3	3
Number of pings per burst	2	2	2	2	2	2	2	2	2
Software version	1.35	1.35	1.35	1.35	1.35	1.35	1.35	1.35	1.35
Deployment name	B1S1_	B1S1B	B1S2A	B1S2B-	B1S4C1	B1S4C2	B1S4C3	B1S5C1	B1S5C1

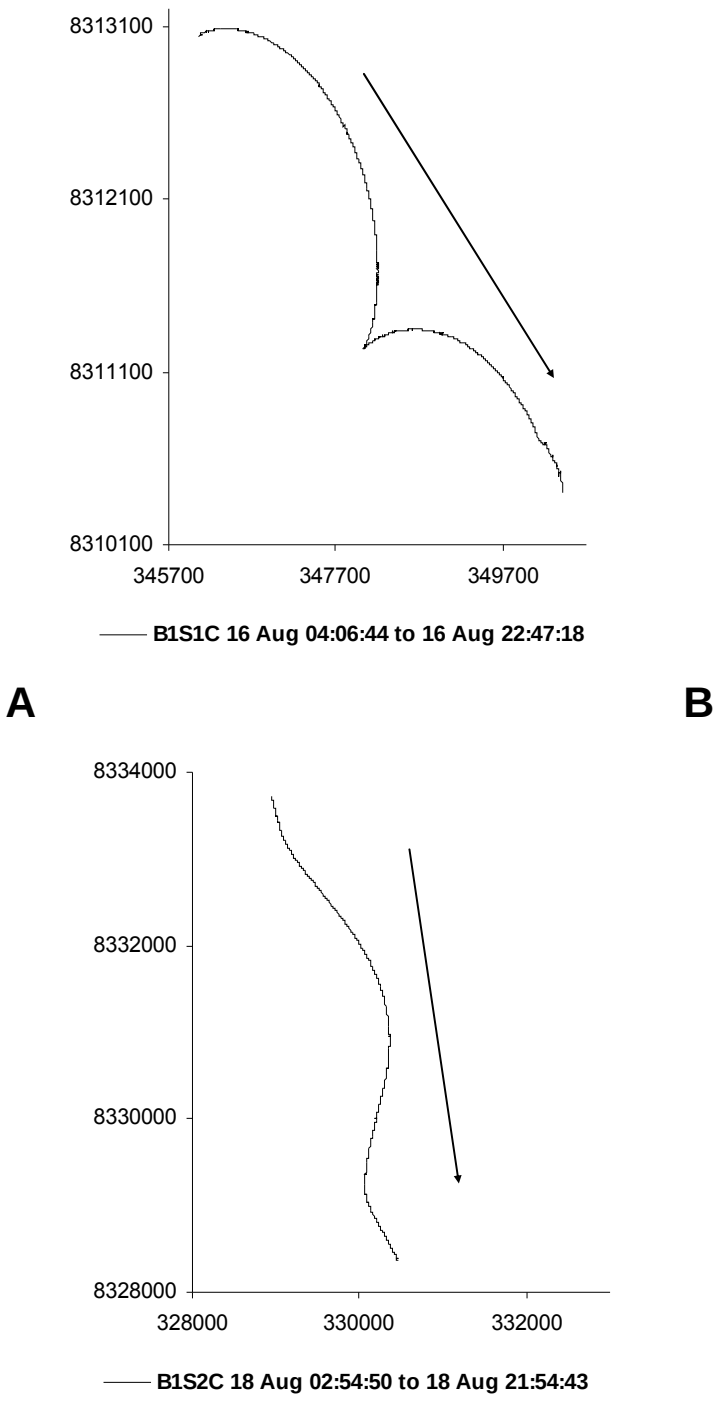

Figure 4. *Position and drift of current profiler at ice floe sites B1S1 (A) and B1S2 (B). Arrows indicate direction of drift. Grid is UTM (m). Relative scale is the same in the two panels.*

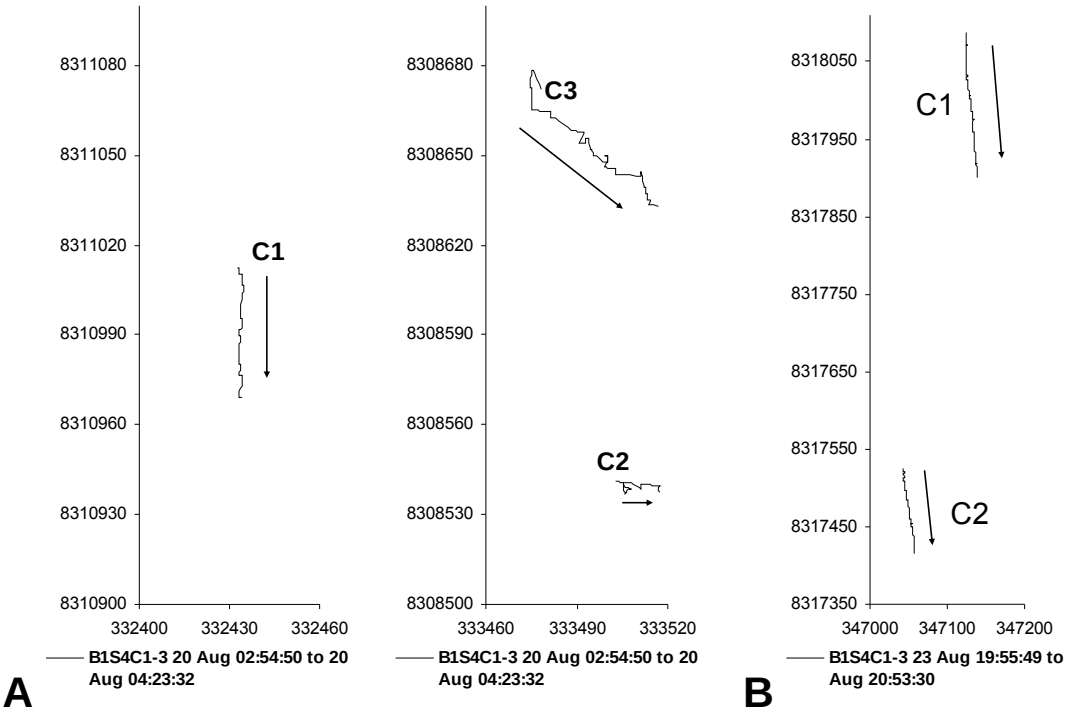

Figure 5. *Position and drift of current profiler at Skippy boat sites S4 C1 to C3 (A) and S5 C1 and C2 (B). Arrows indicate direction of drift. Grid is UTM (m). Throughout each deployment, the Skippy boat was stationary relative to the adjacent floe at each site. Relative scale is the same in the two panels.*

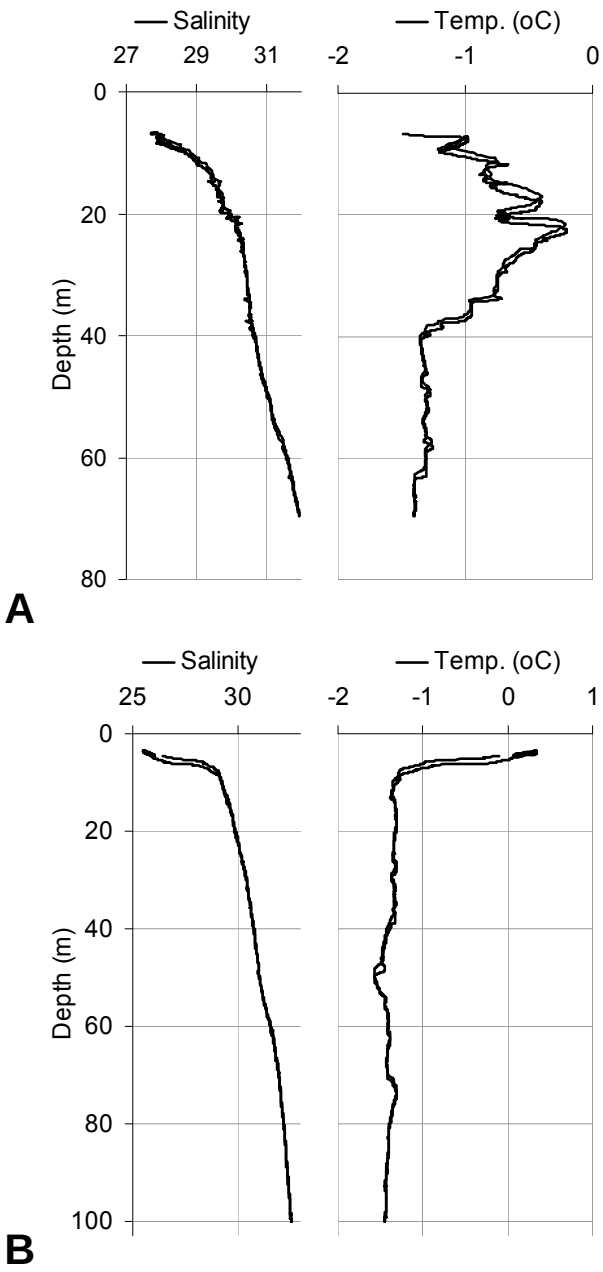

Figure 6. *Salinity and temperature profiles under ice at sites B1S1 (A) and B1S2 (B).*

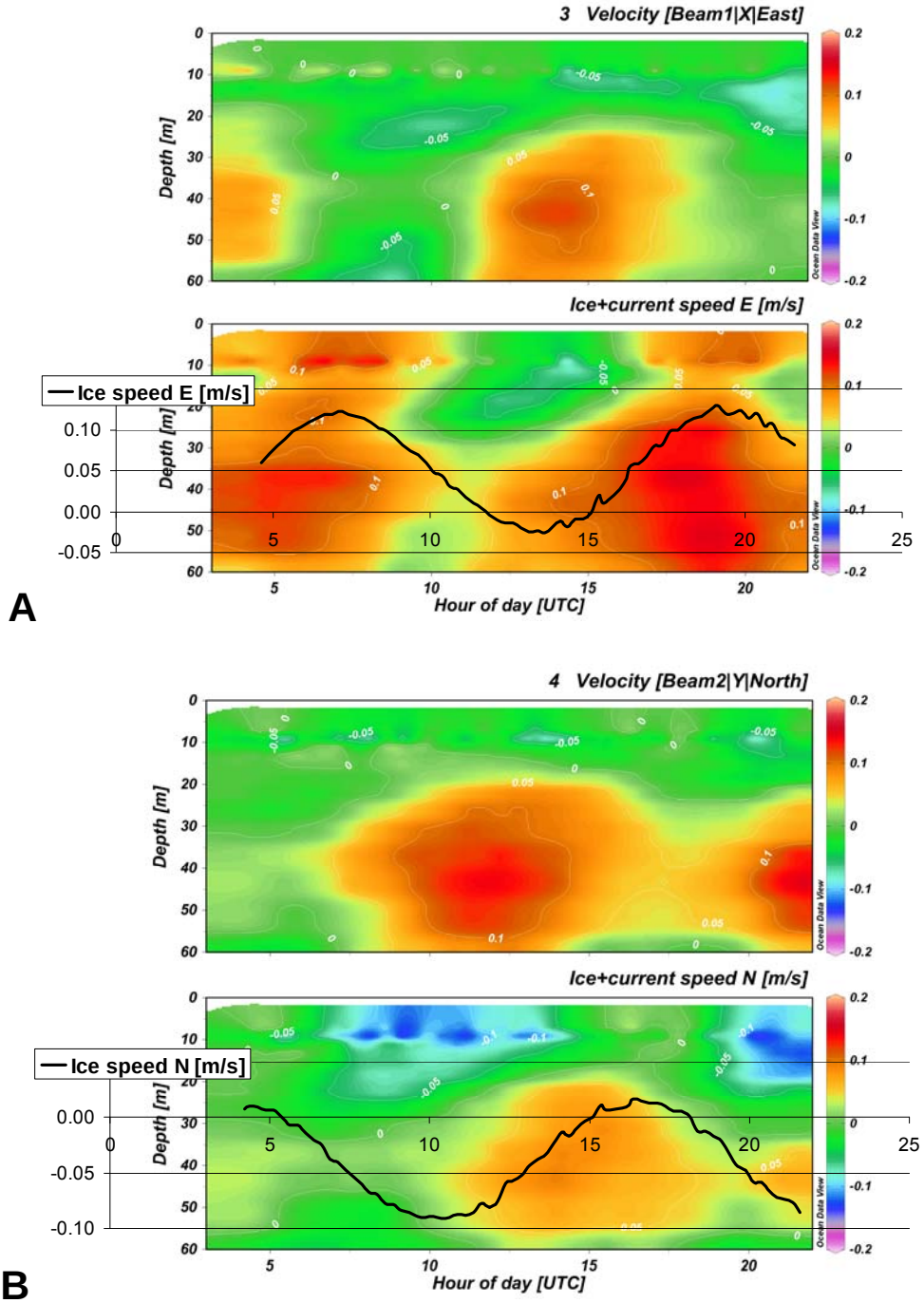

Figure 7. *Magnitude of eastward (A) and northward (B) vectors of ocean currents to 60 m depth at site B1S1. Upper panel shows eastward current speed relative to the ice floe. Lower panel shows absolute eastward current speed. Overlaid line shows eastward (northward) ice speed over the same period, with speed in m/s shown on the scale at far left.*

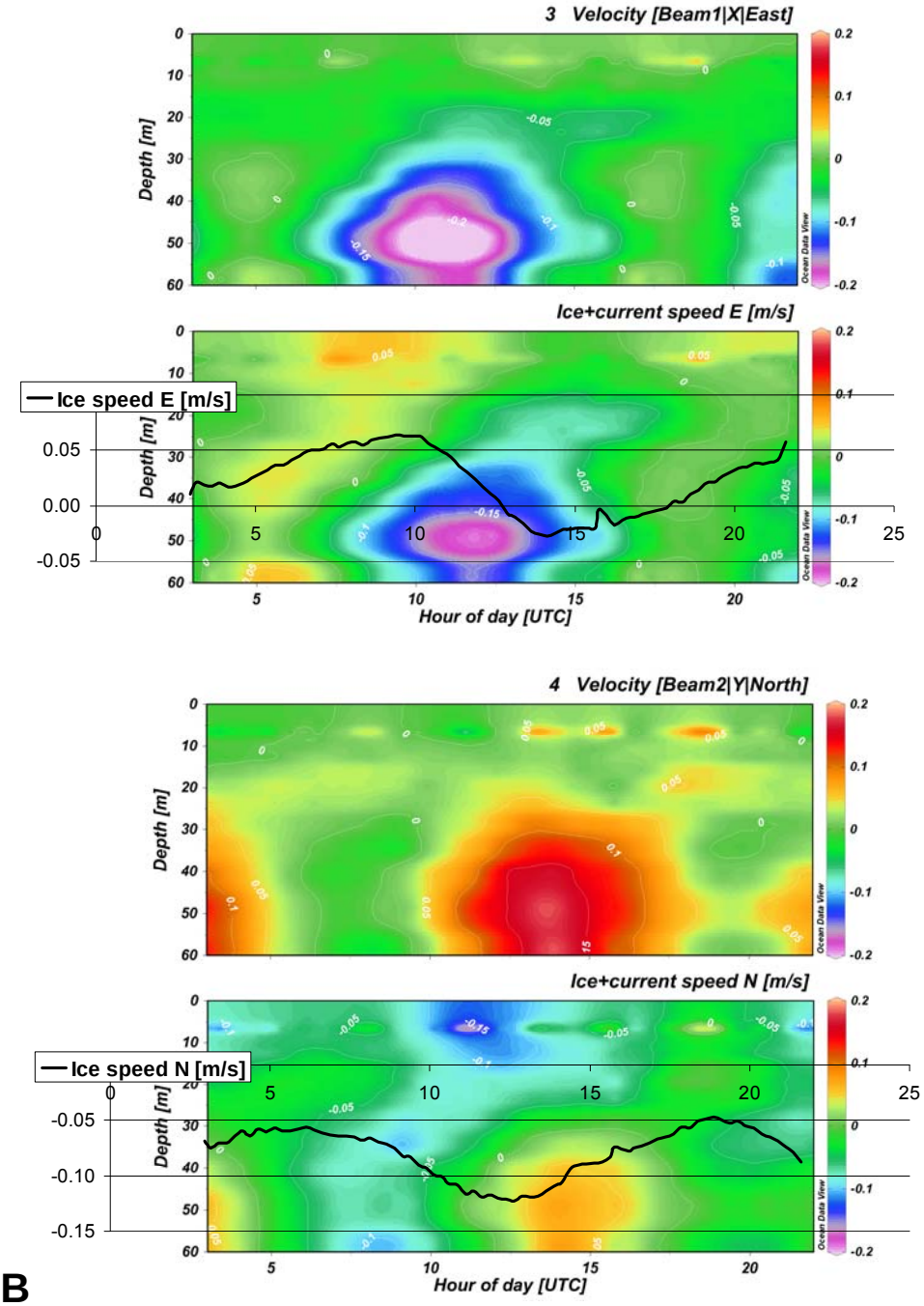

Figure 8. *Magnitude of eastward (A) and northward (B) vectors of ocean currents to 60 m depth at site B1S2. Upper panel shows eastward current speed relative to the ice floe. Lower panel shows absolute eastward current speed. Overlaid line shows eastward (northward) ice speed over the same period, with speed in m/s shown on the scale at far left.*

3.2 Ocean Conductivity-Temperature-Density (CTD) Profiles

3.2.1 Instrumentation

Instrument: Idronaut Ocean Seven 304 CTD-T multi-parameter probe with temperature, conductivity and turbidity sensors (Figure 9).

Figure 9. *An Irdonaut Ocean Seven 304 CTD-T probe about to be deployed.*

Pressure/depth
Range: 0-1000 db
Accuracy: 0.05% F.S.
Resolution: 0.0015 % F.S.

The Idronaut was set to start recording at 6 Hz when conductivity exceeded 0.001 mS cm^{-1} and to cease recording 10 sec after conductivity fell below this threshold, ensuring that the last observations would include atmospheric pressure. Water pressure was derived from raw pressure by subtracting the mean of the last six observations from each observation. Atmospheric pressure by this method ranged from 1.85 - 2.14 db. Standard deviations associated with cast means ranged from 0.00 - 0.06 db, indicating that 95% confidence in water pressure by this method was at most ±0.12 db. Observation depths reported in the accompanying data files are calculated from water pressure (i.e. observed pressure - minimum pressure) as:

Depth(m)=water pressure (db)*1.01724

Temperature
Range: -5 to +35°C.
Accuracy: 0.005°C
Resolution: 0.000°C

Conductivity

Range: 0-64 mS cm^{-1}
Accuracy: 0.005 mS cm^{-1}
Resolution: 0.001 mS cm^{-1}

Turbidity:
The Idronaut Ocean Seven 304 CTD-T is equipped with a Seapoint turbidity sensor which measures side-scattered light. Light source is a pair of 880 nm light emitting diodes; detectors are side-by-side silicon photo diodes. Detectors sense light scattered between 15 and 150° to the side of the emission path, and from a volume within 5 m of the sensor window. It is considered insensitive to ambient light when immersed in water. The sensor
was factory-calibrated in formazin turbidity units (FTU). Specifications for the Seapoint turbidity meter are given in Table 4.

Table 4: Seapoint turbidity meter sensor specifications:

Gain	Sensitivity (mV/FTU)	Range (FTU)	Accuracy (FTU)	Resolution (FTU)
200X	200	25	0.05	0.005
20X	40	125	0.25	0.025
5X	10	500	1	0.1
1X	2	>750	5	0.5

3.2.2 Data Summary

CTD datafiles are organized by deployment date in the following folders:

\OCEAN\ CTD(ASCII&preliminary_QC)\Quality-checked_data

A summary of all CTD casts is presented in Table 5:

Table 5: Irdonaut Ocean Seven 304 Casts conducted in 2011

Station	**Dates**	**Number of Casts**	**Conducted by :**
B1S1 B1S2	15 – 18 Aug.	4	Under-ice physical observations (ice based)
B1S4 B1S5	20,23 August	5	Under-ice physical observations (skippy-boat based)
N/A	15, 16 August	4	Sea Ice Dynamics Group (helicopter based)
All	August 15 -17	25	Sea Ice Morphology Group (ice based)
N/A	August 24	3	Calibration with Rosette

All variables denoted in the file header have been defined in section 3.2.1. A sample of ASCII output for a CTD cast is presented in Table 6:

Table 6: Sample ASCII CTD data

Date	Time	Pres	Temp	Cond	Sal	Turb
20/07/2009	12:35.0	0.13	0.251	22.632	26.4	0.1
20/07/2009	12:35.1	0.13	0.25	22.635	26.404	0.1
20/07/2009	12:35.3	0.13	0.252	22.662	26.437	0.1
20/07/2009	12:35.4	0.13	0.249	22.659	26.435	0.1
20/07/2009	12:35.5	0.13	0.242	22.631	26.406	0.1
20/07/2009	12:35.7	0.13	0.237	22.627	26.405	0.1
20/07/2009	12:35.8	0.13	0.238	22.617	26.391	0.1
20/07/2009	12:36.0	0.12	0.243	22.624	26.396	0.1
20/07/2009	12:36.1	0.12	0.247	22.622	26.39	0.1
20/07/2009	12:36.3	0.13	0.249	22.61	26.373	0.1
20/07/2009	12:36.4	0.14	0.248	22.601	26.361	0.1
20/07/2009	12:36.5	0.13	0.246	22.601	26.364	0.1
20/07/2009	12:36.7	0.12	0.244	22.608	26.375	0.1
20/07/2009	12:36.8	0.12	0.246	22.616	26.383	0.1
20/07/2009	12:37.0	0.13	0.246	22.614	26.38	0
20/07/2009	12:37.1	0.14	0.245	22.604	26.368	0.1
20/07/2009	12:37.3	0.13	0.245	22.602	26.366	0.1
20/07/2009	12:37.4	0.13	0.243	22.606	26.373	0.1
20/07/2009	12:37.6	0.12	0.24	22.613	26.384	0.1

3.3 Ocean Surface Roughness

3.3.1 Instrumentation: Meteorological Ocean Buoy

Instrument : MetOcean Systems Meteorological Ocean Buoy (MOB) System.

The MOB buoy (Figure 10) is used to investigate *in situ* sea surface roughness conditions. Accelerometers are used to generate a 3-dimensional wave-spectrum time series. The MOB also has a Vaisala sonic ultrasonic wind sensor, which measures surface wind speed and direction. There is a GPS receiver on the top of the buoy, and a radio transmitter (160.725 mHz) that transmits a signal that is received by a hand-held directional finder. The buoy weighs approximately 18 kg and has a diameter of 16 inches.

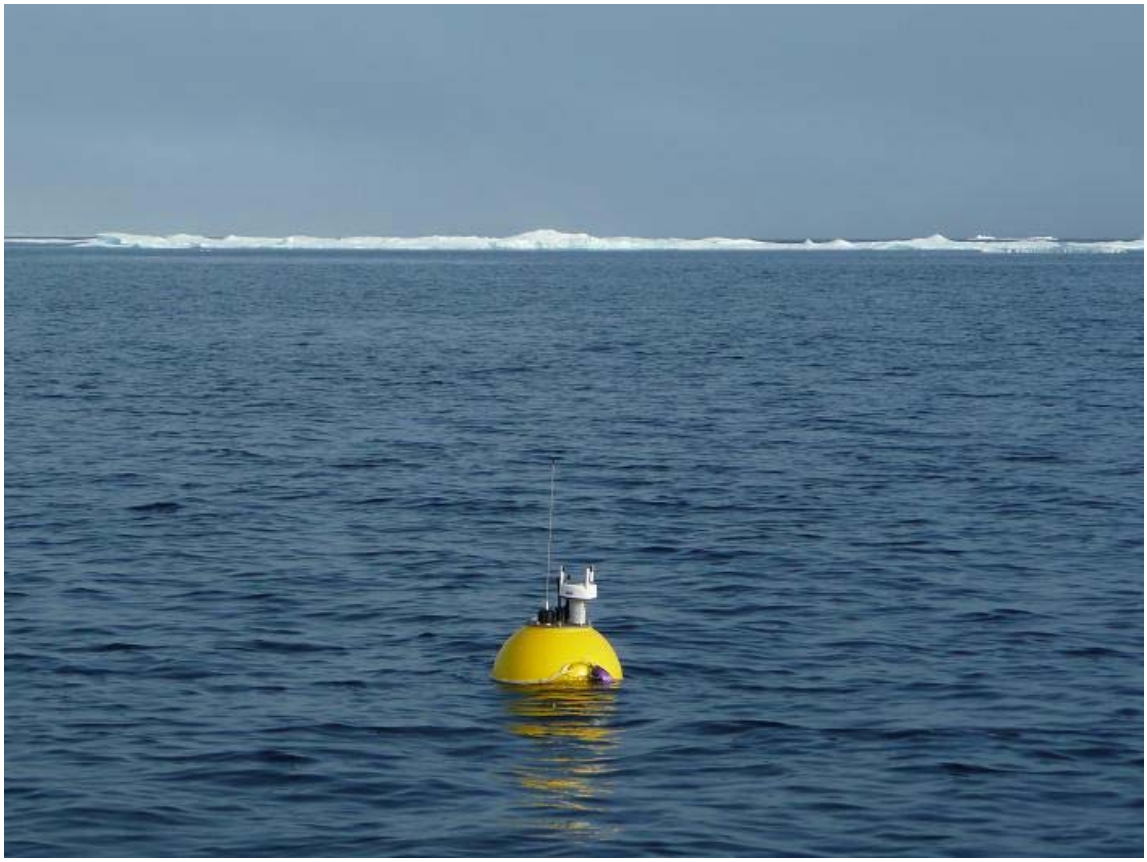

Figure 10. *A MOB during a typical deployment away from the influence of the ship or zodiac.*

The buoy was deployed using the zodiac at least 100 m away from the ship. The buoy is recovered using the zodiac (or the ice cage when the zodiac can't be deployed). The buoy must be on the water for at least 2 hours. This ensures sufficient telemetry to generate various wave parameters including wave spectrum every 15 minutes.

3.3.2 Data Summary

Deployment opportunities were limited to two short deployments on 17 and 18 August 2011. The data sets available from these deployments are very limited in temporal coverage, but are representative of relatively small sea surface roughness encountered arising from high sea ice concentrations.

The MOB has two data sets: 1) Wave spectra, and 2) Ocean surface winds using a Vaisala Ultrasonic anemometer. The wave spectra data appears as two Datawell format files having extensions *.RDT and *.SDT. (Note: Datawell BV waverider software, W@ves21 v2.2.14, is required to open the files." This software can be purchased from Datawell BV http://www.datawell.nl/inhoud.php?id=1). The wave data is in proprietary binary format, and is plotted directly by the supplier software and therefore has no header information. The SDT files contain the main wave spectrum information that includes 2D and 3D power spectral density, significant wave height, wave period, latitude and longitude and position plot. The RDT files contain mainly displacement statistics data that includes, heave distribution, horizontal and vertical projection, mean, standard deviation, skewness and kurtosis.

Ocean surface wind data is in comma-delimited ASCII format and can be easily opened with Microsoft Excel. Datafile header information is as follows:

JHOUR: Hour of the year (Counting 1 from January 1st 00:00 hrs)
HDG: Heading
PITCH: Measured pitch (degrees)
ROLL: Measured roll (degrees)
DN: Wind direction (min)
DM: Wind direction (average, m/s)
DX: Wind direction (max, m/s)
SN: Wind speed (min, m/s)
SM: Wind speed (average, m/s)
SX: Wind speed (max, m/s)
VBAT: Battery Voltage (Volts)

MOB datafiles are organized by deployment date in the dataset at:

\OCEAN\MOBS

3.3.2 Data Visualizations

Data visualizations are presented below in figures 32 and 33.

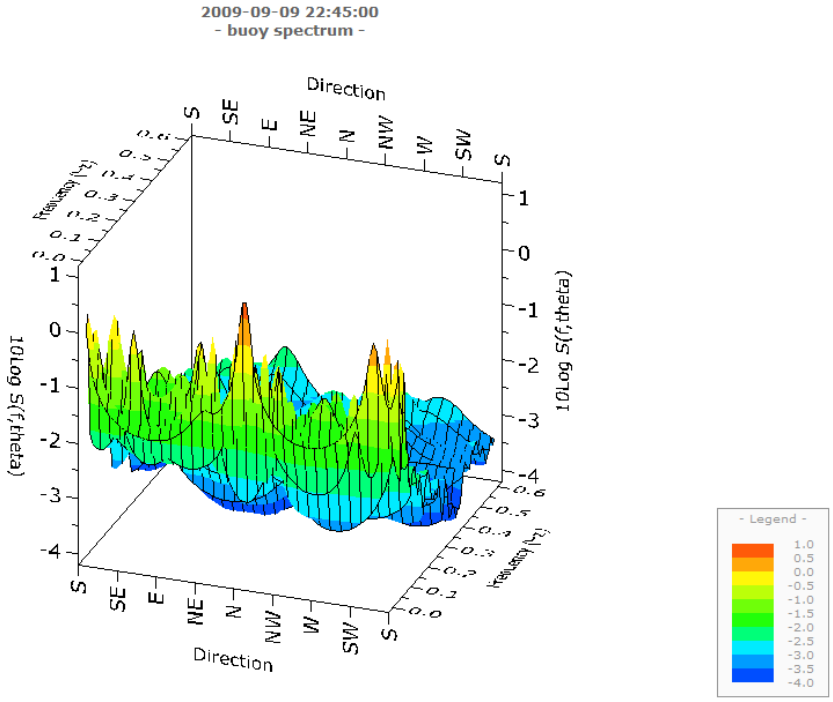

Figure 11. *Three dimensional Meteorological Ocean Buoy spectrum observed on 09 August 2009. The 3D-plot shows spectral density vs. frequency and direction.*

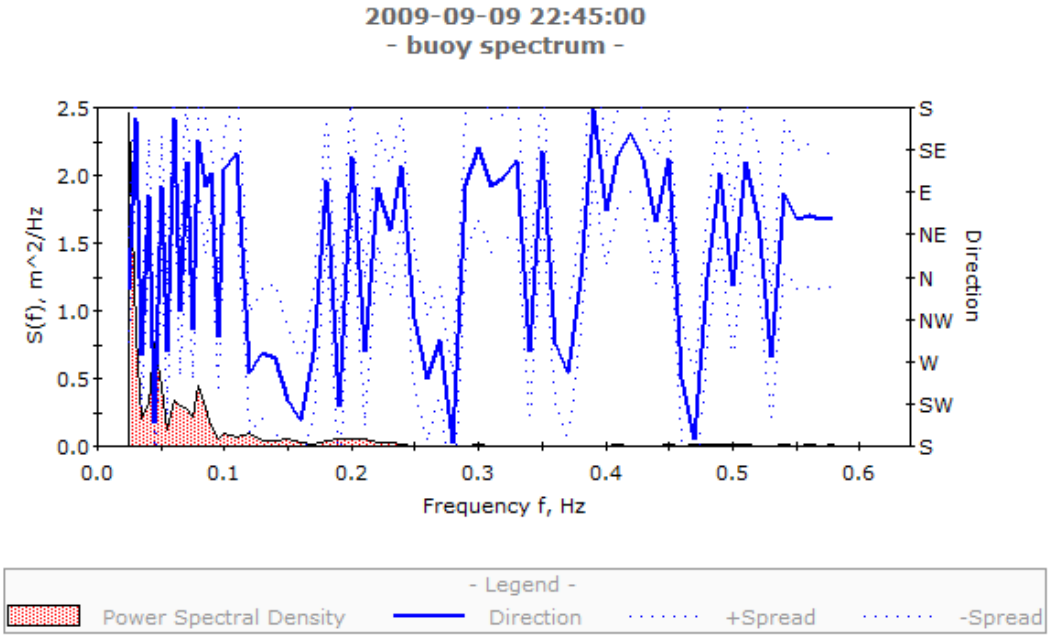

Figure 12. *Two dimensional Meteorological Ocean Buoy spectrum observed on 09 August 2009. The 2D-plot shows Spectral Density vs. Frequency, spread and direction.*

SECTION FOUR: SEA ICE DATA

4.1 Helicopter Electromagnetic Induction System Sea Ice Thickness Surveys

By : Simon Prinsenberg, Ingrid Peterson and Scott Holladay

This report summarises the helicopter survey of the IOL Ice Cruise 2011 and presents examples of data collected with the helicopter-borne sensors during the survey covering August 14-24, 2011 over the Multi-Year (MY) pack ice west of Banks Island in the Canadian Beaufort Sea. The BO105 helicopter onboard the CCGS *Amundsen* was used during the survey and was flown by Robert Pelletier and maintained by the helicopter engineer Eddy Perron. The two week-long survey collected ice thickness and ice roughness data with helicopter-borne Electromagnetic-laser (EM) sensors flown at 5-8m altitude. Video and roughness data was collected with a video-laser system flown at 100-120m altitude along flight paths covered by the EM system. Additional Ground Penetrating Radar (GPR) data was collected simultaneously with the EM sensor; it is designed to measure snow depth, but no snow was encountered on the pack ice. Two MY ice floes, where on-ice sampling by others took place, were extensively sampled by a fine grid EM and Video flight lines. Additional lines were flown along marked EM sled and NRC survey lines and by soft-landing at each marked drill hole location. Four regional surveys were done near the ship using 4-6 parallel grid lines each 10-15km long along which EM-GPR data was collected. This regional data indicated that ice thicker than 4m occurred only 20-40% of the time while thinner ice including melt ponds accounted for 60-80% of the surveyed pack ice. The EM data collection was followed by Video-Laser data collection over the same grid pattern from a 100m altitude to provide a 100m wide video frame width. During the last three regional flights the GPR was replaced by an U. Manitoba camera and video flights were done at a much higher altitude. Further data processing and analysis will occur and all data, plots, photographs and reports will be put on the CCGS *Amundsen* share drive and are available with additional post processing results on the Department Fisheries and Oceans "SeaIce" Website:
http://www.mar.dfo-mpo.gc.ca/science/ocean/seaice/public.html and its FTP data link. All the analysis results including those of the EM sled will be published as a technical report and available on the sea ice website.

4.1.1 Survey Area

The summer 2011 ice survey during the pack ice survey concentrated on the multi year (MY) pack ice west of Banks Island (Figure 13). As seen from the ice chart, the ice consisted mostly of thicker MY ice as the colour variation on the chart mainly indicates an variability in ice concentration rather than a variation of ice type (thickness). A large open water area existed between Banks Island which continued into M'Clure Strait. The open water area was not large enough to generate the long period waves that were seen in the summer survey of 2009 which were capable to move into the pack ice to 300km and broke up the pack ice into smaller floes. A storm, midway through the survey, moved south of the survey area but did not generate these long period waves and did not break of the large floes. The storm however did cause a stoppage of the

survey work and the *Amundsen* hid in M'Clure Strait just at the northwestern tip of Banks Island.

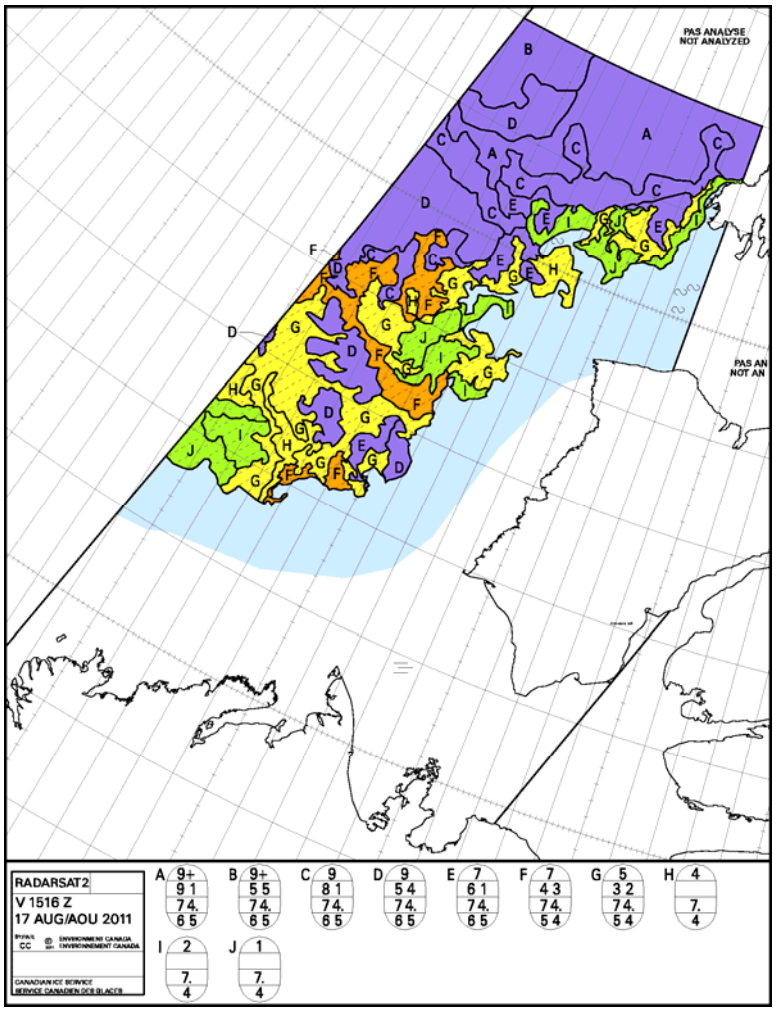

Figure 13. *Ice chart of August 17 representing the ice conditions at the start of the ice survey. The survey was done just below the 75°North latitude, the latitude that runs through the middle of into M'Clure Strait and along and into the ice edge.*

Figure 14 shows the typical ice conditions as seen by a satellite SAR sensor and used to produce ice charts. The B1.S1 floe along which the CCGS *Amundsen* anchored consisted of MY ice, but as seen in later pictures is not as consolidated as it appears on the SAR figure. It was covered by a lot of melt ponds in various stages of decay intermingled with older solid MY pack ice with thicknesses persistently reaching 5-6m. Thus floe B1.S1 was found to be a very inhomogeneous thickness MY ice floe, whose thickness variations are difficult to identify from a SAR image.

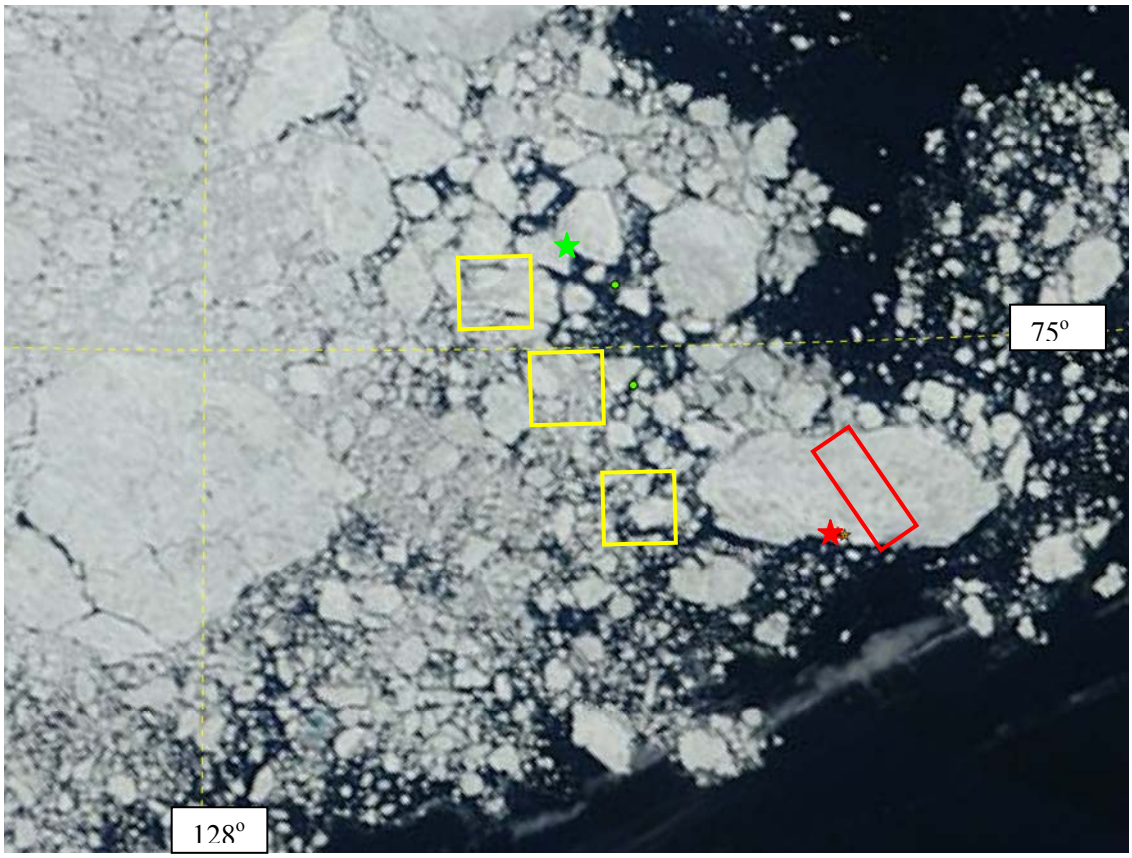

Figure 14. *Satellite Image of August showing the approximate locations of the MY ice floes B1.S1 (Red triangle) and B1.S2 (Green triangle) and the regional areas covered the ice helicopter survey.*

4.1.2 Instrumentation

4.1.2.1 Electromagnetic-Laser Sensor

During the IOL summer 2011 field survey, ice thickness and ice surface roughness were measured with a helicopter-borne electromagnetic (HEM) system, called the “Ice Pic”, built by Geosensors Inc. of Toronto, Canada (Figure 15). As stated in the 2009 report, the sensor package consists of an electromagnetic (EM) sensor with transmitter and receiving coils (transmitter frequencies of 1.7, 5.0, 11.7 and 35.1 kHz) and a laser altimeter. The laser altimeter data provides ice-surface roughness profiles and the height of the EM sensor above the pack ice. The laser is an ADM 3-Alpha Geophysical unit and has a listed accuracy of 1.5cm. The EM sensor measures the distance to the ocean surface water as it is the nearest conductor and the laser measures the distance to the pack ice surface. Together they provide the snow-plus- ice thickness. The sampling rate for the ice thickness and ice roughness data is 10Hz, corresponding to a spatial sampling interval of about 3-4m for the normal helicopter survey speed of 80mph. The ice thickness and ice conductivity are estimated with a 2-layer inversion model representing ice and seawater layers. The calculations are done in real-time on a

computer strapped in the back seat of the helicopter and results displayed approximately 1sec later on a hand-held monitor used by the operator.

Figure 15. *Canadian Coast Guard helicopter showing the fix-mounted sensor equipment.*

The footprint size of the EM sensor depends on the height of the EM sensor above the seawater (Kovacs et al., 1995) and is 16-20m for the “Ice Pic” flying at 4m over 2m thick ice. Several studies have validated the EM ice thicknesses collected by both the “Ice Pic” and “Ice Probe”, a towed HEM system, by comparing EM ice thicknesses successfully with ice and snow thicknesses measured via holes drilled through the ice (Peterson et al., 2003 and Prinsenberg et al., 2008). For flat homogeneous ice over sea water such as refrozen leads, no difference can seen between auger observations and EM helicopter data as the difference are usually smaller than the variability in each data set. Over rough deformed ice, one has to average the auger holes to match the footprint size of the EM sensor, and once this is done the data sets again match normally within ±5cm (Peterson et al., 2003 and Prinsenberg et al., 2008).

4.1.2.2 Ground Penetrating Radar Sensor

Ground Penetrating Radars (GPRs) have the capability to measure snow thickness or freshwater ice thickness (Lalumiere and Prinsenberg, 2009). A one-dimensional processing algorithm provides snow thickness, and if the underlying ice has low salinity, it also provides the ice thickness. For the 2011 survey, the GPR profiles could be

viewed in the helicopter to ensure the data was being logged properly, where as during the 2009 survey the data could only be viewed in a post-processing mode.

The GPR system is a Noggin-NIC 1000 from Sensors and Software Inc. of Mississauga, Ontario. A photograph of a Noggin-NIC 1000 is shown in Figure 16. As stated before in the 2009 report, the Noggin 1000-NIC is 30cm long by 15cm wide and 12cm high. The GPR system was mounted in the middle section of the 206L helicopter mount, with its bottom plate protruding outside the tube exterior (Figure 16). The Noggin-NIC 1000 is a unique GPR system which permits operation and control by a computer with no user interaction. This permits the integration of this GPR as an additional sensor into the Video-laser System. The Noggin-NIC 1000 is a very high resolution GPR system, with a center frequency of 1000 MHz and a waveform sampling interval of 0.1 nanoseconds. The Noggin-NIC was configured to collect 500 points per scan with 4 internal stacks. This results in a scan rate of approximately 30 scans per second. When flying at 60-80 knots, the ground sample spacing is approximately one sample per 1.0-1.5m. This fine spacing permits the GPR to collect snow features at the same fine scale as the laser for surface ice roughness.

Figure 16. *Sensors and Software Noggin 1000-NIC GPR System (left) protruding from section of the mounting tube of a 206L helicopter along with laser/video camera (right).*

4.1.2.3 Video-Laser System

The Video-Laser system consists of the laser and video camera (Figure 16). The 3-Alpha laser altimeter, manufactures by Optech Inc., measures the flying height and ice roughness; for a sampling rate of 30 Hz it provides a 1.5m sample spacing at a flying speed of 80 knots. The digital camera used is an Axis 210 by Axis Communications. Images are typically collected at a rate of 2 Hz but the rate is determined by the logging system based on the image field of view, flying height and speed. Each image is 640 by 480 pixels in size, and with a typical flying altitude of 90m each pixel covers approximately an area of 30cm by 30cm in size. The width of the video frame image equals 1.1 times the height of the video camera above the pack ice surface. Since the helicopter flies low (altitude 4 to 6m) when logging GPR and EM data; digital video images are not recorded during these survey lines. Video data were collected on the offshore flight paths at an altitude of approximately 90-100m, while EM and GPR data were collected on the in-bound flight paths. The Video-laser system also collects laser altimeter data for additional surface roughness determination.

4.1.2.4 GPS Sensors

Both the “Ice Pic” and Video-GPR systems have their own GPS sensors so that the systems can be flown independent of each other when either malfunctioned. The GPS units used are Garmin GPS18’s made by Garmin International Inc., Olathe, USA. The GPSs include an embedded receiver and an antenna, and track up to 12 satellites at a time, while providing fast time-to-first-fix, precise navigation updates once per second. The units are designed to withstand rugged operations, are waterproof and require minimal additional components to be supplied by a system integrator. The “Ice Pic” and Video-GPR systems provide the GPSs with a source of power, and a clear view of the GPS satellites is required. Listed position accuracy are given as <15m, 95% of the time.

4.1.3 Survey Description

The helicopter sensors were mounted on the Canadian Coast Guard helicopter on Friday August 12 and tested inside the icebreaker hanger. The EM sled was also unpacked and put together. Saturday morning the ice breaker was at the ice edge but could not find a suitable floe to moor the icebreaker against (foggy). Sunday (11:00 August 14) morning and ice recco was done to find a suitable MY ice floe for the icebreaker to move to and by supper time the icebreaker was finally anchored to an ice floe. A short flight in the evening was done (7-8pm) in marginal flying conditions; it collected EM and some GPR data (FEM 11031-11032; GPR F521 and F005 to F007). The next day, Monday August 15, there were foggy conditions the whole day and no flying was done; all people were on ice but the floe was found not to be suitable for on-ice sampling. (It should be noted that the start of August 14 (00:00UTM) is the start of the survey clock used by the EM computer to assign sample time stamp numbers in 1/1000th of a

seconds. So the morning ice recco was started at 11:00 local time or 17:00 UTM which is equal to 62064 seconds time stamp on the survey EM clock.)

Tuesday 16 August, a recco flight was again done to find a better MY ice floe and during the ice recco flight ice beacons (09:00-09:30) were placed on three ice island fragments south of the MY ice floe B1.S1 (Figure 17). Data were collected with the EM and Video of the instrumented floe B1.S1 on first flight and of the floe north of the ship on the second flight. During the last flight soft-landing samples were taken over the marked NRC and Sled lines.

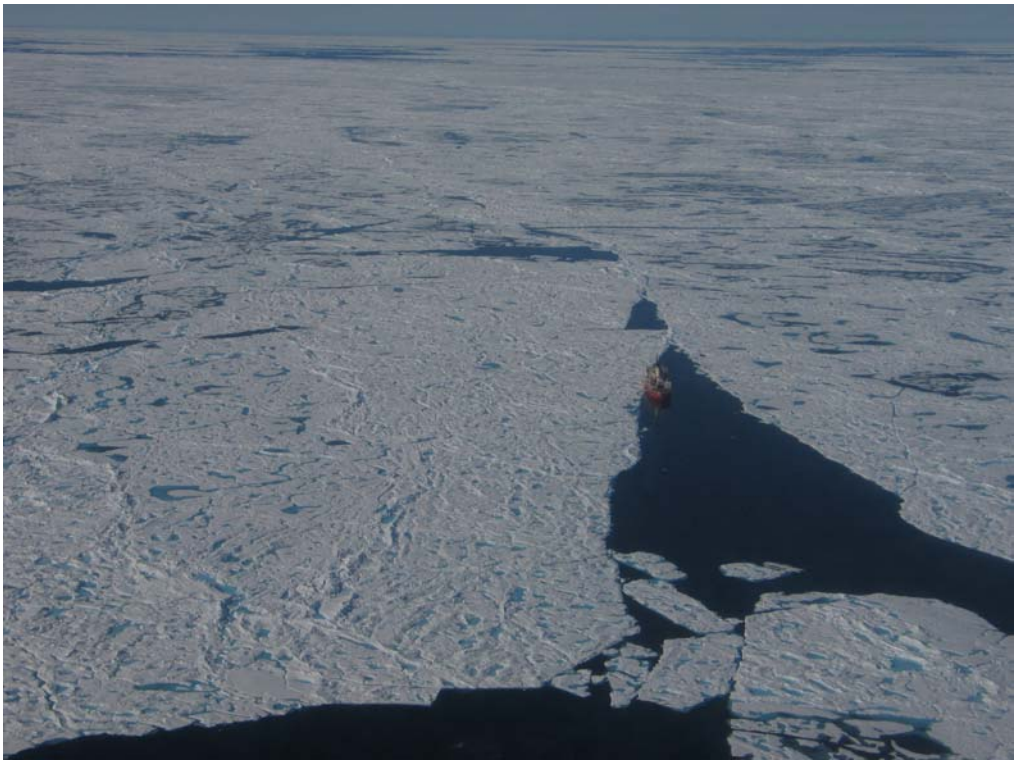

Figure 17. *Picture of B1.S1 site with the sample on-ice instrumentation floe on the left of the ship and the large sampled floe for regional ice distributions on the right.*

After completion of Floe S1 the ship moved overnight to the second MY ice B2.S2. Three sets of EM data lines were collected over the floe B1.S2 in late afternoon when weather cleared (15:00–17:00). As was the case for B1, the floe B2 was the thickest part of any of the floes in the area as can be seen from the picture in Figure 18. The ship was anchored to floe B1.S2 on the SW side and pointing to the South (158), this is opposite of the direction the ship was pointed along the floe at station B1.S1.

On Thursday 18 August the fog did not clear so no low flying with the EM system were done; we only sampled the marked locations on floe B1.S2 where ice thickness data was collected by NRC personnel and by the EM sled.

Figure 18. *Picture of B1.S2 site with people on the ice right (west) of the ship.*

On-ice sampling was stopped on Friday August 19 due to a mishap with people leaving the ship via the "gage", only helicopter and skippy boat sampling is continuing. EM and Video and U. Manitoba camera were used to sample along a N-S grid was flown where an SAR satellite overpass will occur late afternoon (red star area where a old MY ice foe is present 200mx200m. (Regional area now called B1.S3).

On August 20, the icebreaker moved back to B1.S0 where the ice fragments were found. The area is called B1.S4 and is oriented north of ice island fragment. Flew N-S lines video and EM using the beacons fragments as SE and SW (Ship and start of Video) corners. Very solid floe from these corners to North, video lines twice as long as EM lines. Ship moved North where the Red-Star pattern was flown. (13:45) A second N-S lines video and EM was flown from SW and SE (Ship and start of Video) corners (B1-S5). Very solid floe from these corners to North, video lines twice as long as EM lines. The criss-cross over skippy boat and EM final line north. Continue EM line north to get Video ready and flying back to ship very high 3000ft.

Sunday 21 and Monday 22. The ship moved out of the ice to avoid a storm that brought 30-40knts of Southeasterly to Easterly winds. Wave period round 6-7sec, wave amplitude up to 2m and wave length 30-40m. Compared to the summer

2009 when wave periods of 13sec were observed; these waves did not have the long wave lengths to break up the MY ice floes.

Table 7 below lists the EM, GPR and video files collected during the IOL ice survey of August 2011. Where no GPR files were collected the UM camera collected high resolution video data.

date	area	FEM File	GPR files	Video files
Aug 14	B1S0 test floe	11030	Ice recco	
Aug 14	B1-S1 local	11031-11032	227F521	226F005-227F007
Aug 15	B1-S1 local	11034-11035	228F522-228F524	228F008-228F015
Aug 16	B1-S1 region	11036-11037	228F525-228F528	228F016-228F019
Aug 17	B1-S2 local	11038-11039	229F529-229F536	229F020-229F021
Aug 18	B1-S2 local	11040	------	230F022-230F025
Aug 19	B1-S3 local 1	11042-11043	UM Camera	231F026-231F031
Aug 20	B1-S4 local 2	11044-11046	UM Camera	231F032-232F057

Table 8 below lists just the EM collected flight lines; Video lines covered about twice the length along the EM lines at 300-400feet on return flight grid pattern.

Site	Day/time	Sled-NRC lines	Local floe lines	Regional floe lines
B1-S1	Aug 14	------	8x2km lines	8 x2km lines
B1-S1	Aug 16	4 lines ½ km	3x2km lines	4x15km lines
B1-S1	Aug 16	2 lines ½ km	Soft-landing	-----
B1-S2	Aug 17-18	3 lines ½ km	17x2km lines	-----
B1-S2	Aug 18	3 lines ½ km	Soft landing	-----
B1-S2	Aug 19	B1-S2	SAR overpass	4x10km lines
B1-S3	Aug 20	Old B1-S0		6x10km lines
B1-S4	Aug 20	Old B1-S1	Near SAR area	5x10km lines

4.1.4 Data Samples (Ice floes B1.S1 and B1.S2)

4.1.4.1 Ice Thickness profiles from site B1.S1

Ice thickness profiles and video data were collected with helicopter-borne sensors as discussed above. The data string of each data set includes the Lat/Long/time from the GPS sensors. Since the data is collected at a rate of 10Hz, the sample number used in the display plots such as shown below in figure 19 is actually the time in 1/10th seconds starting with the start of the file number (FEM110XX); the actual data is stored as 1/1000th of a second using the computer logging clock with stated at zero at 00:00 UTM time of the first day of the survey August 14 and are referenced to that starting time throughout the survey.

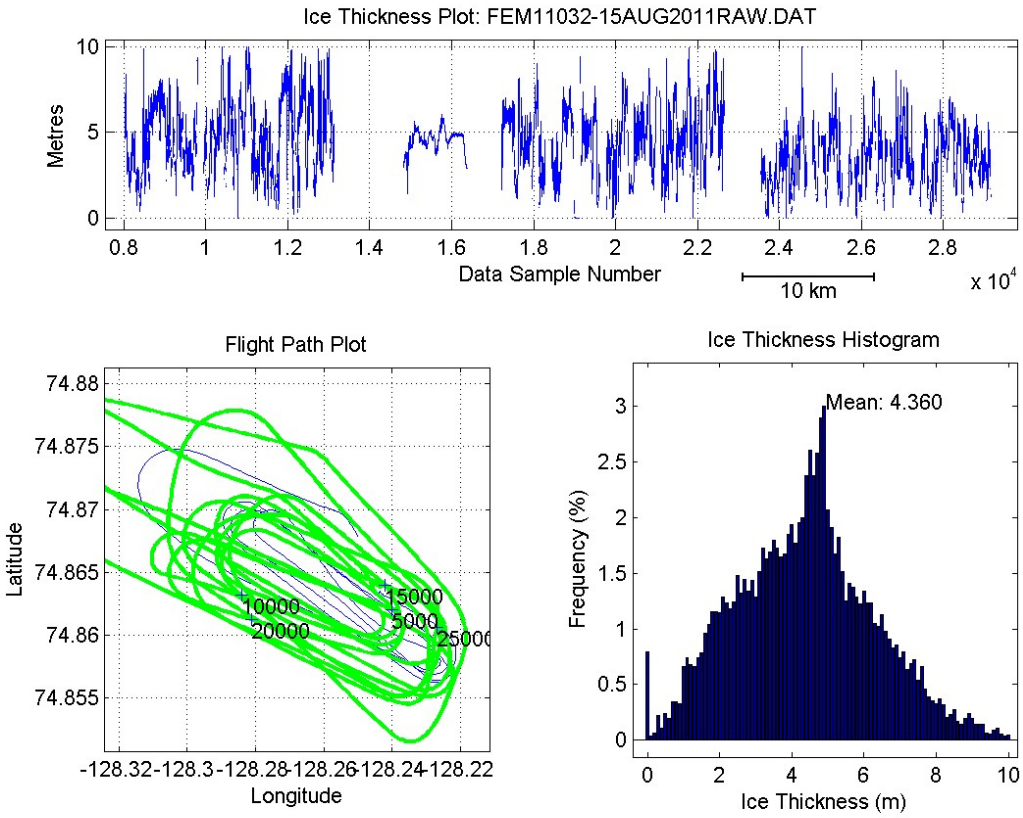

Figure 19. *Thickness profiles (9) across the floe S1 (top) and the flight pattern and ice thickness histogram of the 9 passes over the (1.5km) floe.*

Figure 19 shows 9 passes over the 1.5km B1.S1 thick MY ice floe. The 9 line profiles are shown in the top panel in 3 groups and the flight pattern and summation of the observed ice thickness are shown in the histogram in the two bottom panels. All EM flight passes and Video passes were flown from South to North with return tracks (no sampling) from North to South; this flight pattern makes a race track pattern that looks like a spaghetti plot. The green tracks

represent the tracks along which the ice thickness data was collected and the thinner blue tracks are the tracks when the Video data was collected. The mean ice thickness of the MY ice floe B1.S1 was found to be 4.3m and had a modal thickness of ~5.0m; this modal thickness represents the most frequent observed ice thickness for the S1 floe. The histogram shows that the floe had ridges with thicknesses reaching up to 8 and 10m thick as can be seen in the foreground of the picture in Figure 18.

Several additional passes were made over the line where ice thicknesses were measured by NRC personnel through ice holes and where ice thicknesses were collected with the EM Sled by Klaus Hochheim. Figure 20 made on-board the icebreaker shows four short sections of ice thickness profile of B1.S1 flown over the EM sled-NRC marked line from NW to SE. Shown profiles cover only 400m of the 2km line. The soft-landing EM data of (bottom panel) only represents the first nine bags and thus half the line.

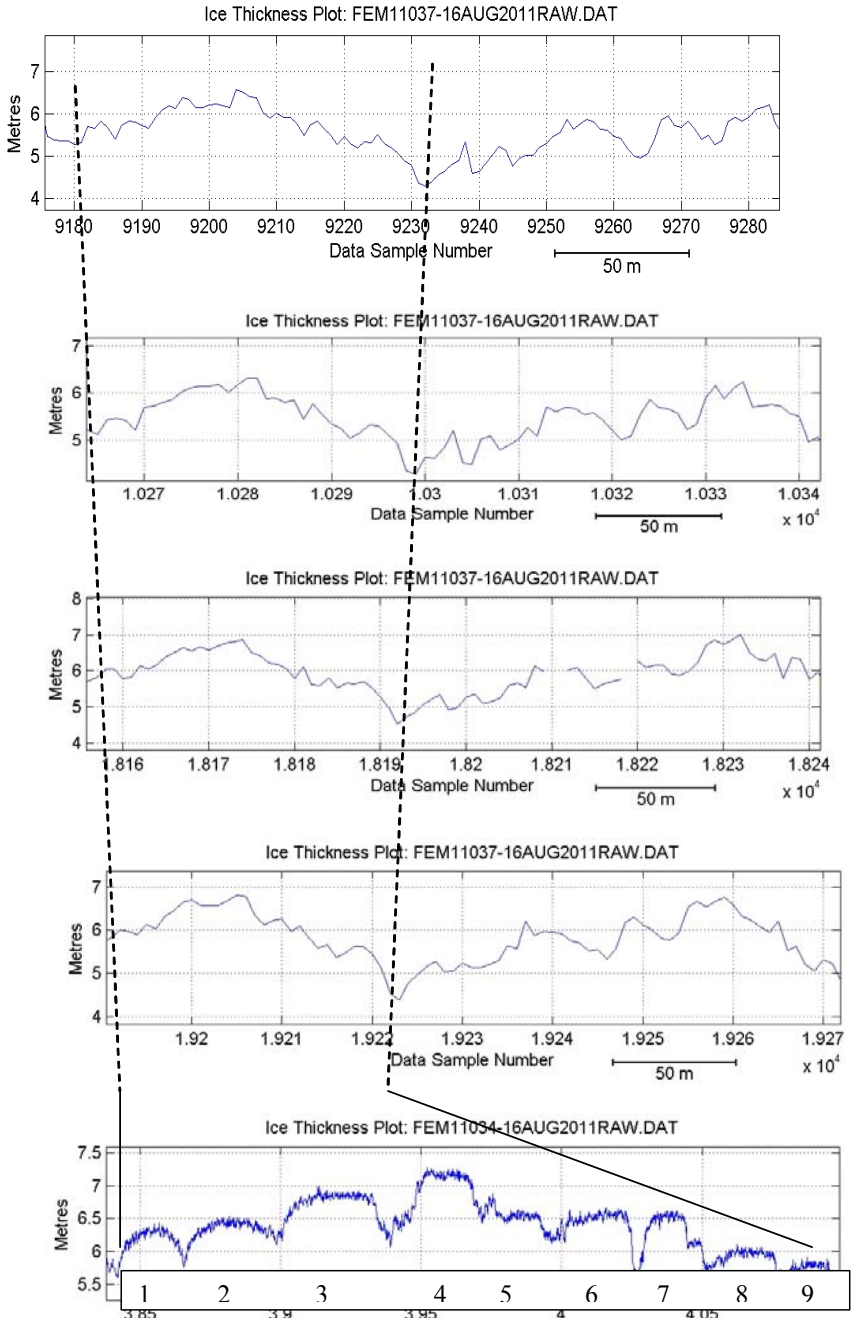

Figure 20. *Ice thickness profiles covering the EM sled-NRC line of floe B1.S1. The top 4 profiles are from flight passes and the bottom profile is from soft-landing at the first nine drill hole locations.*

Figure 20 shows well the repeatability of the separate line data even though the lines may not be perfect aligned along the on-ice markers nor will the speed and height of the sensor and helicopter be the same for each line. The bottom line data of the figure show the soft-landing ice thickness of just the northern nine marked locations along the line. All profiles are based on time series data, so the flat stops on the soft-landing profiles represent places were the helicopter soft-

landed and collected the data. Gear and personnel along the marked line stopped the completion of the soft-landing profile. Bag four shows a flat stop in the time series where the helicopter soft landed and read a thickness of just over 7m, it is the thickest point in all the flight profiles (at 9205 sample number of the first profile). Data is stored in Lat/long/time format derived from the sensors GPS units. However since the floe was drifting at around 150m/hr, the EM and Video data over the instrumented floes was converted by post-processing to xy floe co-ordinates to remove the drift of the floe.

4.1.4.2 Ice Thickness profiles from site B1.S2

Floe B1.S2 was located northwest of floe B1.S1 as shown in the SAR image Figure 14. As with the first floe, the section of the floe selected to do on-ice sampling was again the thickest part of the floe as can be seen in the picture (Figure 18). Three groups off passes were done over the floe; each pass was about 1.5 to 2.0km long and contained the thicker part of the flow where on-ice sampling was being done. One group of five ice thickness profiles from the floe B2 is shown in Figure 21.

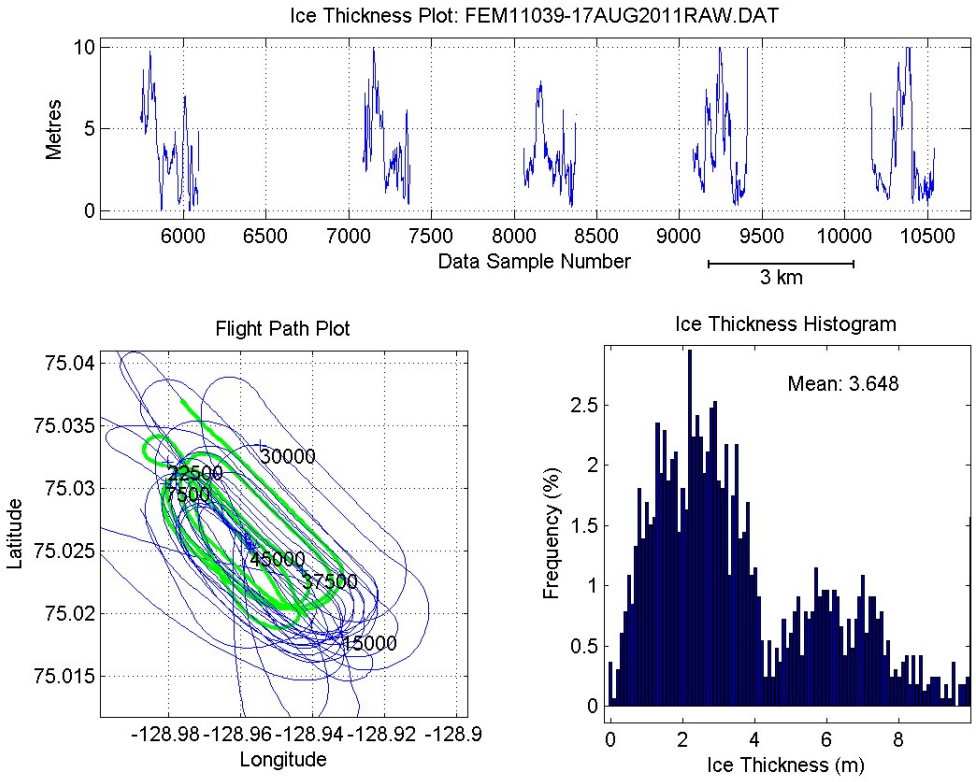

Figure 21. *Thickness profiles (5) across the floe B1.S2 top) and the flight pattern and ice thickness histogram of the 5 passes over the (1.5km) floe.*

Figure 21 shows five passes over the B1.S2 thick MY ice floe. The five-line profiles are shown in the top panel and is from the first of three groups of line profiles from B1.S2. The flight pattern and summation of the observed ice

thickness are shown in the histogram in the two bottom panels. The three groups of profiles show the same pattern: the on-ice sampling floe was the thickest part of the floe having thicknesses between 5 and 8m as seen in the ice thickness histogram. Attached to this thick floe was a section much thinner and has thickness values between 1 and 4m. The ice thickness histogram (Figure 9) shows a mixture off these ice thicknesses having a mean of 3.6m that represent neither part of the combined floe. The histogram has thickness peaks at 6.0 and 7.5m representing the on-ice sampling floe and peaks at 1.5 and 2.5m for the thinner attached floe. Ice thicknesses reach up to 8-10m in ridges; one such ridge separated the thicker part of the floe from the thinner part as can be seen in the floe's picture (Figure 18).

Several additional passes (3) were made over the line parallel to the icebreaker where ice thicknesses were measured by NRC personnel through ice holes and where ice thicknesses were collected with the EM Sled by Klaus Hochheim.

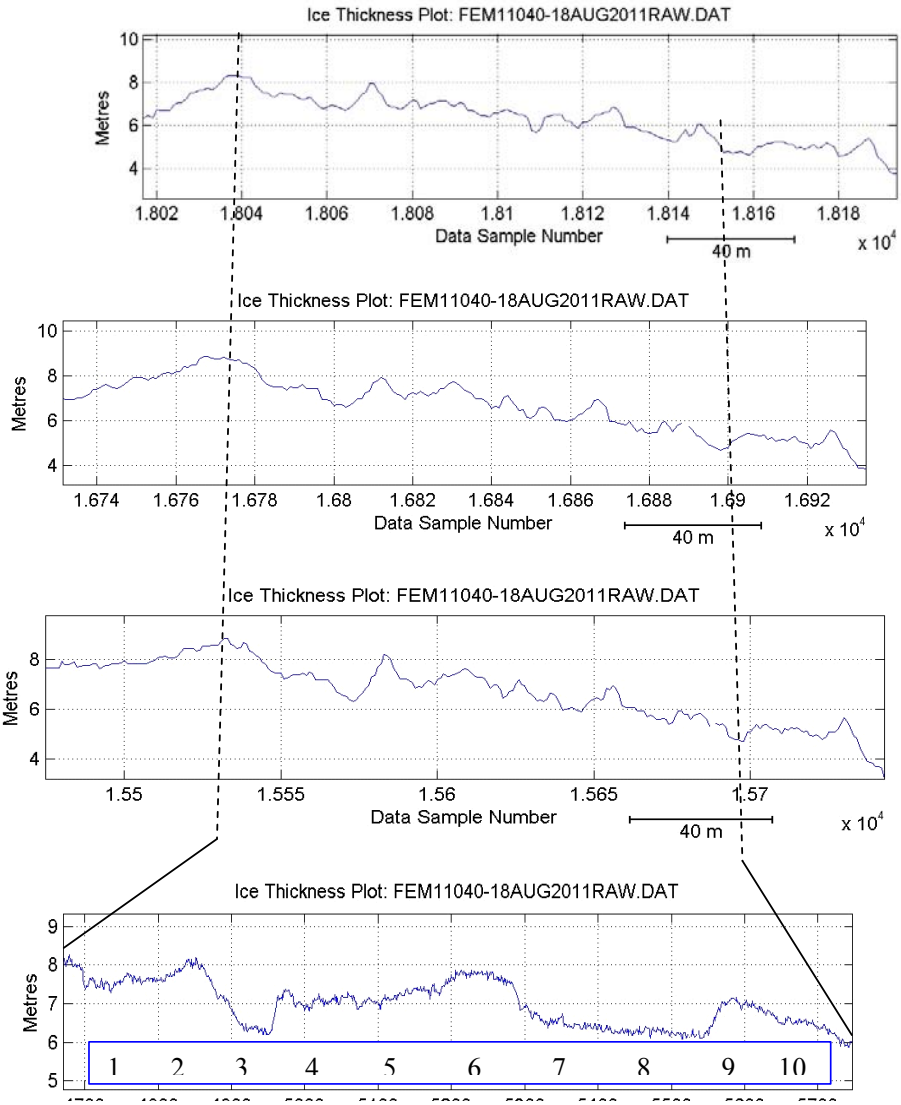

Figure 22. *Ice thickness profiles covering the EM sled-NRC line of floe B1.S1. The top 3 profiles are from flight passes and the bottom profile is from soft-landing at the 10 drill hole locations along the line parallel to the icebreaker.*

Figure 22 was made on-board the icebreaker and shows three short sections of ice thickness profile of B1.S2 flown over the EM sled-NRC marked line from NW to SE. Shown profiles cover only 150m of the 2km line. The soft-landing EM data of (bottom panel) represents the ten locations along the line parallel to the icebreaker. Other lines perpendicular to the icebreaker could not the flown due to the present of the icebreaker. Post-processing has concentrated so far on the B1.S2 and has removed the ice floe drift from the Lat/long/time format and transferred it X-Y coordinates of the floe. This allows for better comparison of the Helicopter EM data with the EM sled data and the NRC ice hole data (Figure 23) and using the video data to make floe specific mosaics overlain with EM data.

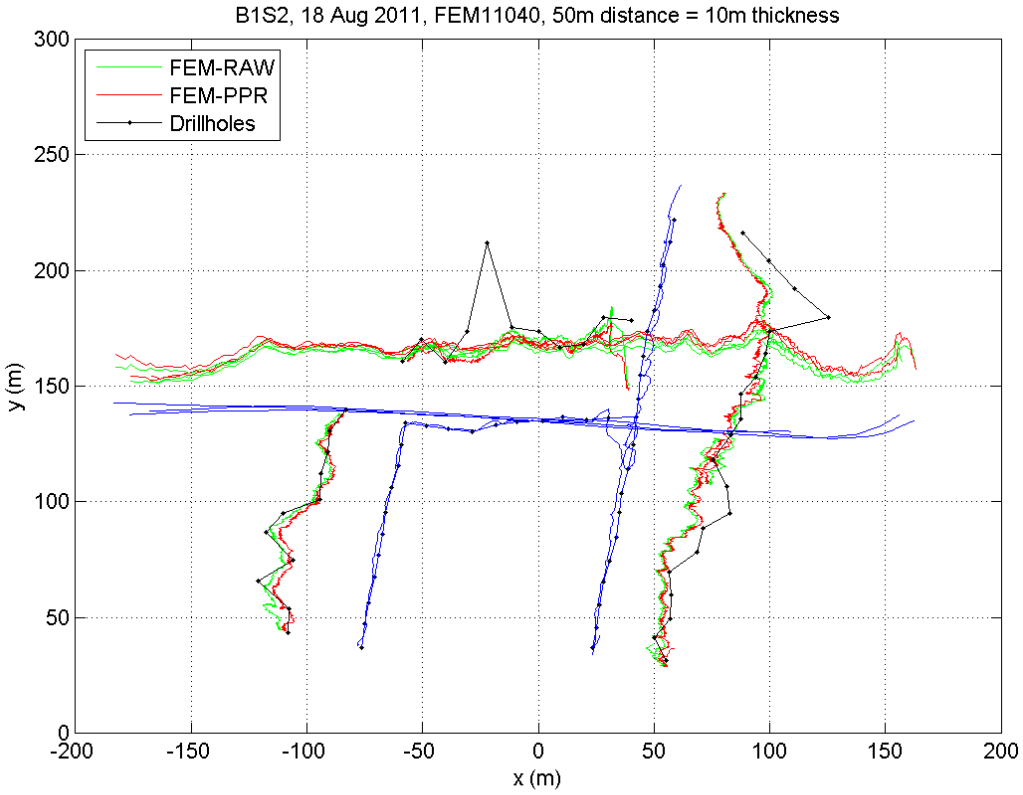

Figure 23. *Ice thicknesses along marked ice hole lines (black dots along blue lines) of floe B1.S2 with the icebreaker located along the y-axis between x= -50m and x= +50m; the pattern make a shape of a chair. The 3 EM fight passes are also shown as blue lines and run parallel to the ice breaker (seat of the chair). The ice thicknesses EM red and green) and NRC drill hole (black dots along black lines) are plotted relative to these blue lines as 10m for 50m xy distances.*

The OIL survey was the first time that the EM helicopter and EM sled data from thick MY ice could be compared to ice hole data. The EM helicopter and sled data has been extensively compared to thinner first year ice data but not the thicker MY ice data because to acquire this ice hole data takes a lot of effort and time that can not be done during helicopter surveys due to the high cost of helicopter logistic costs. In addition to the present surveys have been mostly done in coastal regions of the Mackenzie delta and Labrador Sea where no MY ice is present. The OIL survey thus provided this unique opportunity to compare the two MY ice data sets and the results of the B1.S2 floe is shown in Figure 11. The footprint of the EM data over which the EM data is averaged is about three times the distance of the sensor to the surface of the ocean water. So for 5m ice and flying at 5m altitude the foot print is about 30m thus actually covering three ice hole data locations separated by 10m. The EM will thus sense the ocean water at 5m even though some parts of the ice floe within the footprint extend to deeper depths and those could be measured through the ice holes. The EM observations thus provide an ice volume thickness over a large foot print and ignore some of the deeper high salinity ice keels. The ice hole data provide high detailed site specific ice thicknesses but do not provide a average thickness around drill hole nor can it provide an regional perspective of the overall pack ice conditions. Each data set provides different information of the pack ice conditions. The data in Figure 23 shows that overall the variability of the EM and drill hole data shows the same variability but that as expected the drill hole data do catch some of the thicker part of the ice floe.

The soft landing data from both floes are compared to the NRC drill hole data in Figure 24. As expected the drill hole data do show large ice thicknesses for the thicker pack ice (>8m) but do compare well in the 5-7m range that were the high range thicknesses seen in the large regional data surveys away from the B1.S1 and B1.S2 floes. The data from B1.S1 had a much narrower ice thickness range as compared to the B1.S2 floe.

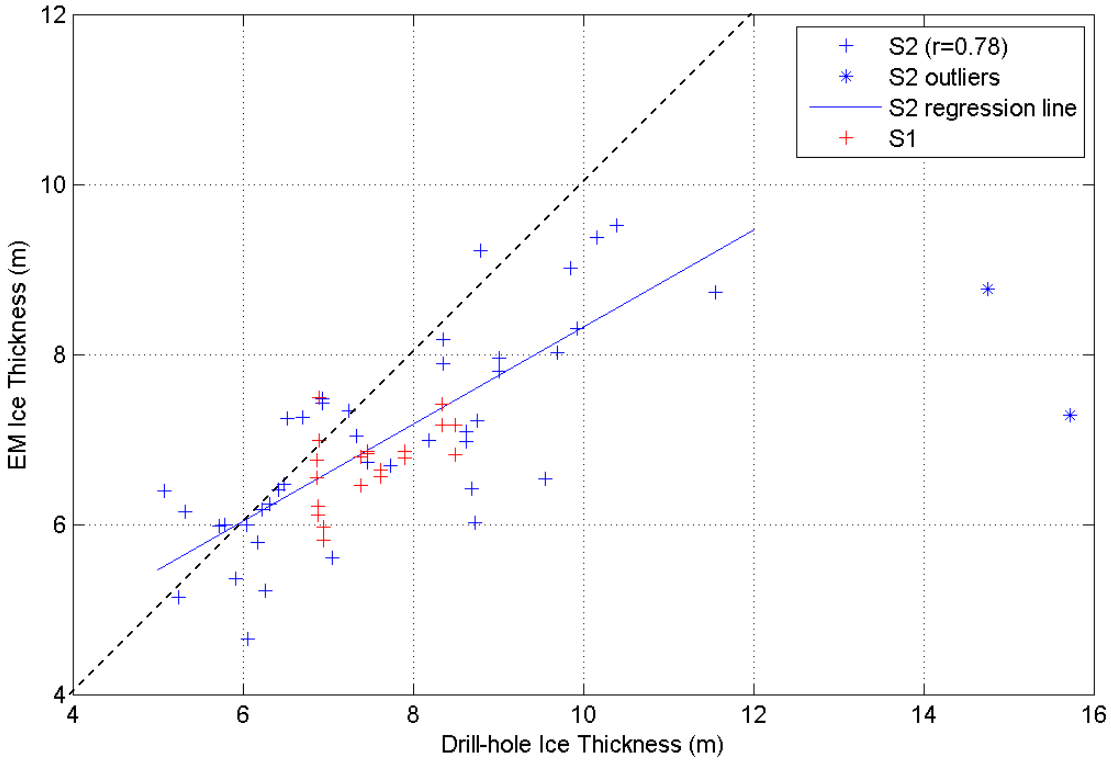

Figure 24. *Comparison the site specific EM soft-landing and NRC drill hole data of the B1.S1 and B1.S2. The S1 floe data are in red and the S2 floe data are in blue.*

4.1.4.3 Video data

The video data has been used to make mosaics (e.g. Figure 25 & 26) to enhance the information obtained by the EM sensor (snow+ice thickness) and the GPR sensor (snow depth). Here we show first two mosaics of the B1.S2 that captured the icebreaker and people on the ice. These can be put together as well and the data of the EM over flights can be overlain once the video frames Lat-Long coordinates have also be transferred to the floe coordinates.

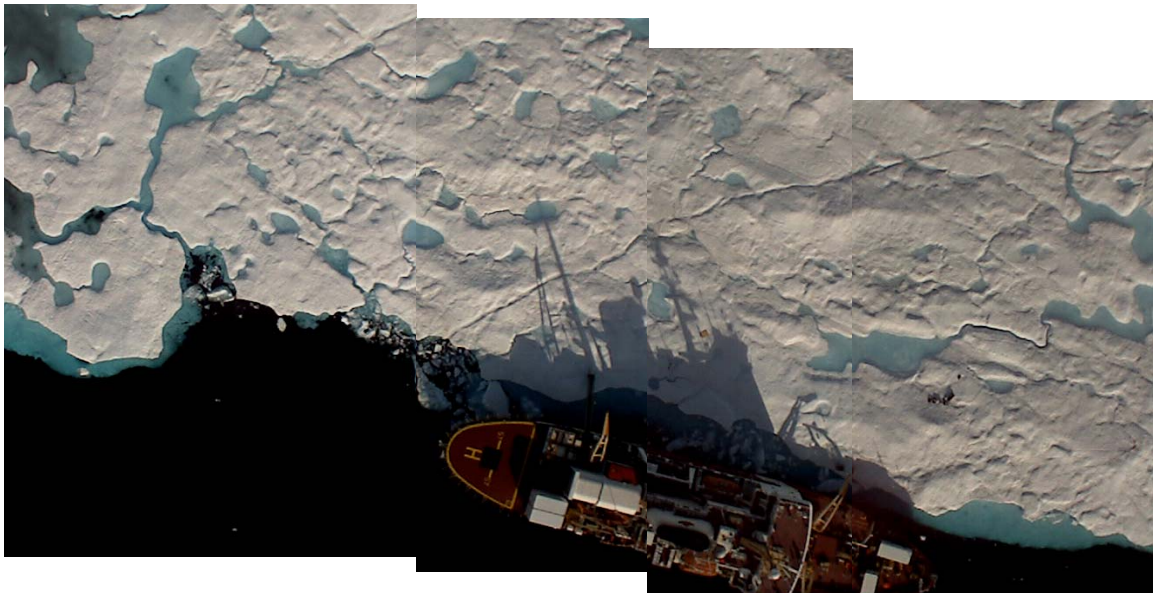

Figure 25. *Mosaic constructed of four overlapping video frames showing the Amundsen anchored to floe B1.S2. Video frame with is 100m.*

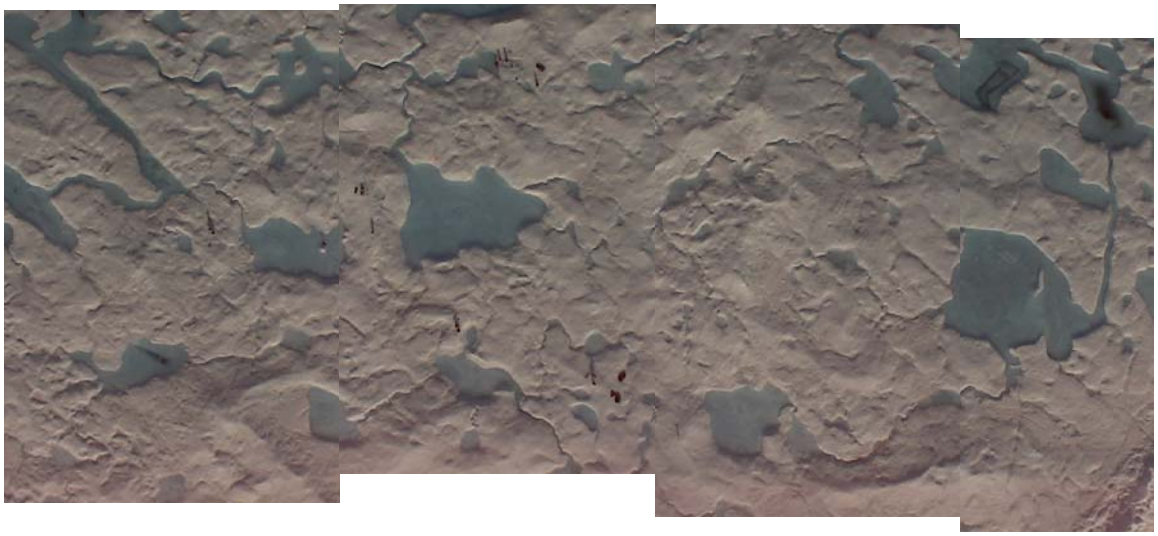

Figure 26. *Mosaic constructed of four overlapping video frames showing people on the ice on the floe B1.S2. Video frame width is 100m.*

The resulting figure is shown below (Figure 27). It shows the EM helicopter flight and soft-landing data and the drill hole data. It shows that the helicopter flight passed over a melt pond while the ice hole and sled track detoured just below the melt pond. It is very hard to lay out an 100m straight line without running into melt ponds.

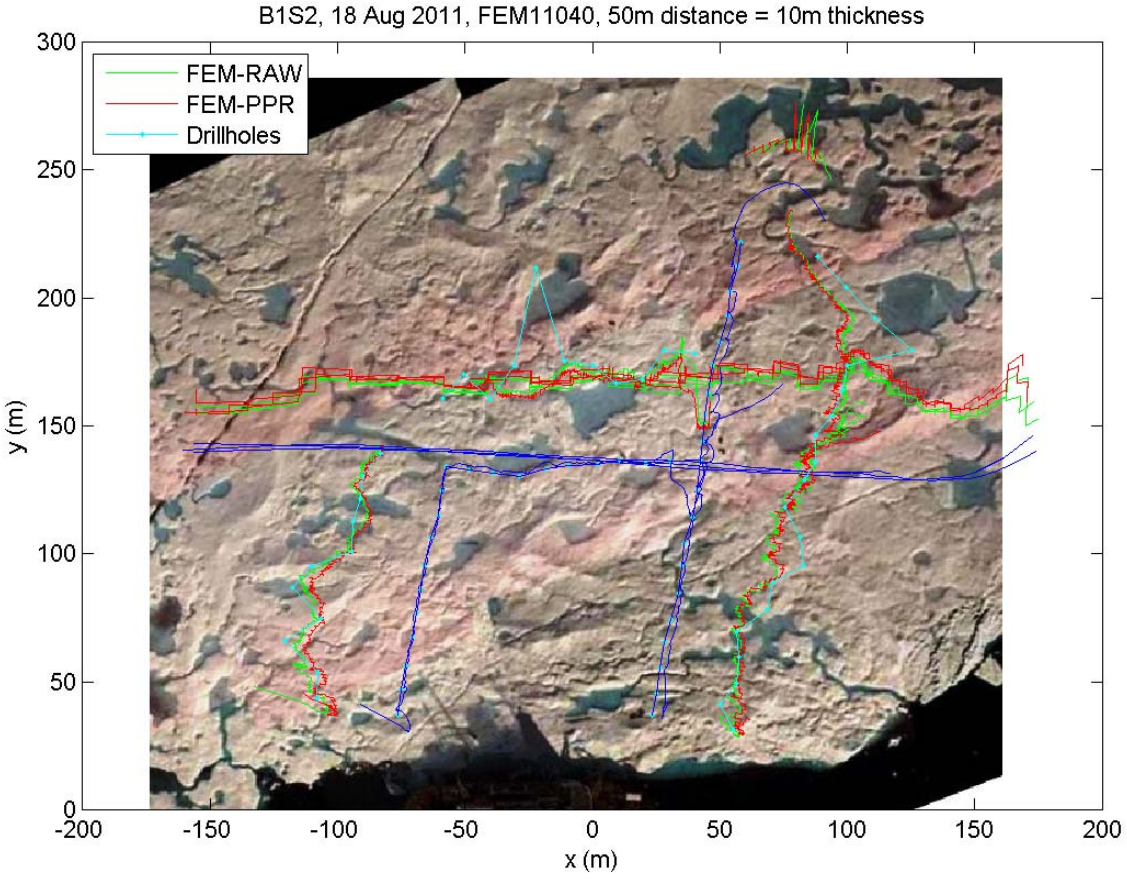

Figure 27. *Mosaic of the MY B1.S2 ice floe overlain with the helicopter EM flight and soft-landing data.*

4.1.5 Data Samples (Regional sampling)

When the helicopter data sampling (video and ice thickness) of the MY ice floes had been completed, regional ice surveys were done along parallel 10-15km lines. The large floe to the North of the ice breaker and MY ice floe B1.S1 was sampled and shown below in Figure 16. The histogram shows that this part of the pack ice consisted of 40% of ice thicker than 4m; while remaining the pack ice (60%) including melt pond areas was less than 4m thick. As seen in the SAR image (Figure 14), the floe appears to be very compact and the floe component where the on-ice sampling was done (Figure 17) was one of the most solid and thicker parts of the floe. But as seen in the picture, other areas of the floe consisted of thinner areas and contained a lot of melt ponds that were actually bottomless.

Four parallel EM-GPR lines were flown in the NW direction and four video lines were flown back at 100m altitude in the SW direction. The main worry with this data and any summer EM data are the presence of melt ponds with the large floe itself. These melt ponds are protected from wind waves and there associated mixing. It appears the melt water within the melt ponds are not well mixed with the under-laying ocean waters. They thus appear as ice thickness of 2-2.5m with the ice floe and this affect disappears at the edges of the flow were the wave mixing is present. The MY ice away from the melt ponds consistently showed values between 5 and 10m. Further analysis is ongoing to see if the fraction of melt ponds along each flight line can be inferred from laser brightness or GPR data.

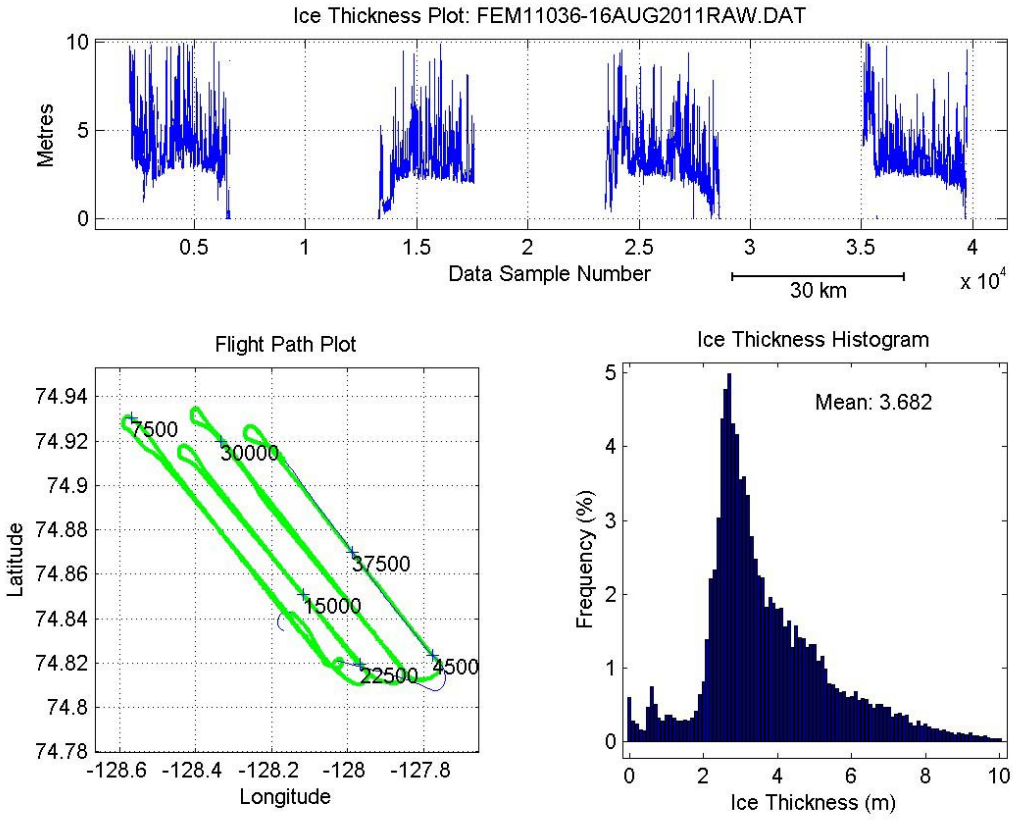

Figure 28. *Regional ice thickness survey over the large ice floe north of Floe B1.S1 the CCGS Amundsen was anchored to.*

The Video data can also be used by an algorithm that uses pattern recognition in grey scale to make mosaics. It provides rapid details on the pack ice conditions frown over by the video and is used to determine floe and lead distributions. For the most north-eastern return flight path of the grid shown in Figure 16, a short mosaic is shown in Figure 29. The mosaic shows the distribution and presence of melt ponds that typical occurred throughout the area of the pack ice west of Banks Island which the helicopter ice survey flew over. A mixture of melt pond with and without bottoms within the pack ice where we assume the vertical mixing of the melt water is limited. Near the edges of the consolidated floes (~1/2 km), wave mixing did appear to mix the melt water into the ocean surface layer as seen by EM Line profiles (Figure 30).

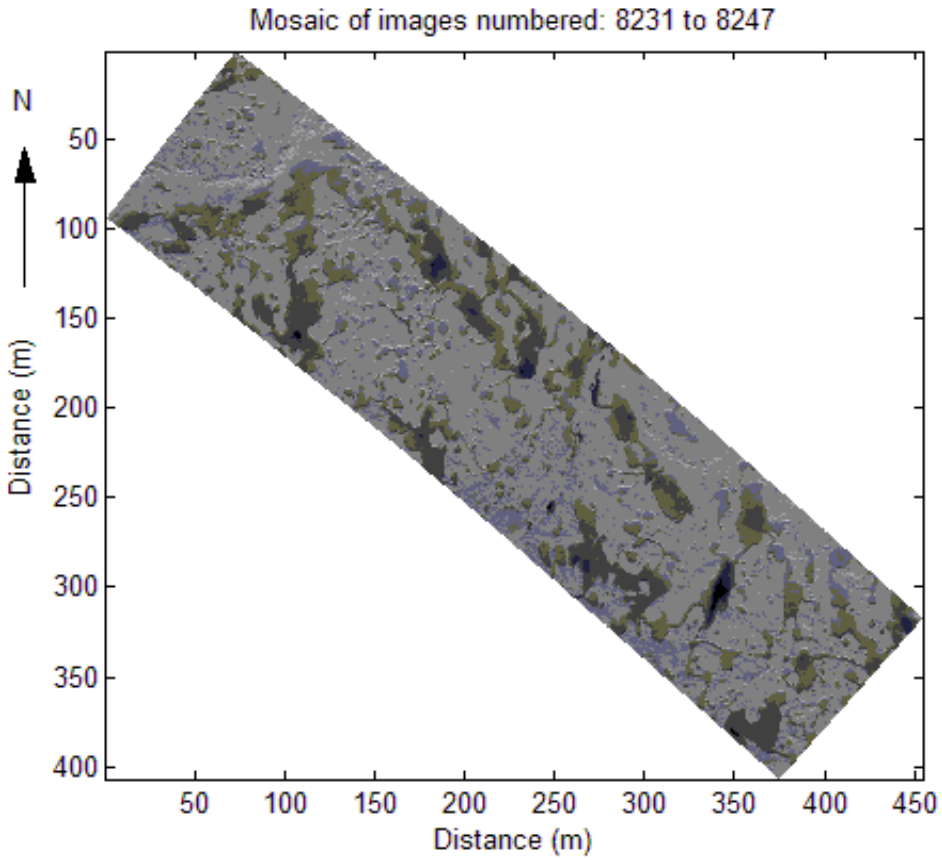

Figure 29. *Short mosaic along the return flight of the most North-Eastern flight line shown in Figure 16 covering the large MY floe the north of floe B1.S1.*

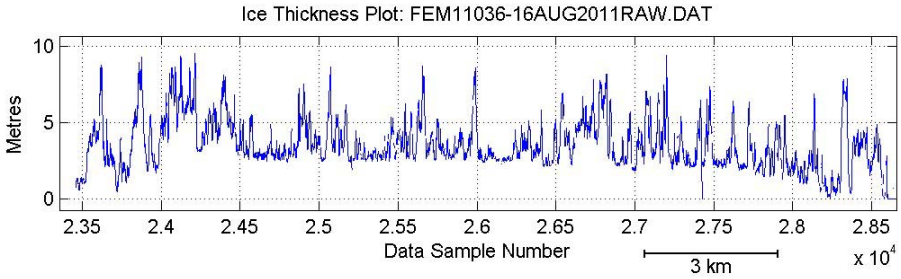

Figure 30. *Single EM profile the 3th of the four lines shown in Figure 16 covering the large MY floe the north of floe B1.S1.*

After the on-ice surveys were stopped, there was more time to do regional surveys when favourable weather conditions did occur. Three additional regional survey ice thickness plots are shown in Figures 31, 33 and 34, along with short video mosaics from these lines in Figure 32.

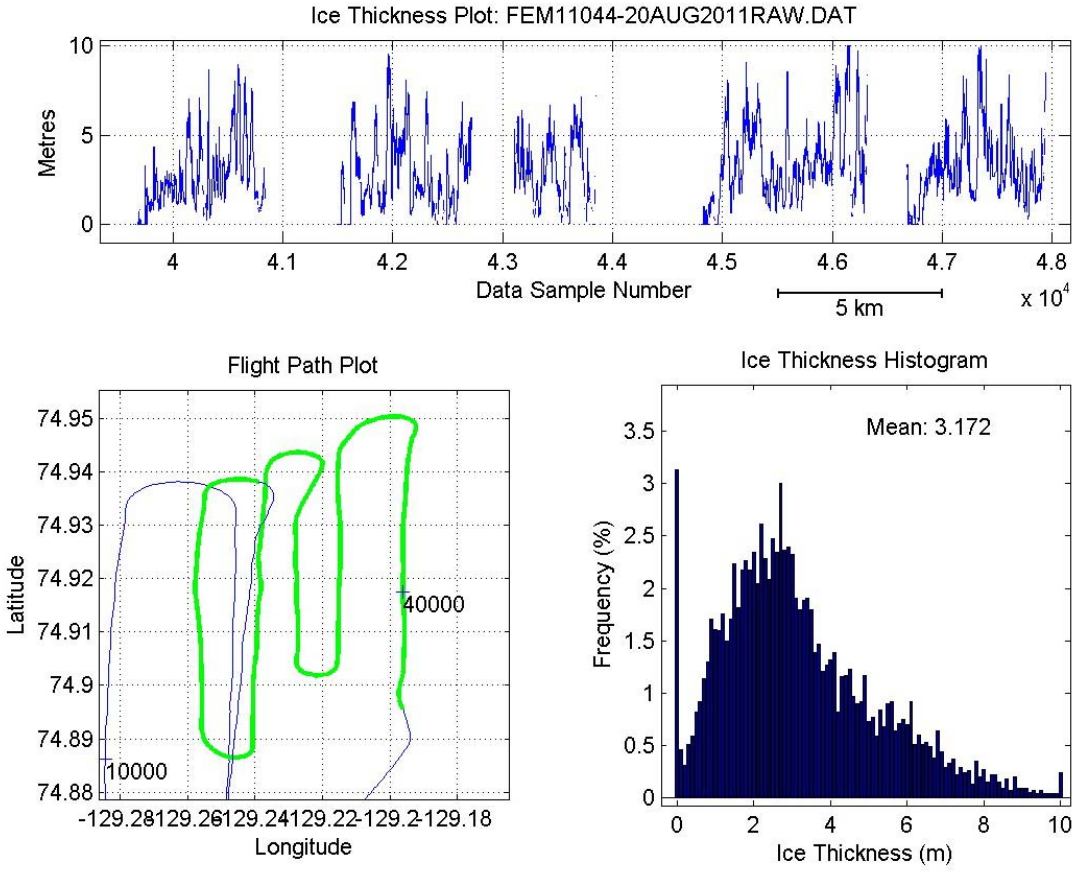

Figure 31. *Regional ice thickness survey (FEM 11044) of August 20. Ice thicker than 4m makes up only 20% of the area surveyed, yet some ridges do reach 10m.*

Figure 32. *Three video mosaics of the pack ice properties found alone the three regional ice surveys done on August 20 and whose ice thickness profiles are shown in Figure 19 (first video frame 23110), Figure 21 (first video frame 26349) and Figure 22 (first video frame 31391).*

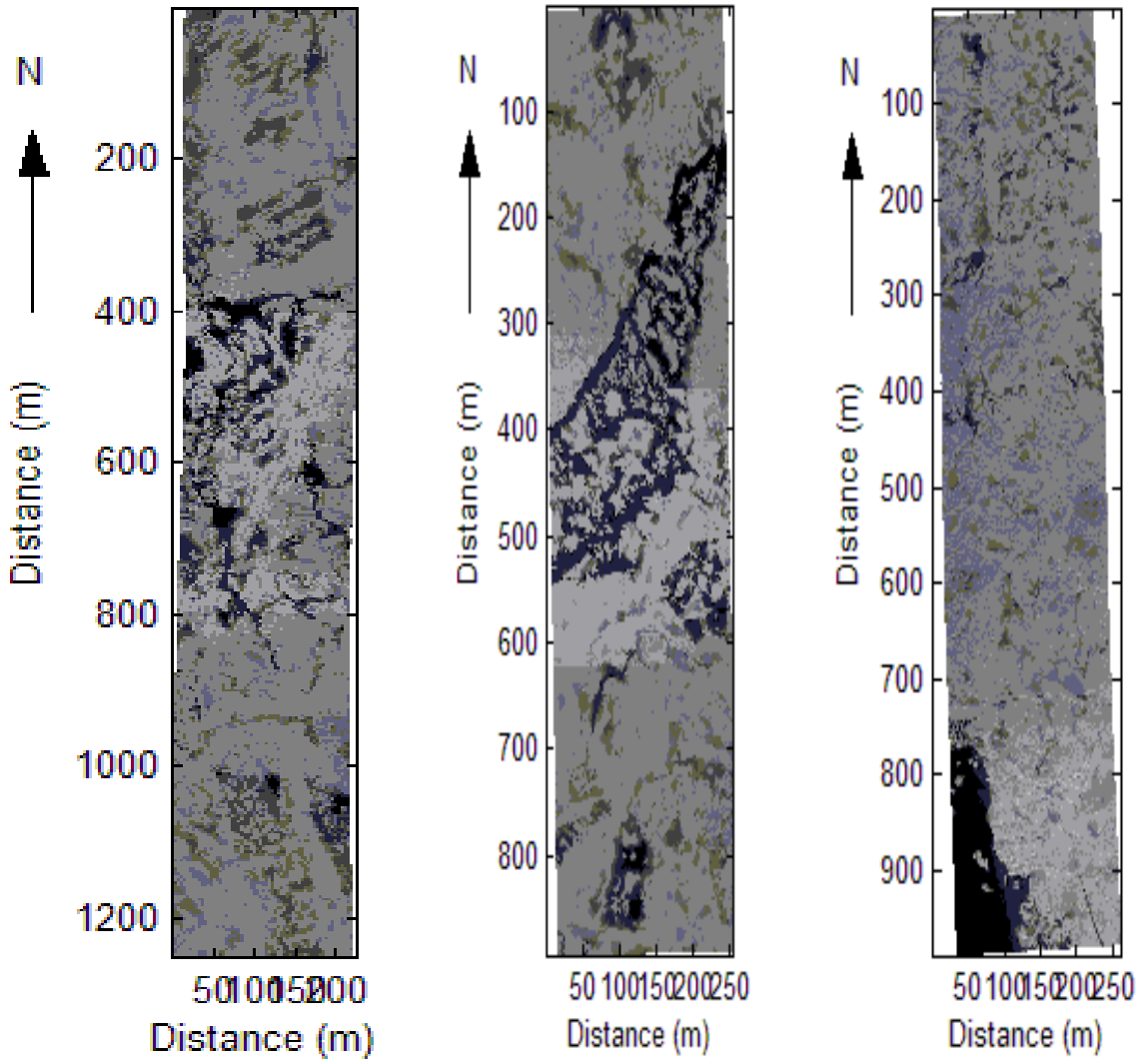

Mosaic F037-23110
EM flight FEM11044

Mosaic F043-26949
EM flight FEM11045

Mosaic F049-31391
EM flight FEM11046

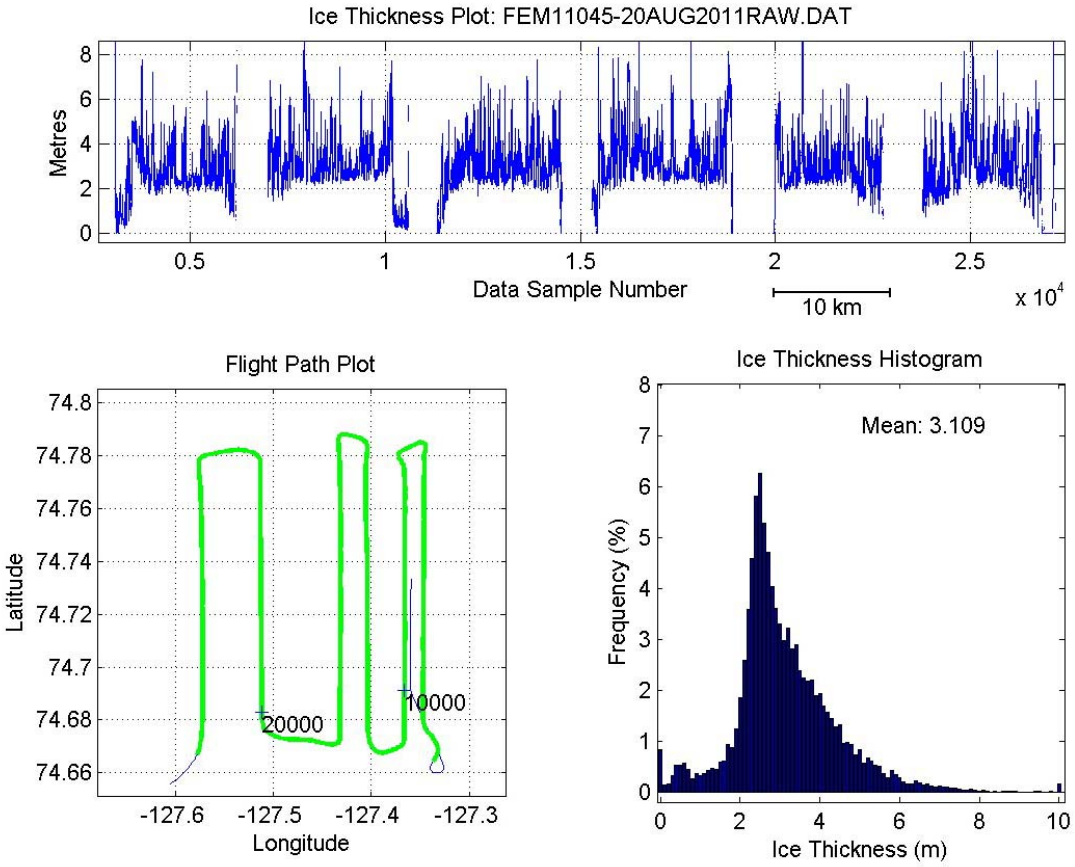

Figure 33. *Regional ice thickness survey (FEM11045) of August 20. Ice thicker than 4m makes up only 20% of the area surveyed, yet some ridges are up to 10m thick.*

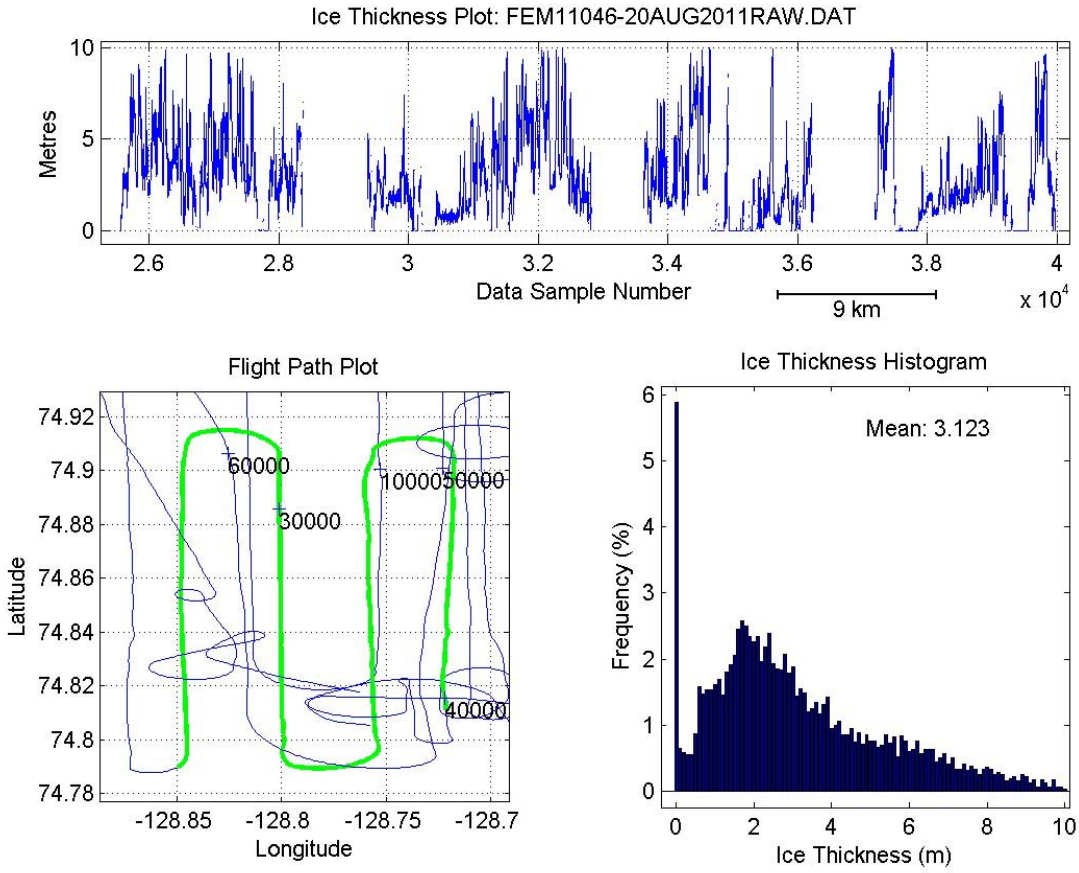

Figure 34, *Regional ice thickness survey (FEM11046) of August 20. Ice thicknesses greater than 4m occurred 40% over the area surveyed.*

4.1.6 Conclusions

Analysis of this data set will continue. So far most effort has been made to look at the MY ice floe B1.S2 to bring together the EM flight and soft-landing data and compare those to the NRC ice hole data set. This was the first time such a drill hole data set was available from thick MY ice and where the EM helicopter and EM sled could sample along the same lines. The comparison of the data sets from both the B1.S1 and B1.S2 MY ice floes indicate that the ice thickness properties represented by these two different observation technologies agree very closely for the average floe thickness of 5-7m where as the thicker parts the floe (>8m) the large foot print averaging and the high saline keels that caused an underestimation of the EM thicknesses as compared to those directly measured through ice holes. The sampled floes were the thickest floes in the region as the four regional surveys indicate that floes thicker than 4m occurred only between 20-40% of the time. Most of the pack ice 60-80% consisted of ice (including melt ponds) thinner than 4m.

The EM sled and EM helicopter sensor can also provide the bulk conductivity of the ice layer the EM signal travels through. Since the ice strength is related to the amount of brine pockets, the relative bulk ice conductivity can indicate the difference in ice strength between parts of the pack ice. Such an variability in ice conductivity was observed between the two MY ice floes B1.S1 and B1.S2 as shown in the EM sled data shown in Figures.35 and 36. The

conductivity of floe B1.S1 was larger than the conductivity of floe B1.S2, further analysis and comparison with NRC ice strength data is required.

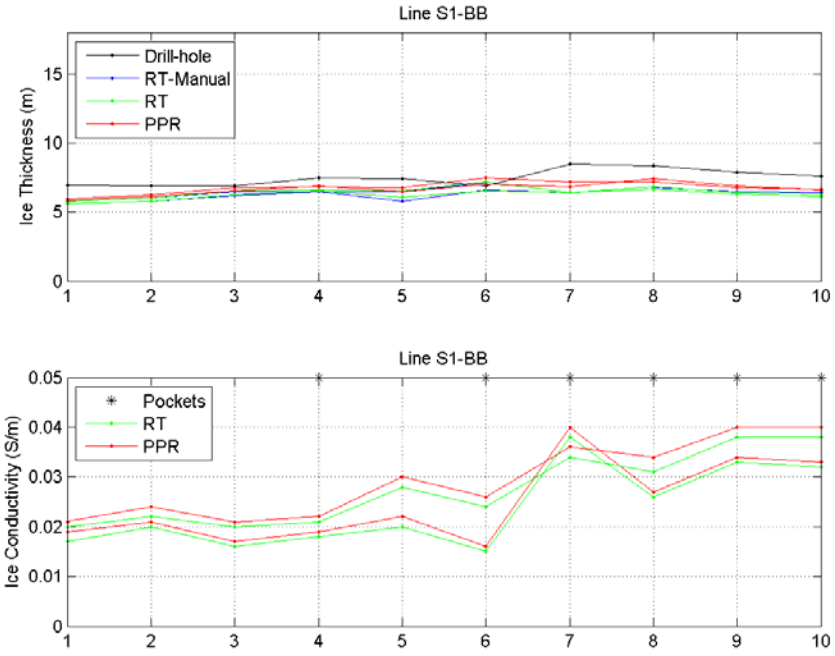

Figure 35. *Comparison of EM sled and NRC ice hole data (top) and ice conductivity (bottom) from MY ice floe B1.S1.*

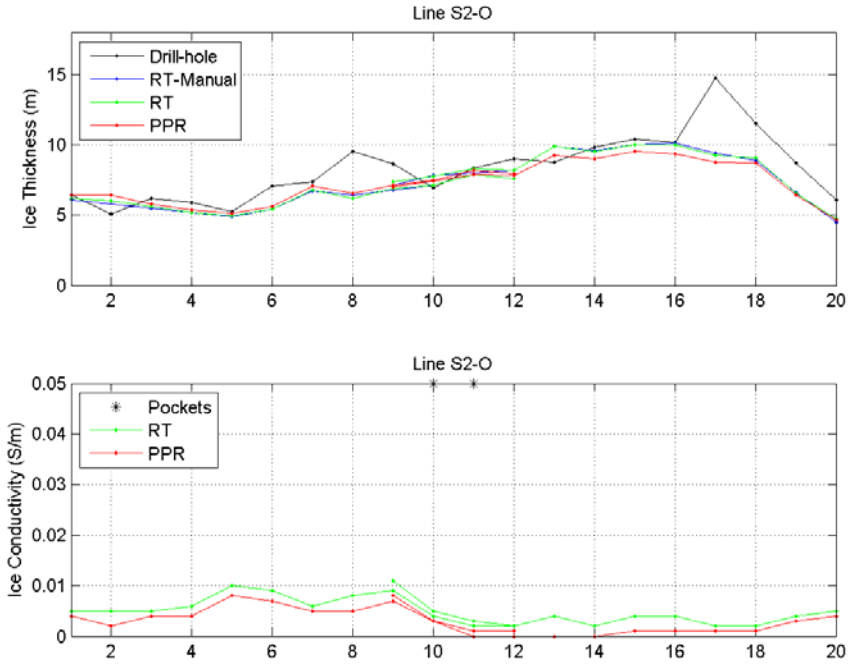

Figure 36. *Comparison of EM sled and NRC ice hole data (top) and ice conductivity (bottom) from MY ice floe B1.S2.*

For the first part of the survey, the GPR was used and then replaced by the U. Manitoba camera. The GPR is designed to measure the snow depth by inferring the snow depth from the strong ice-snow interface echo and from the weaker snow-ice echo. Since there was no snow on the MY pack ice, the GPR data provided no useful snow information as it does during winter surveys. An 1.5km section of the GPR data from the first regional ice survey north of floe B1.S1 appears to show very strong water echos (Figure 37). These areas are where the laser indicates a flat surface which we interpret as being a melt ponds. So it may be possible that these locations and their line section lengths can be used to determine the spatial distribution of melt ponds along the EM transect as the EM and GPR data are being collected simultaneously. Thus even though the GPR data was considered not to be too useful in summer no-snow conditions, it may actual be beneficial to determine the melt pond spatial fraction along the EM summer transects

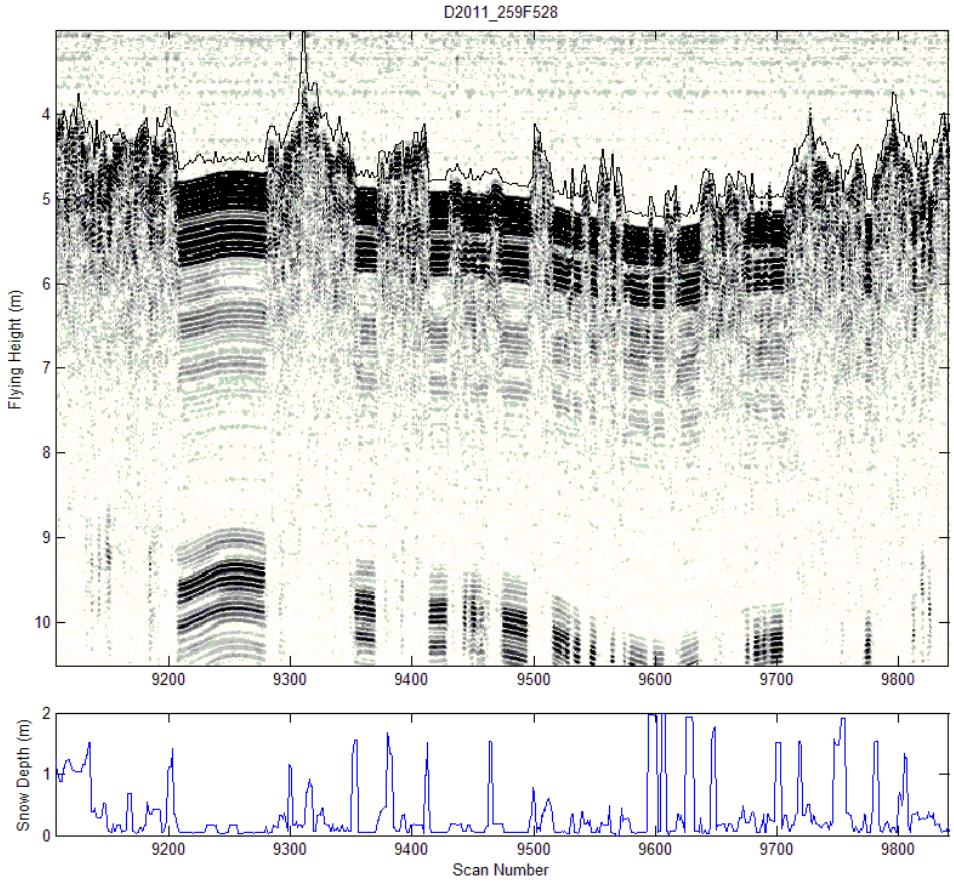

Figure 37. *Section (1.5km) of GPR data over the large floe North of MY ice floe B1.S1.*

This report shows only some of the data figures, mosaics and photograhs; all the ice thickness data of the survey in digital and plot forms along with more pictures are available through DFO Maritimes through the DFO Maritimes "Seaice Website". http://www.mar.dfo-mpo.gc.ca/science/ocean/seaice/public.html and the data link; ftp://starfish.mar.dfo-mpo.gc.ca/pub/ocean/seaice/.

4.1.7 Data Summary

HEMI Data is located in the database at:

\SEA ICE\HEMI

The IcePic™ system generates two data files, stored in the \Survey directory of the console's hard disk drive (C:), whenever it logs data. The base filename is FEMxxxxx.yyy, where xxxxx is a number which increments automatically, and the filename extension yyy is either RAW or TXT. The RAW file is a binary file which captures all data generated by the system during operation as a series of time-stamped data packets. The TXT file is a series of ASCII records, each corresponding to one Sample Run. The Sample Runs are numbered sequentially, starting with the value 1, after every power-up.

Data fields in the TXT file are:

SR #
Mean latitude (N or S, degrees, decimal minutes)
Mean longitude (E or W, degrees, decimal minutes)
Start time (milliseconds since midnight, GPS time)
End time (milliseconds since midnight, GPS time)
Mean ice thickness (m)
Standard deviation ice thickness (m)
Mean ice conductivity (S/m)
Standard deviation ice conductivity (S/m)
Mean sensor altitude (m)
Standard deviation sensor altitude (m)
Final normalised fitting error in sample run
Final # iterations in sample run

The RAW file may be transcribed using program EISXcribV1 to yield an ASCII summary file (FEMxxxxx.IPP) and a binary summary file (FEMxxxxx.DAT) which can be interpreted by the Sensors by Design DAT Viewer program for Matlab.

The IPP file is a column-oriented ASCII data file. IPP data columns are :

1 TimeStmp –System timestamp in milliseconds since 0000 Sunday morning.
2 GPSTime –GPS time of week in seconds since 0000 Sunday morning.
3 Lat –Latitude in degrees and decimal degrees
4 Lon –Longitude in degrees and decimal degrees
5 TimeDelay_lsr –Time delay between laser sample and 0.1 second system "tick"
6 Laser –Laser altimeter output
7 Laser_Return –Strength of laser return, out of about 6500
8 iLaser_Warn –warning character (decimal code for the ascii symbol)
9 Mfid –Manual fiducial (incremented with pushbutton adjacent to user interface)
10 RadAlt –Radar altitude if present and connected to console
11 Pitch –Sensor pitch
12 Roll –Sensor roll

13 SysCurr—Console DC current draw (should be ~5.5-9A if Pic only operating)
14 SysVolt --Console DC supply voltage (normally about 28V)
15 IntTemp –Internal temperature in C of console
16-23 (curr_FDEM_dat_pkt(j),j=1,8)--8 columns of EM data in ppm (parts-per-million)
24-31 (curr_FDEM_Zero_pkt(j),j=1,8)--8 columns of EM baselevel data in ppm
32 NParam –Number of parameters in inversion model, normally 3 for real-time data
33 NIter —Number of iterations during inversion of this sample
34 RMN —Normalized RMS fitting error in ppk during inversion of this sample
35 Sig_{ice} –ice conductivity estimate
36 T_{ice} –ice thickness estimate
37 $Sig_{seawater}$ –seawater conductivity (normally fixed in real time)
(there can be more T and Sig column pairs if additional layers are used for inversion)

4.2 Surface Electromagnetic Induction System Sea Ice Thickness Surveys

4.2.1 Introduction

Sea ice morphology surveys (topography and ice thickness) were conducted using variety of techniques including 1) physical sampling (drilling for ice thickness, free board), 2) surface and helicopter based Electromagnetic Induction (SEMI/HEMI) measurements, and 3) on ice LiDAR measurements to characterize the surface topography. These are all reported in different sections of the report, the intention of is section is to summarize the SEMI data collected during Leg 2A.

DFOs Surface Ice Sensor™ (SIS™) was used to measure ice thickness on transects sampled by NRC and by CEOS along the perimeter of the LiDAR survey area. The SEMI data will provide a second estimate of ice thickness complimenting the 2" auger measurements. The SEMI data provides an integrated ice thickness measure over an area 3x the ice thickness. This is the first time this instrument was used to measure multi-year ice, therefore the auger measurements are used as reference in the inversion of the SEMI data, this is still a work in progress (need to transfer inversion software to CEOS).

4.2.2 Data Summary

All SEMI data is located in the database at:

\SEA ICE\SEMI

4.2.2.1 B1S1

Figure 38 shows a map of site B1S1 visited August 15 -16. SEMI surveys were conducted along NRC lines 1 and 2 and around the perimeter of the 50x50m LIDAR scan site. Auger measurements were made along NRC_L1 only and at locations indicated around LiDAR site (Figure 38, Table 9). Table 10 summarizes the SEMI surveys conducted while at B1S1.

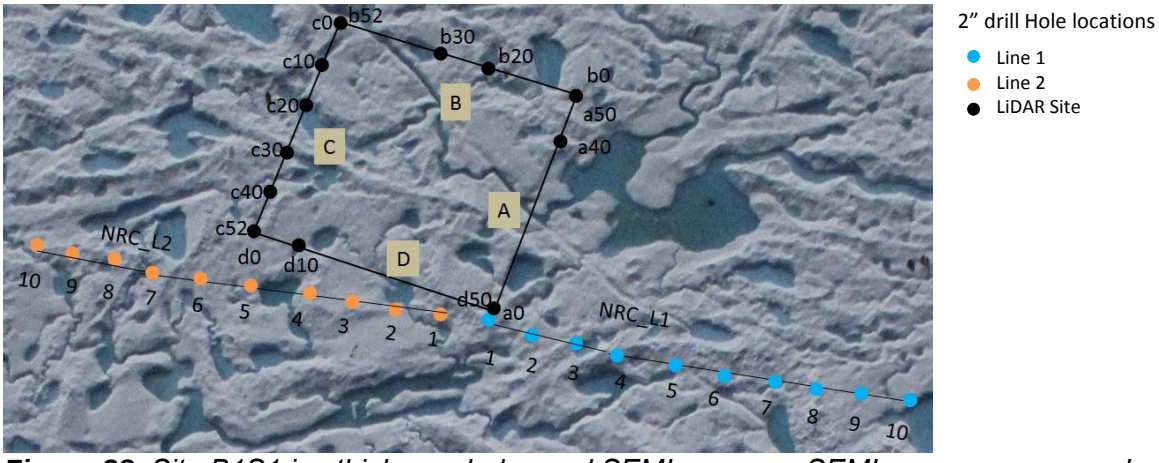

Figure 38. *Site B1S1 ice thickness holes and SEMI surveys. SEMI surveys were conducted along line NRC_L1 (blue) and NRC_L2 (orange) surveyed August 15, and adjacent to the LiDAR site.*

Table 9.. Auger ice thickness measurements surrounding the LiDAR site.

Time (UTC)	Site	Station	CTD Serial#	Ice thickness	Ice freeboard (m)	Snow depth (m)	Profile depth (m)
2011 Aug 16 16:37:16	B1S1	a0	228	7.34	0.76	0.1	70
2011 Aug 15 22:25:31	B1S1	a40	228	8.14	0.74	0.01	
2011 Aug 15 20:32:00	B1S1	a50	228	5.71	0.31	0.2	70
2011 Aug 15 00:00:00	B1S1	b10	228	>8m			
2011 Aug 16 21:20:47	B1S1	B20	228	7.07	0.31	0.05	30
2011 Aug 16 21:03:14	B1S1	B30	228	7.22	0.65	0.1	30
2011 Aug 16 20:42:47	B1S1	c0	228	7.63	0.57	0.05	30
2011 Aug 16 20:19:03	B1S1	c10	228	7.16	0.20	0.04	30
2011 Aug 16 19:48:35	B1S1	c20	228	7.45	0.25		30
2011 Aug 16 17:21:12	B1S1	c30	228	7.75	0.62		30
2011 Aug 16 17:08:45	B1S1	c40	228	8.14	0.80	0.1	30
2011 Aug 16 16:59:13	B1S1	c52	228	7.8	0.90		30
2011 Aug 15 23:15:30	B1S1	d10	228	7.67	1.64		

Table 10. Summary of SEMI transects at Site B1S1.

Date UTC)	Box	Site	Line	Start UTC	END	Continuous	Stepped	File	Comments
80/15/2011	1	1	NRC-2	20:50:01			1	200	
				20:51:42			2		
							3		
				20:53:27			4		around pond
				20:54:48			5		
				20:55:38			6		
				20:56:31			7		
				20:57:33			8		
				20:58:30			9		
				20:59:26			10		
					21:03:35	1	10 to 1		location 10 to 1 and back to GPS (origin)
			LiDAR_D				D0	201	
							D10		
							D20		
							D30		
							D40		
							D50		
			GPS		21:17:04	21:18:45			Continuous back to origin.
80/16/2011	1	1	NRC-1	3:35		1		202	Line 1 1 to 10
				15:45:30			10		long stop at 10
				15:46:07			9		
				15:46:38			8		
				15:47:20			7		
				15:48:00			6		
				15:48:48			5		
				15:49:55			4		
				15:50:55			3		
				15:51:40			2		
				16:52:20			1		
				19:54:50					back to origin
				16:10:00			A	203	Lidar loop
				10:11:53			B		
				10:14:15			C		
				10:16:20	10:17:28		D		
							GPS		END

4.2.2.2 B1S2

The site map for B1S2 is shown in Figure 39. This site was visited Aug 17-18. NRC obtained auger ice thickness data along lines NRC_L1 and L2, CEOS obtained some additional auger ice thicknesses and CTD data from drill locations surrounding the LiDAR site, these are presented in Table 11. Table 12 summarizes the SEMI surveys conducted on site.

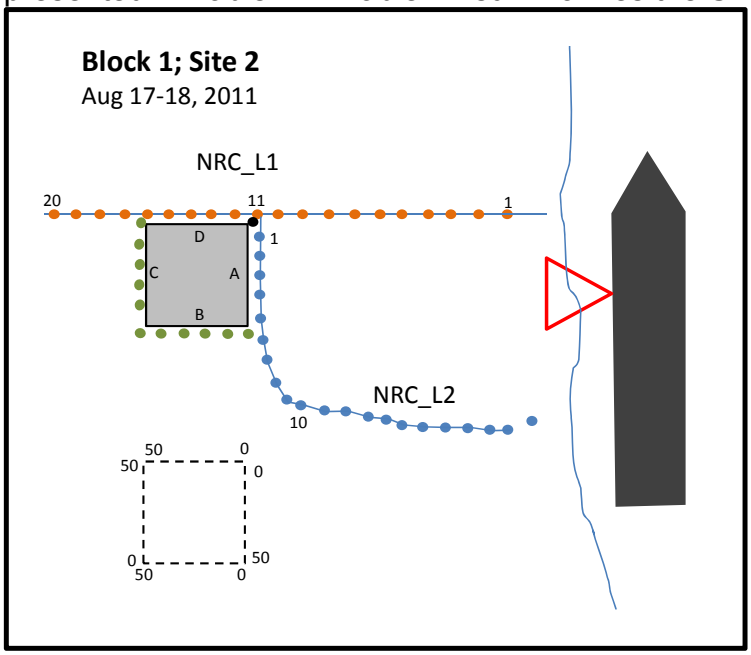

Figure 39. *Sketch map of site B1S2 visited August 17-18, 2011*

Table 11. Summary of SEMI transects at Site B1S2.

Time (UTC)	Site	Station	CTD Serial#	Ice thickness	Ice freeboard (m)	Snow depth (m)	Profile depth (m)
2011 Aug 18 03:30:20	B1S2	B0	228	7.53	1.2	0.02	30
2011 Aug 18 03:14:19	B1S2	B10	228	6.48	0.6	0.02	30
2011 Aug 18 02:54:14	B1S2	B30	228	6.53	1.1	0.02	30
2011 Aug 18 02:45:44	B1S2	B40	228	6.2	0.9	0.02	30
2011 Aug 17 22:28:48	B1S2	C10	228	7.58	0.98	0.02	100
2011 Aug 17 22:15:36	B1S2	C20	228	10.87	0.84	0.03	30
2011 Aug 17 21:39:57	B1S2	C30	228	8.63	1.03	0.02	100
2011 Aug 17 21:17:36	B1S2	C40	228	7.08	1.48	0.02	100

Table 12. Summary of SEMI surveys conducted August 17-18, 2011.

Date UTC)	Box	Site	Line	Start UTC	END	Continuous	Stepped	File	Comments
8/17/2011	1	2	1	22:08:00		1	11 TO 1	204	paused to adjust yellow cable at flag 1.
						1	1 TO 20		
					22:23:52	1	20 to GPS		GPS near flag 11
						1			
8/18/2011	1	2	2	1:11:10			GPS	205	evening of 17th, 19:11 local (mtn) 8/17/2011
				1:11:54			1	205	
				1:12:46			2	205	
				1:13:33			3	205	
				1:14:07			4	205	
				1:14:54			5	205	
				1:15:26			6	205	
				1:16:07			7	205	
				1:16:54			8	205	
				1:17:35			9	205	
				1:18:37			10	205	
				1:19:37			11	205	
				1:20:16			12	205	
				1:21:47			13	205	
				1:22:47			14	205	
				1:23:16			15	205	
				1:23:49			16	205	
				1:24:17			17	205	
				1:24:33			18	205	
				1:25:33			19	205	
				1:26:04			20	205	
				1:27:03			21	205	extra? On hummock close to floe edge
				1:27:51	1:33:10	1	21-1	205	back to GPS position (origin)
8/18/2011	1	2	1	1:35:58		1	GPS	205	19:35:58 local (MTN) 8/17/2011
				1:36:20		1	11-1	205	
				1:39:58			1	205	
				1:40:45			2	205	
				1:41:24			3	205	
				1:41:54			4	205	
				1:42:28			5	205	
				1:43:00			6	205	
				1:43:47			7	205	
							8	205	
				1:45:35			9	205	
				1:46:04			10	205	
				1:46:48			11	205	
				1:47:17			12	205	
				1:47:46			13	205	
				1:48:25			14	205	
				1:48:58			15	205	
				1:49:29			16	205	
				1:50:06			17	205	
				1:50:40			18	205	
				1:51:04			19	205	
				1:51:29			20	205	
				1:51:56	1:53/46	1		205	continuous back to GPS
8/17/2011	1	2	1	1:57:38		1	GPS	206	snoopy line B,C; origin
				1:59:08	2:00:30	1	A	206	start from GPS
				2:00:30	2:03:09	1	B	206	stop at 40m mark, metal auger equipment at 50, stuck auger piece in melt pond, go to 10m starting point on line C
					20:05:20	1	C	206	end of line C
					20:05:55	1	1	206	back along line 1 to GPS (origin)
					20:06:57	1	GPS	206	stopped, lines around melt ponds

4.2.2.3 B1S1

Preliminary estimates of ice thickness along transect NRC_1 is shown on Figure 40. The sea ice thickness measurements along vary considerably along this transect. The SEMI integrates ice thickness over 18m vs. 2". The presence of melt ponds and voids in in ice (suggesting sea water intrusions/rubble ice) causing SEMI estimates of ice thickness to be lower.

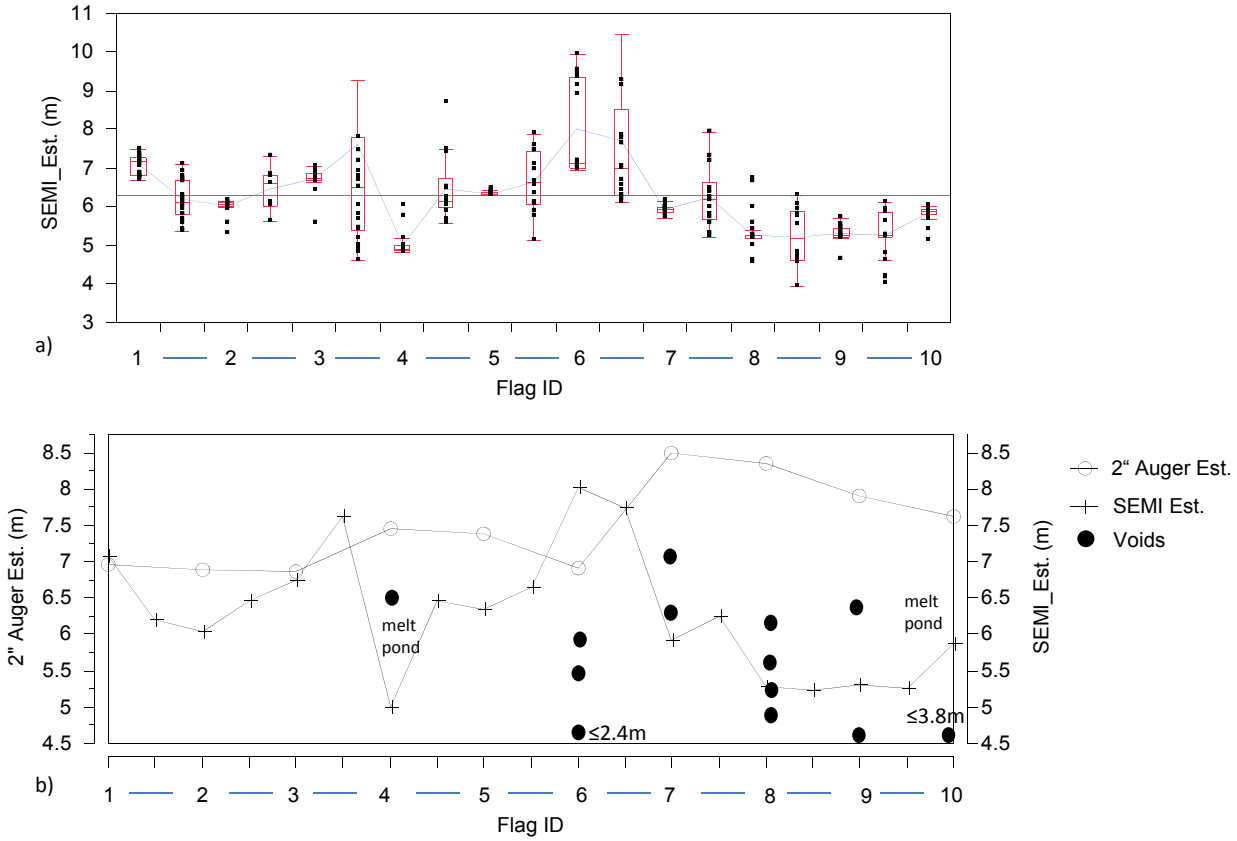

Figure 40. *a) SEMI ice thickness estimates at flagged sites and mean estimates between flags (-) using a preliminary inversion. b) Mean SEMI estimate of ice thickness along Line 1 (6.3 m (0.88 SD) versus 7.5 meters (SD = 0.61) from the 2" auger data.*

4.2.2.4 B1S2

SEMI ice thickness estimates along NRC_L2 (File 205) are presented in Figure 41. The SEMI surveys are in agreements with the 2" drill data estimates with the exception of site 6.located adjacent to a large melt pond. Mean ice thickness estimated by the SEMI was 6.96m. (SD 1.4 m) vs. 7.3m for the auger est.(excluding outlier), and 7.7 m including the outlier.

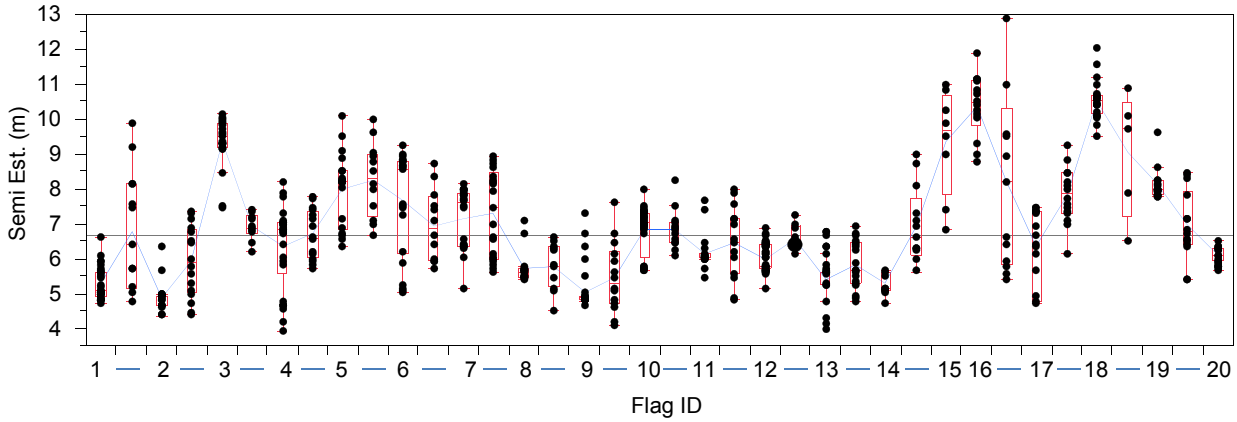

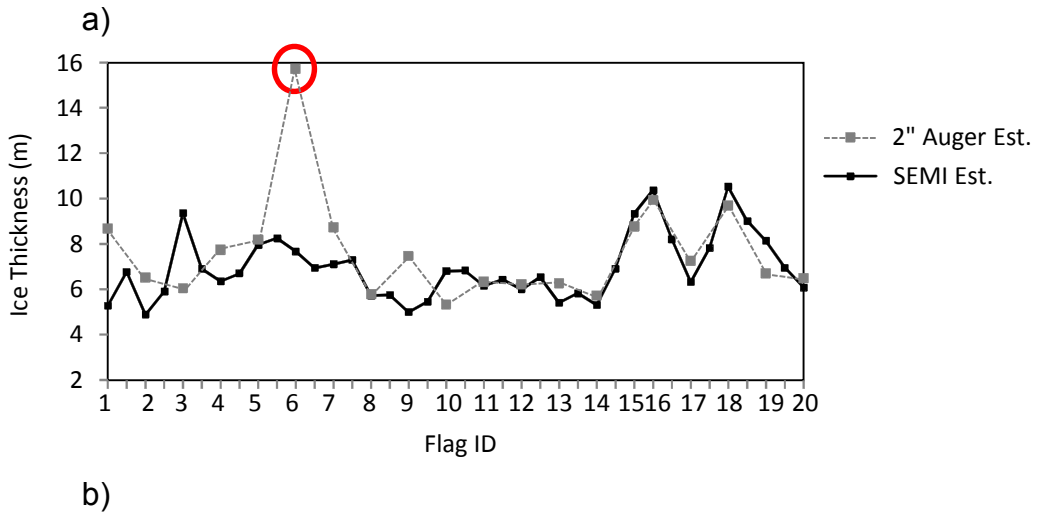

***Figure 41.**. a) SEMI estimates of ice thickness along line 2 (B1S2), b) comparison of SEMI and 2" auger data with one outlier located adjacent tot a large melt pond.*

SEMI ice thickness data along NRC_L1 is shown in Figure 42A. The mean ice thickness along this line was estimated at 7.01 m (SD 1.86), the mean ice thickness estimate based on the auger data was 8.3m (SD 2.4 m). The general trends in ice thickness along the line are comparable; the SEMI data tends to integrate ice thickness over a much larger area (including adjacent melt pond features etc.).

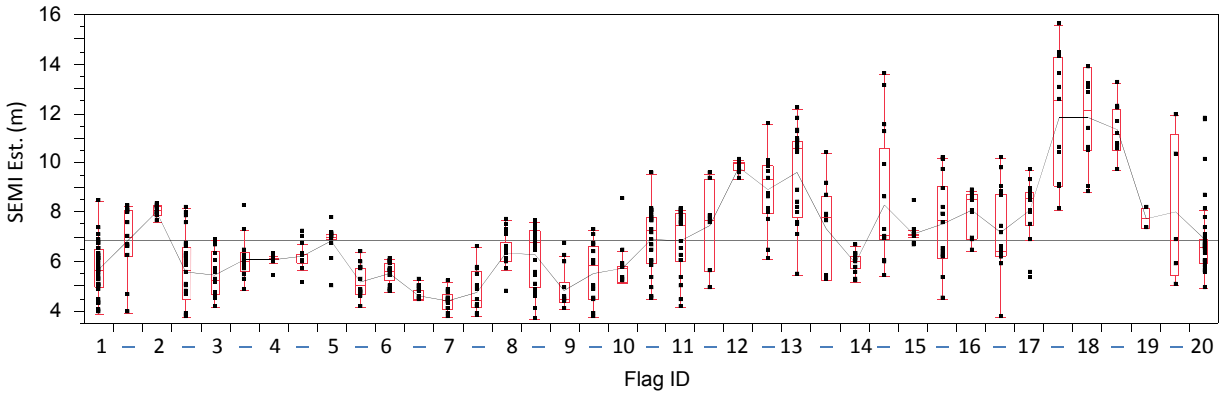

a)

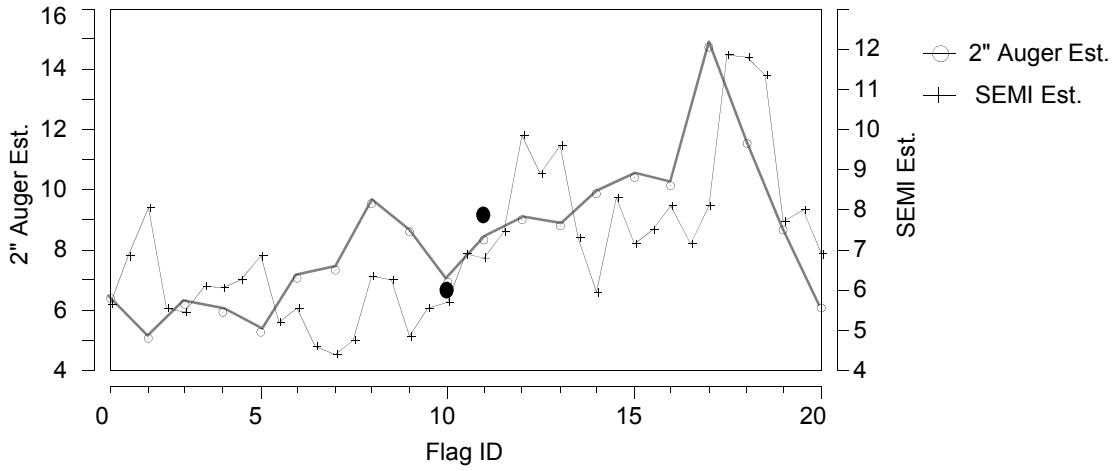

b)

Figure 42. *a) SEMI ice thickness estimates along line 1 (B1S2), b) comparison auger and SEMI estimates of ice thickness.*

4.3 Aerial Photographic Surveys

4.3.1 B1S1

Aerial photographic surveys conducted were conducted where possible over sites visited by the on-ice teams. Site B1S1 had three transects flown over it to provide detailed coverage of the floe at 1300, 2500 and 3000 ft (Table 13); this data supplements to satellite data collected by IOL for that area. Site B1S2 adjacent to the ship was not covered by aerial photography although some video transects where obtained by the helicopter coincident with the EM surveys.

Table 13. Summary of transects flown adjacent to the Amundsen at B1S1.

Transect_heading	Altitude (ft)	**Time (UTC)**	**Alt**	**Lat**	**Long**
				N74	W128
1_300	1300	21:32:00	1300	49.570	07.928
2_300	2500	22:18:00	3000		
3_120	3000	22:23:00	2500		

4.3.2 B1S2

Three photographic/EMI Surveys were flown on August 20 between 1:24 and 21:30 UTC (Figure 43).

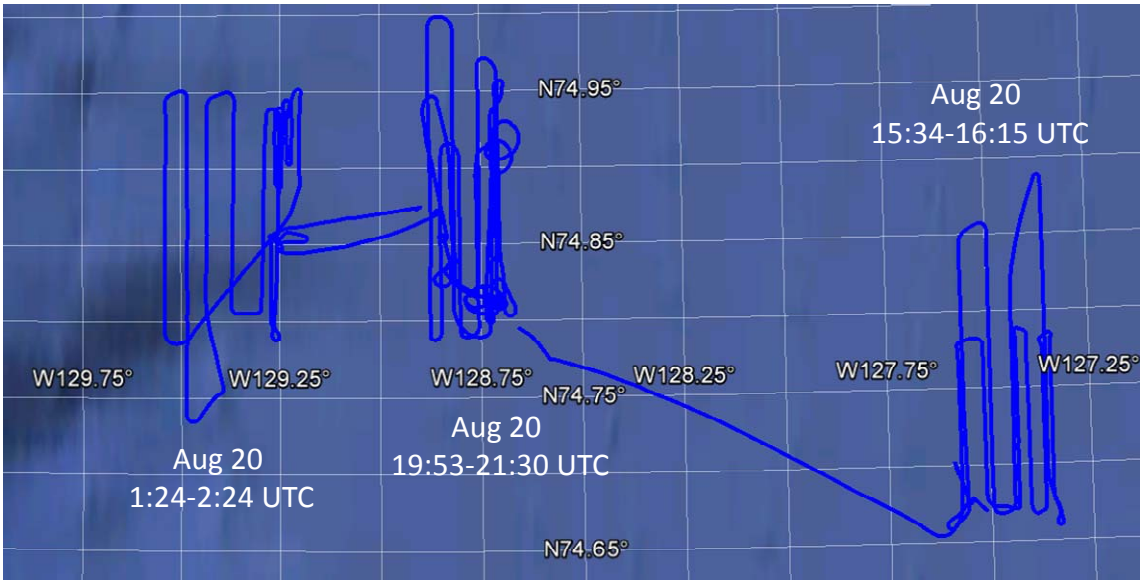

Figure 43. *Photographic and EMI surveys flown Aug 20 (UTC).*

The first survey was flown on Aug 19 in the evening around 19:24 local time (1:24 UTC, Aug 20) (Figure 44), photographic and video data where obtained in an area west of the ship coinciding with a RADARSAT acquisition that evening Seven transects were flown at altitudes ranging from 500-800 ft. due to low cloud cover (Table 14).

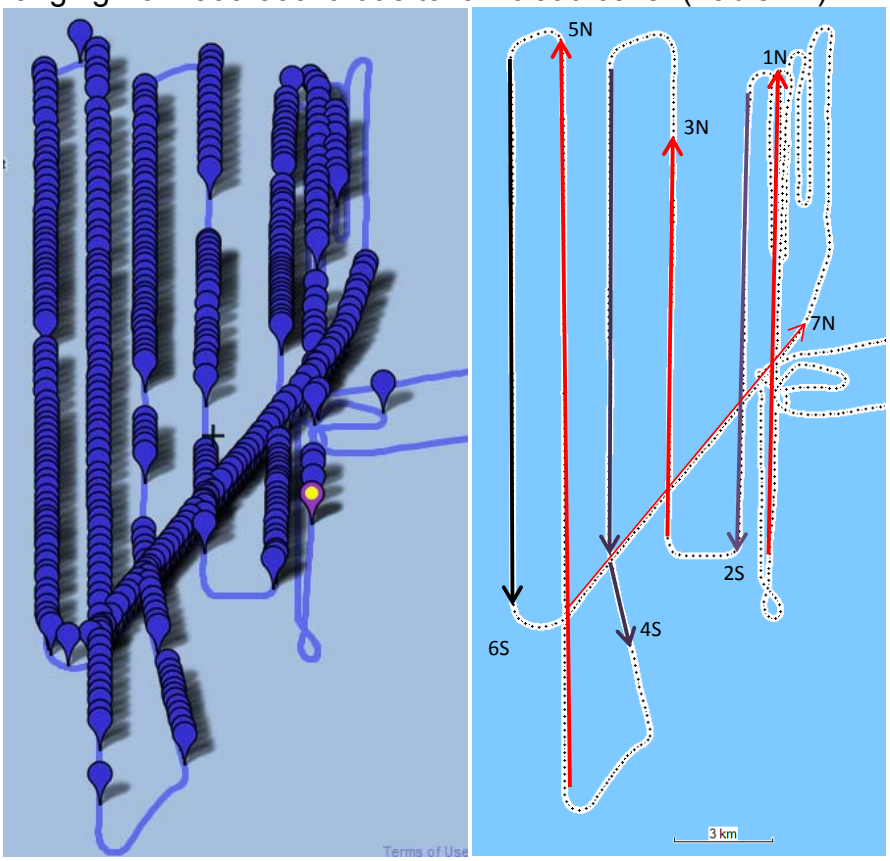

a) b)

Figure 44. *a) Photo locations of survey flown August 20 (1:24-2:24 UTC); b) transect designations.*

Table 14. . Summary of photo frames per transect flown August 20, 1:24-2:24 UTC, B1S2. Each photo frame number corresponds to the file name of the photo..

Transect	Altitude (ft)	Frames	Comment
1N	500	2789-2823	low cloud, marginal
2S	400	2831-2882	low cloud; vaiable altitude
3N	590	2891-2927	low cloud; vaiable altitude
4S	750	2922-3000	low cloud; vaiable altitude
5N	800	3002-3077	low cloud; vaiable altitude
6N	800	3085-3155	low cloud; vaiable altitude
7S	800	3163-3209	low cloud; vaiable altitude
Misc	60-130	3210-3221	

Low level HEMI surveys were flown following the aerial photographic surveys to obtain local ice thickness data (summarized elsewhere). GPS data was collected during this and subsequent flights and embedded into the digital imagery using Geosetter software (http://www.geosetter.de/en/). The camera time (UTC) and GPS time (UTC) were offset by (-54) seconds. The software allowed the offset to be used to obtain the correct GPS location data. The photo locations were saved in .kmz files. Each .kmz file (one per survey) can be opened in Google Earth (Figure xa), were thumbnails of each photo frame can be queried for location information etc. (Figure 45b). This information is intended for data browsing only. Additional software will be required to generate geocoded imagery for import into ArcMap based on the embedded geo-location data.

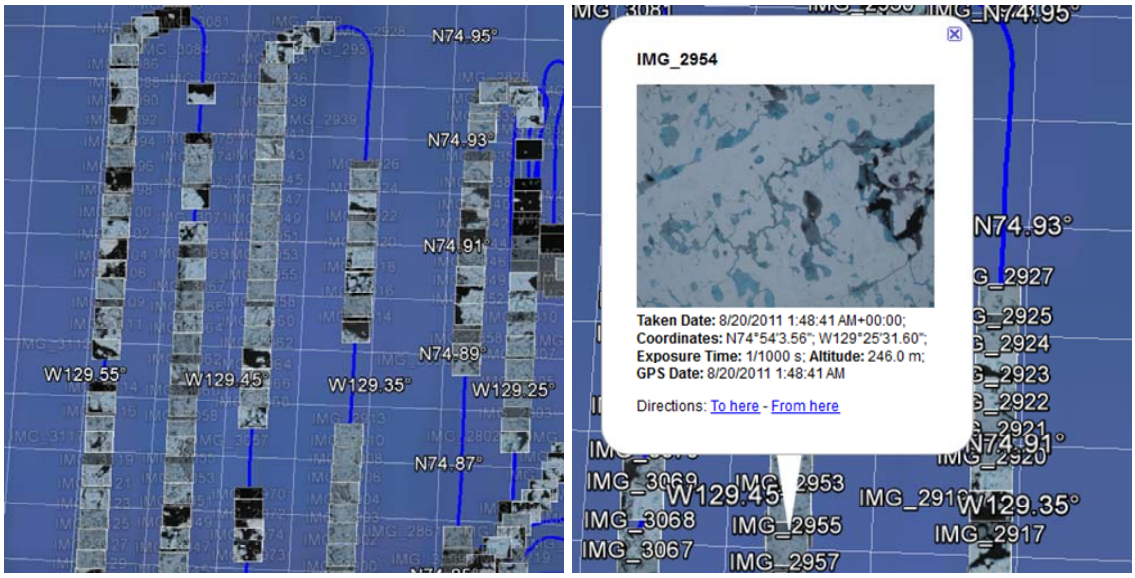

a) b)

Figure 45. *a) Geo-tagged image locations in Google Earth ©; b) each thumbnail can be queried; kmz files where created for each photo survey associated with B1S2.*

Two more aerial surveys were flown on August 20 (UTC), to obtain general ice cover information in anticipation of a storm event that was anticipated to occur August 21-22 in addition to obtaining more sea ice thickness data. The intension of the photographic data was to obtain pre- and post-storm ice cover information to assess the impact of the storm event on ice conditions in the area (flow size, etc). The survey flown starting 15:34 UTC comprised of approximately 4 transects flown at about 800 ft altitude, the maximum altitude given a low cloud ceiling are summarized in Figure 46. The other survey starting at 19:53 (UTC) is summarized in Table 15.

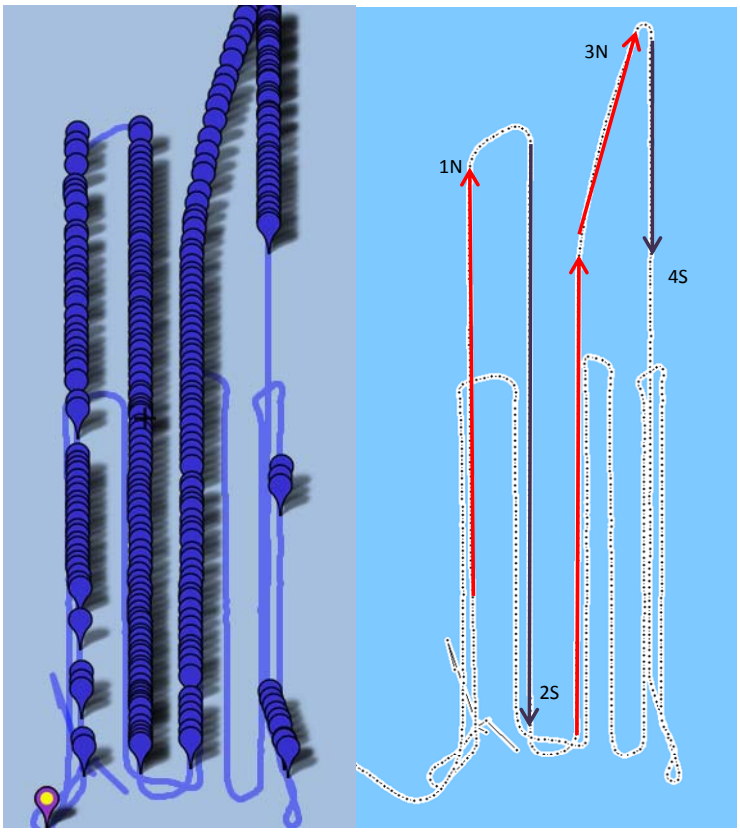

***Figure 46**. a) Photo locations for survey flown on Aug 20, 15:34-16:15 UTC, b) transect designations.*

Table 15. Summary of photo frames per transect flown August 20, 15:34-16:15 UTC, B1S2. Each photo frame number corresponds to the file name of the photo.

Transect	Altitude (ft)	Frames	Comment
1N	800	2789-2823	low cloud, marginal
2S	800	2831-2882	low cloud; vaiable altitude
3N	800	2891-2927	low cloud; vaiable altitude
4S	800	2922-3000	low cloud; vaiable altitude

Subsequent surveys (post-storm) were not flown due to fog and low ceilings. Software is commercially available to import the geo-tagged photos into ArcMap.

4.3.3: Data Summary

All Aerial survey photography can be found in the database at:

\SEA ICE\AERIAL PHOTOGRAPHIC SURVEYS

4.4 LiDAR Sea Ice Surface Surveys

4.4.1 Rationale

Three-dimensional digital elevation data was acquired at unprecedented spatial resolution over ice, snow and pond surfaces by terrestrial laser scanning (LiDAR). The data offers the potential for high accuracy quantification of pond coverage, lateral pond dimensions and form, snow drift morphology, surface microstructure and scales of surface roughness.

4.4.2 Technical Specifications of LiDAR System

Terrestrial laser scanner: Leica Scanstation C10 (wavelength 532 nm, green)

- Optics: oscillating mirror
- Pulse Rate: ≤50,000 Hz
- Range: 300 m at 90 % albedo, 134 m at 18 % albedo (Leica Scanstation Datasheet, 2009), approximate albedos of snow, ice and water are 90 %, 60 % and 0 % (total absorption) respectively
- Ranging Accuracy: 6 mm at 50 m range
- Operating Temperature: 0 to +40°C
- Levelling: mounted on surveying tripod approximately 2 m above the terrain and oriented to level with a digital bubble level and dual-axis compensator

4.4.3 Methods

A square 50 x 50 m site was selected for remote, non-invasive sampling at each of the two ice floes. Sites were chosen where surface morphology was considered representative of the full ice floe and over areas adjacent to the positions of NRC sampling transects so that the ice morphology and thickness data sets could be combined. Sites were surveyed with levelling apparatus and control points were positioned both at the site corners and mid-points of edges. Four pegged-out black bags at site corners acted as control points for aerial reconnaissance and four HDS target reflectors located approximately 1 m above the ice at mid-points of site edges acted as control points for registering separate LiDAR scans.

At each site, LiDAR data was acquired over the non-invasive sampling site from five positions (Figures 47 and 48). At each scan position, the following routine was carried out: (1) setup of LiDAR platform and tripod at local high point outside site; (2) heating of scanner inside case and on tripod during start-up; (3) preliminary low-resolution (rapid) scan to heat internal motor; (4) acquisition of images around full 360 x 270 degree field-of-view; (5) acquisition of primary scan of relevant area at ≥0.05 m resolution and (6) acquisition of target positions as separate, individual scans. The target reflector array (theoretically) stayed immobile throughout data acquisition so that the five separate LiDAR scans could be registered to single point cloud.

This method was also carried out for acquiring LiDAR data at the Scatterometer Site (Section 4.4).

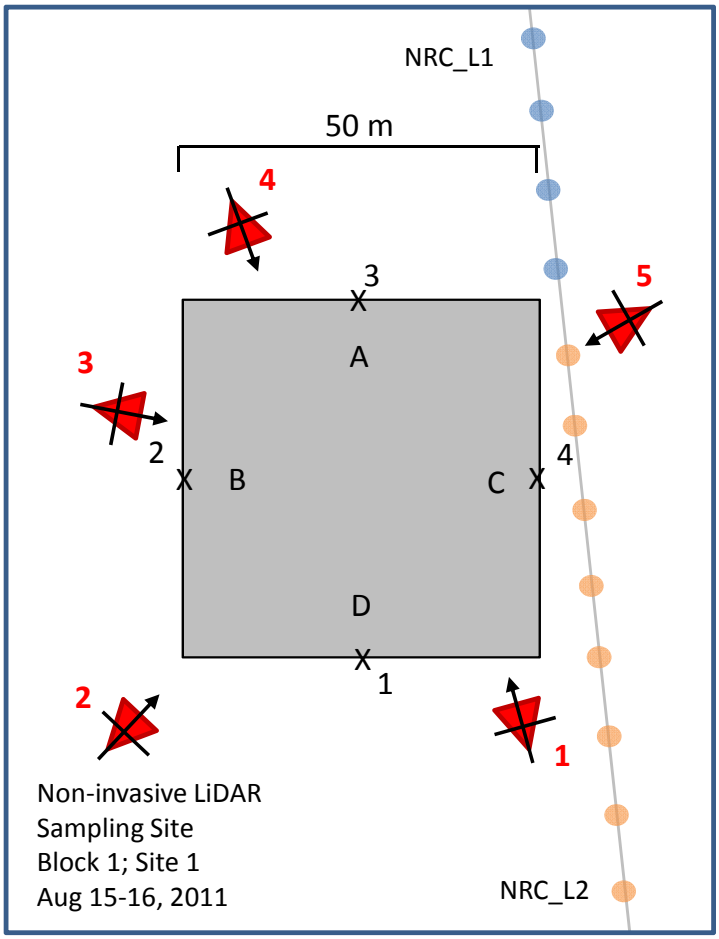

a)

b)

Figure 47. *a) Site map of Block 1 Site 1 with the non-invasive area given in grey, scan positions and orientations given by red triangles and black arrows and target positions given by crosses and numbers; b) Photograph of Block 1 Site 1*

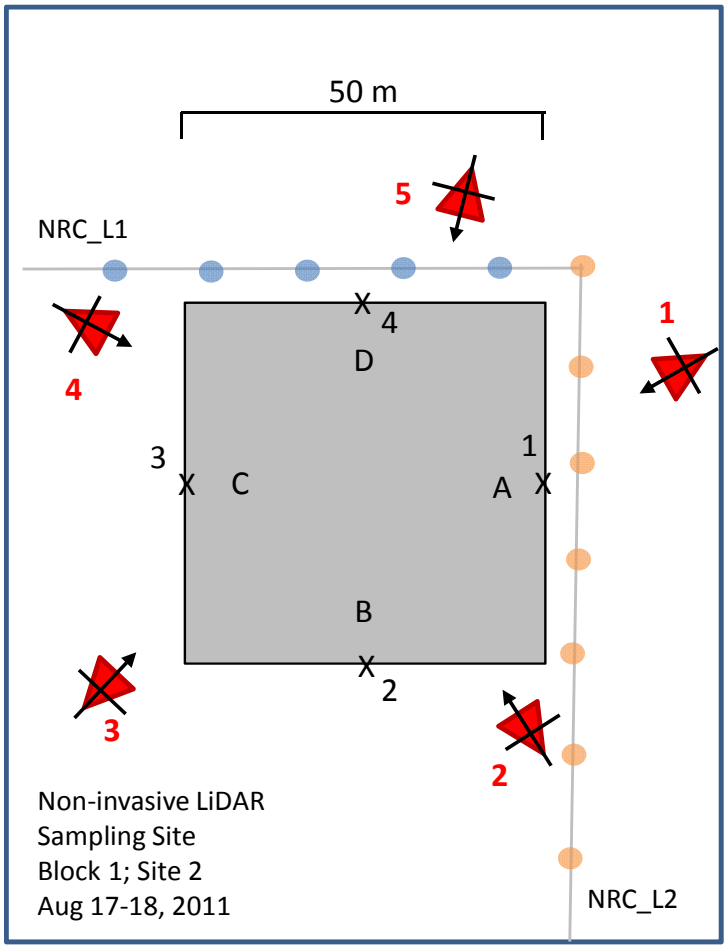

a)

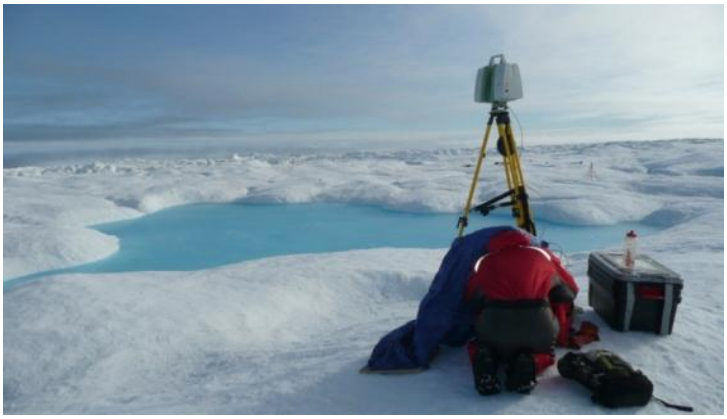

b)

Figure 48. *a) Site map of Block 1 Site 2 with the non-invasive area given in grey, scan positions and orientations given by red triangles and black arrows and target positions given by crosses and numbers; b) Photograph of Block 1 Site 2.*

Table 16. Log of activities during cruise, where M = morning, A = afternoon and E = evening.

Date	Session	Activity	Notes
Aug 11		Transit	
12		Transit	Equipment Prep
13		Transit	Equipment Prep
14		Transit	Equipment Prep
15	M	Site Prep	Box 1 Site 1: Surveying 50 x 50 m Non-invasive Sampling site
	A	Acquisition	Box 1 Site 1: LiDAR at Non-invasive Site
16	M	Acquisition	Box 1 Site 1: LiDAR at Non-invasive Site
	A	Acquisition	Box 1 Site 1: LiDAR at Scatterometer Site
17	M	Transit	
	A	Site Prep	Box 1 Site 2: Surveying 50 x 50 m Non-invasive Sampling site
	E	Acquisition	Box 1 Site 2: LiDAR at Non-invasive Site
18	M	Acquisition	Box 1 Site 2: LiDAR at Non-invasive Site
	A	Acquisition	Box 1 Site 2: LiDAR at Scatterometer Site
19		Transit	
20		Transit	
21		Transit	
22		Transit	
23		Transit	
24		Transit	

4.4.4 Data Summary

All LiDAR data is available in the database at:

\SEA ICE\LIDAR

Examples of the LiDAR data acquired at Block 1 Site 2 are given in Figures 49 and 50. It is clear from comparisons between Figure 49 and aerial photographs that there is little shadowing over the area of interest. Registered LiDAR data have a spatial resolution of approximately 3 cm and in most cases ponds appear to absorb the green light totally. However, over the large pond to the left of the site there are consistent returns from the surface acquired from one of the scan positions. It is hypothesised that solar radiation reflecting off the pond surface directly opposite to the scanner during this one scan was strong enough to register in the sensor as returning laser energy. Figure 50 emphasizes how well the laser scanner picked up the larger-scale ridges/hummocks and pond features at Block 1 Site 2.

Post-processing will initially focus on data clean-up and filtering of anomalous points and reflections from precipitation above the site.

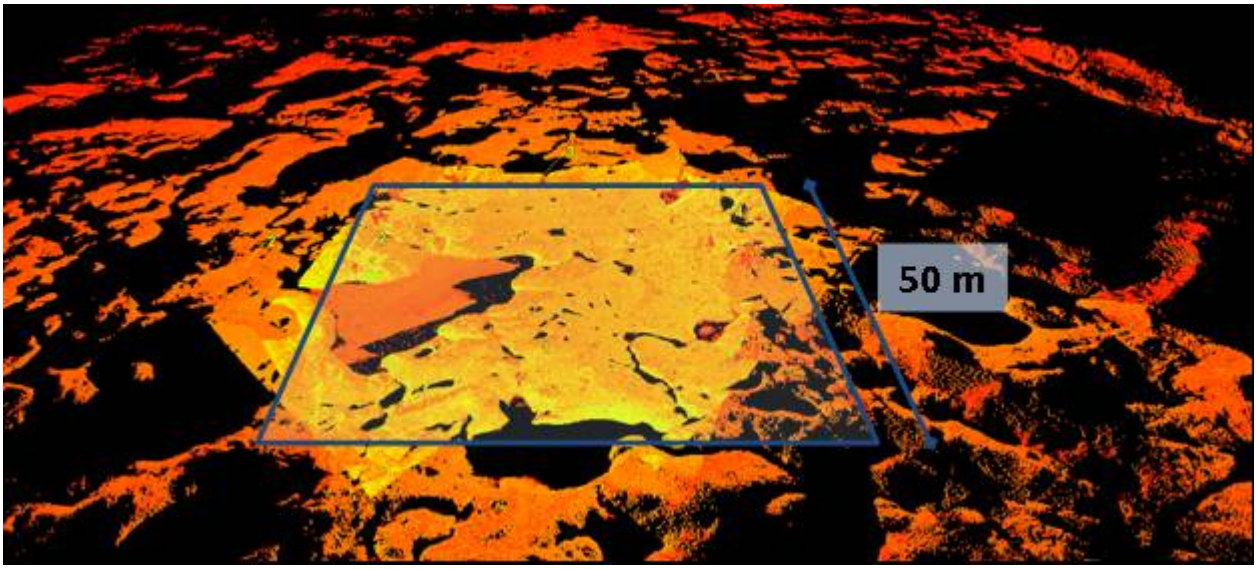

Figure 49. *Full LiDAR point cloud (i.e. made up of five registered scans) of Block 1 Site 2 with non-invasive site highlighted. LiDAR returns are given in orange with a brighter colour indicating a higher return intensity.*

Figure 50. *Full LiDAR point cloud of Block 1 Site 2, zoomed in from Figure 3.6 to show absorption over melt ponds.*

4.5 Active Microwave Measurements (C-Band Scatterometer)

4.5.1 Instrumentation: C-Band Scatterometer

Polar-orbiting spaceborne microwave synthetic aperture radars (SARs) provide valuable sea ice information for science and navigation purposes irrespective of cloud cover and darkness. The recent proliferation of next-generation dual-polarimetric and fully-polarimetric SARs such as Envisat-ASAR, Radarsat-2, Alos-PalSAR, and TerraSAR-X, has stimulated research into expanding its utility as a tool for ice type identification, ice-open water discrimination, ice floe tracking, demarcating ridged versus level ice areas, and as an information source for geophysical, climatological, and biogeochemical studies of polar snow and sea ice.

During ArcticNet Leg 2A, a scatterometer capable of providing dual-polarimetric and fully-polarimetric parameters in the same frequency (C-Band) as spaceborne SARs ENVISAT-ASAR and RADARSAT-2 was deployed over homogeneous multiyear sea ice targets in the Beaufort Sea with the aim of assessing the utility of multi-parameter polarimetric data for discriminating old, multiyear floes from younger ice types, and for detailing the influence of seasonal melt processes on sea ice signatures. The scatterometer was ship-mounted at approximately 8.2m height (Figure 51), with scans collected at each site during key periods of the local diurnal cycle (morning, solar noon, evening) and/or during coincident C-band satellite overpass times.

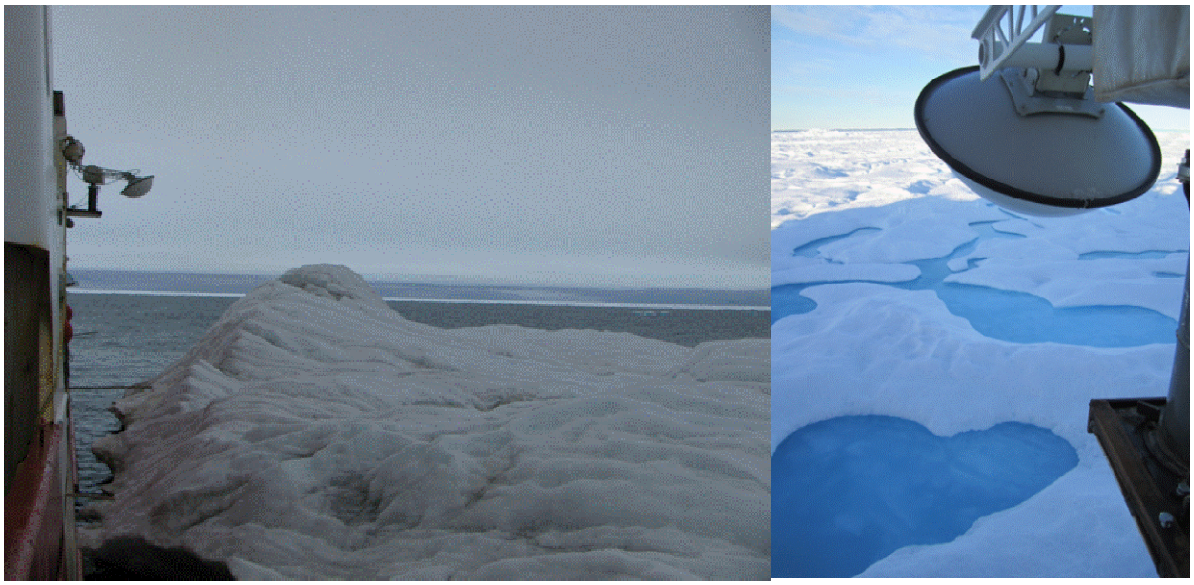

Figure 51.Ship -mounted scatterometer (left) and view of surface at B1S1 from behind the mount (right).

In addition to the collection of C-band polarimetric scattering signatures, data were collected to characterize the properties of the ice and melt ponds affecting the sea ice scattering signature. Data were collected at physical sampling sites (designated PS-1, PS-2, …) at each site, in the vicinity of the scatterometer footprint (Figure 52). Physical sampling data are summarized in the ice physical property data section.

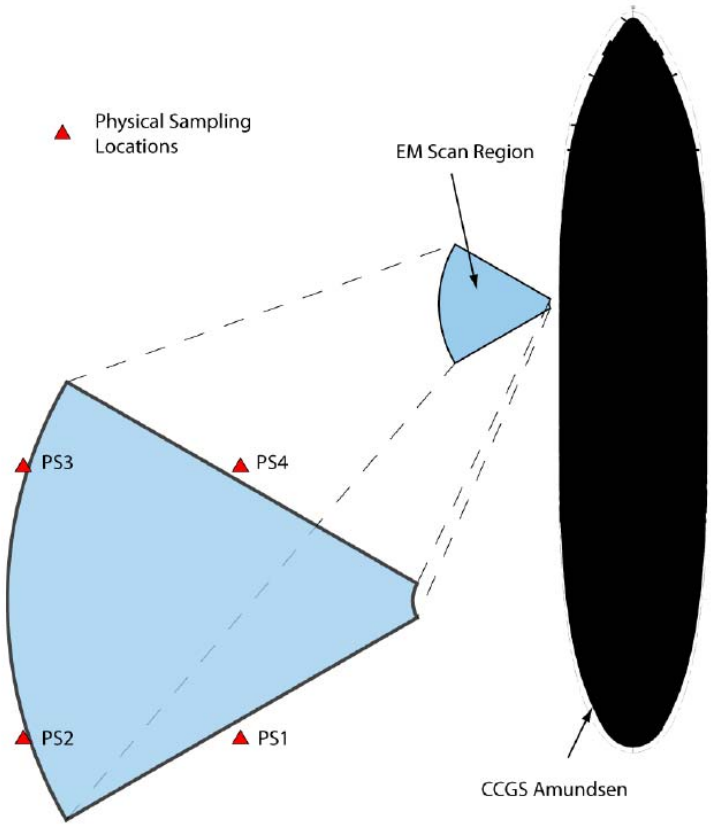

Figure 52. *General schematic of physical sampling (PS) locations with respect to the ship position. Sampling occurred at the edge of the scan region. Sites were numbered sequentially as visits were made at each station, and may not correspond to the locations depicted in the figure.*

4.5.2 C-Band Polarimetric Scattering

Specifications of the radar scatterometer are given in Table 17. The scatterometer scans the surface over an adjustable range of incidence angles (θ) and across a specified azimuth range using a *Kipp and Zonen* tracker. A single scan comprises several linear frequency-modulated continuous wave (FMCW) or *chirp* pulses, at a centre frequency of 5.5 GHz, in H and V polarization states. The backscatter amplitude and phase to the radar in all four linear transmit-receive polarization states (HH, HV, VV, and VH) is recorded at each incidence angle, and comprises and average of several azimuthal data blocks (independent samples) across the specified azimuth. A larger azimuth yields a greater number of independent samples of the surface for a single scan.

Table 17. Specifications of the C-band scatterometer.

C Band Polarimetric Scatterometer Specifications	
Frequency	5.5 GHz (C Band)
Antenna Beamwidth	5.4°
Bandwidth	500 MHz
Range Resolution	0.30 m
Modes	HH, VV, HV, VH
Noise Floor	Co-polarized Channels: -36 dBm^2
	Cross-polarized Channels: -42 dBm^2
External Calibration	Trihedral Corner Reflector

The complex scattering amplitudes of all azimuthal data blocks within an incidence angle scan line are represented by the average covariance matrix [C]:

$$[C] = \begin{vmatrix} Svv S^*vv & Svv S^*vh & Svv S^*hv & Svv S^*hh \\ Shv S^*vv & Svh S^*vh & Shv S^*vh & Svh S^*hh \\ Svh S^*vv & Svh S^*hv & Shv S^*hv & Shv S^*hh \\ Shh S^*vv & Shh S^*hv & Shh S^*vh & Shh S^*hh \end{vmatrix}, \qquad \text{(Eqn. 1)}$$

where * refers to the complex conjugate (Ulaby and Elachi, 1990; Zebker and van Zyl, 1990). Average microwave backscatter coefficients (σ°, in dBm^2) of linear and cross-polarised transmit-receive combinations are produced from cross-products derived from Eqn. 1. Additional parameters which describe the backscattering properties of the surface are also derived, including the *co-pol* ratio, r_{co} (Eqn. 2); the *cross-pol* ratio, r_{cr} (Eqn. 3); the total power, or *Span* (Eqn. 4); the *co-pol* channel phase difference, φ_{VVHH} (Eqn. 5); and the *co-pol* channel correlation coefficient, ρ_{co} (Eqn. 6):

$$r_{co} = \frac{\left\langle \left| S_{VV} \right|^2 \right\rangle}{\left\langle \left| S_{HH} \right|^2 \right\rangle} = \frac{\sigma^\circ{}_{VV}}{\sigma^\circ{}_{HH}}; \qquad \text{(Eqn.2)}$$

$$r_{cr} = \frac{\left\langle \left| S_{HV} \right|^2 \right\rangle}{\left\langle \left| S_{HH} \right|^2 \right\rangle} = \frac{\sigma^\circ{}_{HV}}{\sigma^\circ{}_{HH}}; \qquad \text{(Eqn.3)}$$

$$Span = \sigma^\circ{}_{HH} + \sigma^\circ{}_{VV} + 2(\sigma^\circ{}_{HV}); \qquad \text{(Eqn.4)}$$

$$\rho_{co} = \frac{\left|\left\langle S_{VV} S_{HH}^{*} \right\rangle\right| \sqrt{\left(1 + \frac{1}{SNR_{VV}}\right)\left(1 + \frac{1}{SNR_{HH}}\right)}}{\sqrt{\left\langle \left|S_{VV}\right|^{2} \right\rangle \cdot \left\langle \left|S_{HH}\right|^{2} \right\rangle}}; \qquad \text{(Eqn.5)}$$

$$\phi_{VVHH} = \tan^{-1}\left(\frac{\mathrm{Im}(S_{VV} S_{HH}^{*}}{\mathrm{Re}(S_{VV} S_{HH}^{*})}\right); \qquad \text{(Eqn.6)}$$

where $\langle ... \rangle$ indicates spatial averaging, and Im and Re denote real and imaginary components (Ulaby and Elachi, 1990). The above is not an exhaustive list of parameters which can be derived from the polarimetric response of a target; interested users should refer the extensive literature on full polarimetry and its potential use for more information. A complete review of scatterometer specifications, calibration routine, signal processing, near-field correction, calibration procedure, and error determination can be found in Geldsetzer et al. (2007).

4.5.3 Scatterometer Data Summary

Table 18 outlines the scatterometer scan data collected during ArcticNet 2A.

Table 18. Scatterometer scan data collected during ArcticNet Leg 2A*. Dates and times are in UTC. Sites and session IDs are shown in the first column, with each site and session ID representing a unique feature or floe scanned. ID designations are "EM" for sites with no surface physical sampling, "CAL" for a system calibration, "PS" for sites with surface physical sampling data, and "WS" for open water scans.*

Site-ID	*Date (mm.dd)*	*Start Time (hh.mm)*	*Number of scans*	*Notes*
B1S1-EM0	08.14	21:42	20	On B1S1 station but prior to commencement of ice activities
B1S1-CAL	08.15	03:10	3	RADAR calibration scans
B1S1-PS1	08.15	14:12	20	PS1 sampling at B1S1
B1S1-PS2	08.15	18:52	28	PS2 sampling at B1S1
B1S1-PS3	08.16	01:51	22	PS3 sampling at B1S1
B1S1-PS4	08.16	13:30	46	PS4 sampling at B1S1
B1S2-PS1	08.17	18:55	15	PS1 sampling at B1S2
B1S2-PS2	08.18	01:34	13	PS2 sampling at B1S2
B1S2-PS3	08:18	14:45	11	PS3 sampling at B1S2
B1S2-PS4	08.18	19:34	9	PS4 sampling at B1S2

S3-EM1	08.20	00:00	1	MYI Floe
S3-EM2	08.20	00:33	1	MYI Floe
S3-EM3	08.20	00:59	4	MYI Floe
S3-EM4	08.20	01:46	5	MYI Floe
S3-EM5	08.20	03:02	4	MYI Floe
S3-EM6	08.20	12:42	2	MYI Floe
S3-EM7	08.20	13:36	4	MYI Floe
S3-EM8	08.20	14:59	5	Ice Island
S4-WS1	08.21	19:35	5	Open water in S4
S4-WS2	08.21	02:40	5	Open water in S4
S5-EM9	08.23	13:38	3	MYI Floe
S5-EM10	08.23	15:09	3	MYI Floe

Scans were typically conducted over an incidence angle range of 20° to 65° (5° spacing), and an azimuth width of 50°, though settings were occasionally modified to maintain the radar beam within a homogeneous field of view. Example angular dependencies (incidence angle range 20-65°) of co-polarized and cross-polarized microwave backscatter coefficients (σ°_{VV}, σ°_{HH}, and σ°_{HV}) from B1S1 at 10:00 (top) and 14:00 (bottom) in Figure 7.3. An external calibration scan was conducted on 15 August using a trihedral corner reflector. Full calibration and the development of a new calibration reference file for ArcticNet 2A data will require post-processing. All scan data included in the initial dataset, and presented here, were processed from raw format using an internal (system) calibration and are useful for preliminary analysis and plotting only. Please contact the team lead for updated calibration information.

The preliminary processed ASCII scatterometer files follow the same naming convention, and are organized into month-day folders as follows:

\SEA ICE\SCAT

It should be noted that there was an ongoing date/time synchronization problem in the scatterometer central processing unit. The operators have taken care to record LST, UTC, time on laptop, and the CPU time. The filename of each scan is linked to the CPU time.

4.5.4 Data Visualizations

A comparison of scatterometer polarization data for different ice types is presented below in figure 53.

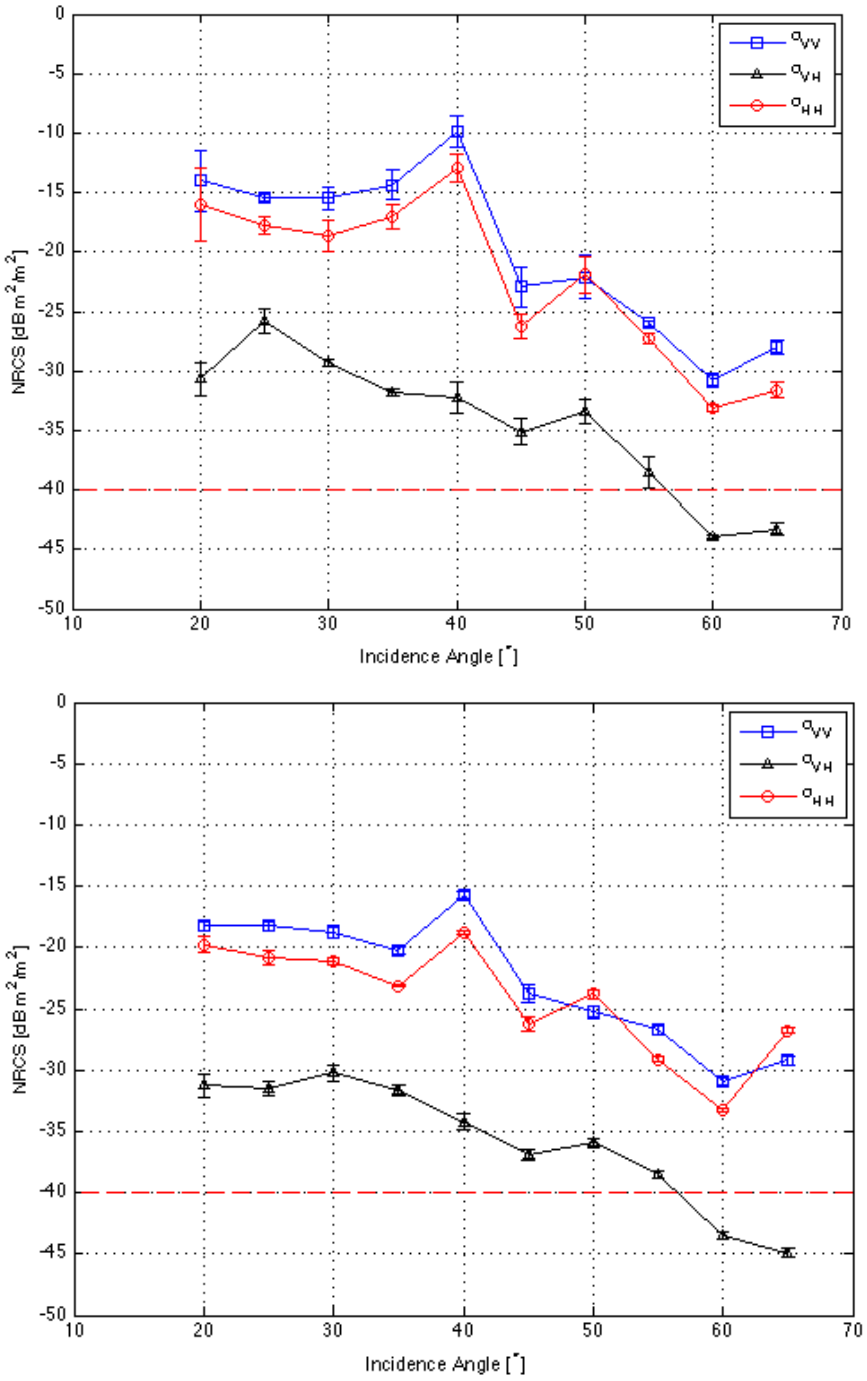

Figure 53. *Co-polarized and cross-polarized backscatter coefficients (σ°VV, σ°HH, and σ°HV) as a function of incidence angle for two scans, 10:00LT (top) and 14:00LT (bottom) during B1S1-PS1 and B1S1 PS-2, respectively.*

4.6 Sea Ice Physical Sampling (Ice Cores)

4.6.1 Methodology

Typical Sea ice physical sampling activities include, but are not limited to:

- Take ice cores from a location with the same snow depth close to were the snow pit is/was done (even at the same spot). Extract one core for temperature, and one for salinity.
- Freeboard (FB): determine FB from a core hole using a ruler.
- Thickness (h_i): determine h_i using an ice thickness gauge.
- Temperature (T_i): Measure at surface or snow/ice interface immediately after removing snow cover. Temperature profiles at intervals in the ice using temperature probe: immediately after extracting core, use drill to make hole to the center of ice core at a known distance from the surface, insert temperature probe to measure temperature. Shade the sensor from direct solar radiation. If T_a is colder than ice temperature, then observe maximum ice temperature. If T_a is warmer than ice temperature, then observe minimum ice temperature. Determine depth interval of temperature measurements depending on ice core thickness. Keep in mind that measuring the profile quickly is better than a high vertical resolution.
- Estimate the length of the ice core thickness (does it match the thickness gauge observation).
- Salinity: Extract an additional core. Cut it in 5 - 10 cm intervals immediately after retrieval and place in whirl-pack bags or buckets. Bring back to ship and allow to melt so that conductivity and salinity can be measured.

Figure 54: *On-ice team taking an ice core for temperature and salinity profiles (top left), and sampling area, depth, temperature and salinity of meltponds (lower right).*

At each station, physical properties of sea ice in the vicinity were observed. The temperature at depth within the visited ice floe(s) was determined by coring the floe and drilling holes in it at 10 cm intervals, starting 5 cm from the ice surface. After each hole was drilled a fast-response digital temperature probe was inserted and the result recorded. The surface temperature of the ice surface was also recorded. A second core was pulled at each station and cut in the field at 10 cm intervals in order to determine the salinity profile within the ice floe (Figure 55).

Figure 55: *An ice core being cut into 10cm segments for eventual salinity analysis*

When it was possible for personnel to work on the ice, a no-walk zone was designated along the port side of the CCGS *Amundsen* (semi-circular area with a radius of 30m) to preserve a natural surface for the passive and active microwave measurements On-ice physical sampling activities were conducted in close proximity to this no-walk zone. For ice thicknesses of 0 cm (e.g. grease or frazil ice) to less than 10 cm, the measurement intervals were modified to whatever was possible.

Ice cores are taken using a Kovacs Enterprises Mark II Coring system, which extracts cores with a 9cm diameter (www.kovacsicedrillingequipment.com). Ice temperature profiles (10cm interval) were measured in the field using a drill and a Hart Scientific Model 1522 temperature probe. Additional Ice cores were brought back to the ship for profile measurements (10cm interval) of salinity, by cutting about 10cm core pieces into (nearly) cubical shapes. The pieces, from which all sides that had been subject to drainage or exposed to the atmosphere were removed, were melted for measurements of conductivity using a Hach Sension5 portable conductivity meter (Hach, Loveland USA), with measurement accuracy of +/- 0.01.

By measuring the temperature and salinity of the sea ice it is possible to calculate the brine volume present in the sea ice and thus get an estimate for the ice porosity. The total thickness and freeboard of the ice floe was also recorded. Pictures were typically taken of the

various snow/sea ice/ocean surfaces encountered at each station. Where melt ponds occurred on the sea ice surface, melt pond salinity, temperature and depth was recorded.

4.6.2 Physical Sampling Data Summary

Ice cores were extracted adjacent to the scatterometer site at B1S1 and B1S2 using a 9 cm diameter core barrel (Kovacs© Mark II Coring System), photographed next to a measuring rule, sectioned into 10 cm intervals, transferred to a lab, melted and measured for conductivity and salinity (S_i, ‰) using a *Hach sension 5* portable conductivity meter model 51975-00 calibrated with a conductivity standard (Table 19). A second core was extracted at each site and sampled for temperature (T_i, °C) in drill holes at 10 cm intervals using a temperature probe (Figure 7.4). A third core was taken at B1S1 and B1S2 and transferred to the cold lab on the ship shortly after extraction for thick section (5mm) structural analysis and photography.

Table 19. Ice core data collected by the EM team during ArcticNet Leg 2A.

Site	*Session*	*Date (mm.dd)*	*Time (hh:mm)*	*Notes*
B1S1	PS1	08.15	15:53	Drained white ice 0-17cm;
B1S1	PS2	08.15	20:00	Hummock; drained white ice 0-45cm; milky layer 60-65cm
B1S1	PS3	08.16	03:50	Flat area adjacent melt pond; drained white ice 0-6cm
B1S1	PS4	08.16	14:00	Core taken with contaminants group
B1S2	PS1	08.17	19:30	Banding; drained white ice 0-6cm, milky layer 7-22cm; rest is bubbly
B1S2	PS2	08.18	01:50	Banding; drained white ice 0-6cm, milky layers 13-14cm, 55-64cm, and 66-67cm
B1S2	PS3	08.18	15:10	Small hummock surrounded by melt ponds; drained white ice 0-5cm
B1S2	PS4	08.18	21:40	Large hummock; upper 2cm is disaggregated granular layer

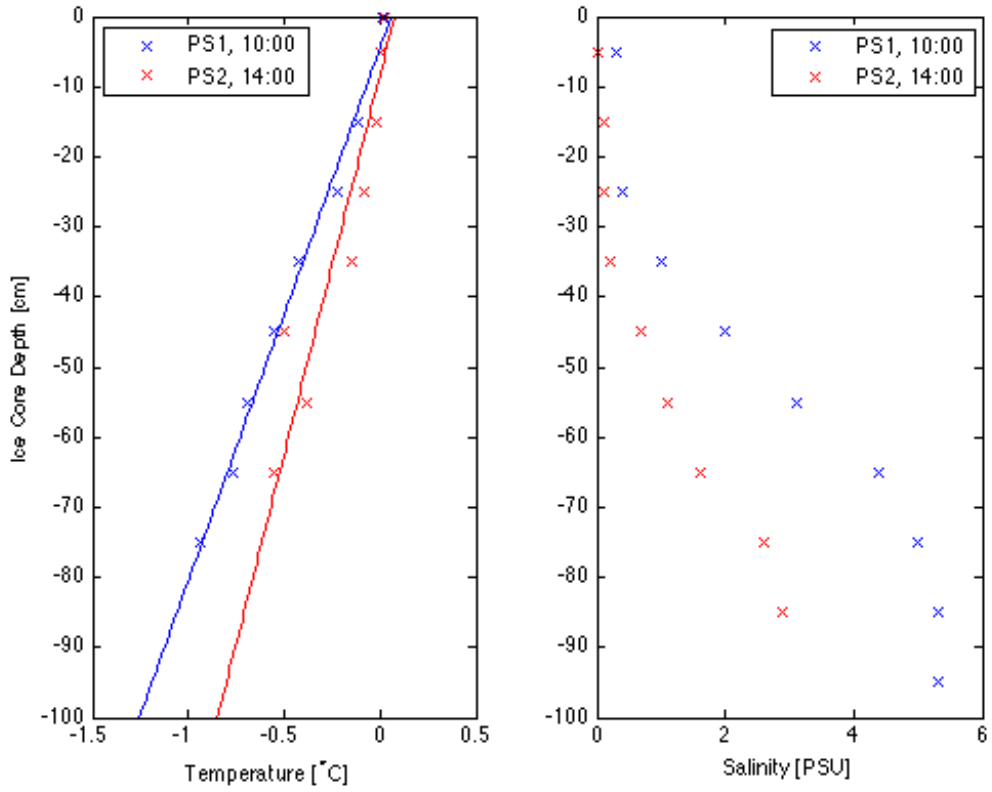

Figure 56. *Temperature and salinity data from ice cores extracted during PS1 (10:00LT) and PS2 (14:00LT) at B1S1.*

Physical sampling data is available in the database at:

\SEA ICE\ICEPHY

The information contained in this file is well-described, and organized by date. Ice core profiles are recorded from the top, down (where surface = 0 cm depth).

4.7 Infrared Photography

4.7.1 Introduction

An infrared (IR) camera FLIR was employed for measuring sea ice temperature profiles during the IOL *Amundsen* cruise on Aug. 11 - Aug. 25, 2011. Actual IR measurements were conducted on 15 – 18 August, since the work on sea ice was not allowed after 18 August.

4.7.2 Methods

1) The IR camera should be turned on at least 20 min prior to measurements.
2) An ice core approximately 1 m. length is placed on the core barrel box.
3) The ice core must be protected from direct solar radiation. We used a piece of plywood ~ 1.5 m. x 1.5 m.) to shade the core, as shown in the pictures below (Figure 7.5 and 7.6).
4) An IR image is taken at a distance of three metres from the core; thus, the ice core and the core barrel box are in the same frame. The camera settings are left at the factory default.
5) Button **S** on top of the camera is pressed once for preview and then once again (1 second long) for saving the image.
6) Pictures taken by the IR camera are stored on a regular SD memory card.

Figure 57. *Taking IR image of an ice core, Aug. 17, 2011*

4.7.3 Post-Processing

The IR camera takes two images (IR and visible) at the same time. However, the IR and visible images are not the same size. The area captured by the IR mode is a subset of the visible image. An example of visible and IR pictures taken by the camera are shown in Figure 58.

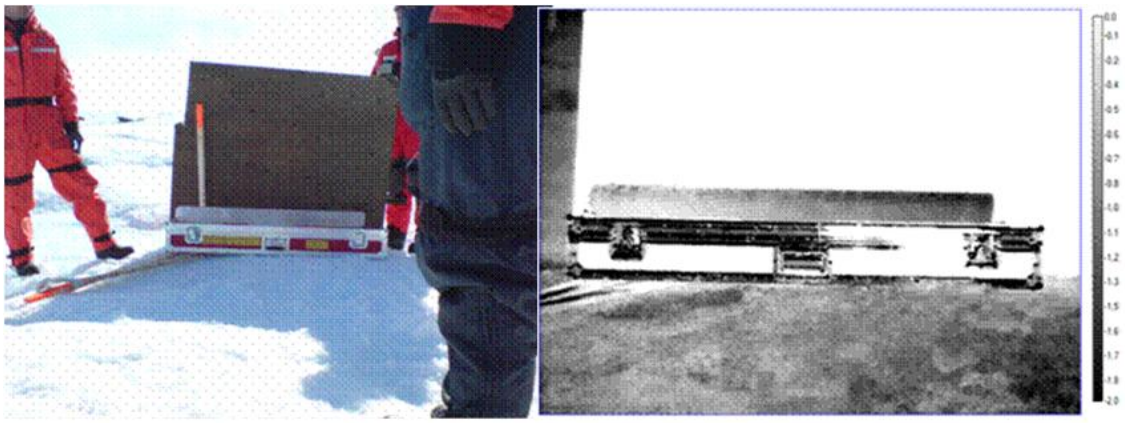

Figure 58. *An example of visible and IR images taken by IR camera. Box1 Site2 PS1, 17 August 2011, between 13:00 – 15:00 LST. Size of the core barrel box used as a scale is 127 cm.*

Using ExaminIR software it is possible to extract temperatures along the ice core. A line is drawn along the length of the core and the temperatures are extracted. We recommend using 3 or 4 lines to calculate the average temperature profile since such an operation reduces noise.

4.7.4 Comparison With Contact Measurements

Figure 59 demonstrates comparison between the temperature profile extracted from IR image (Figure 7.6, right-hand image) and actual temperature probes (contact measurements every 10 cm along the ice core). A good agreement between IR and contact measurements is observed in Figure 59.

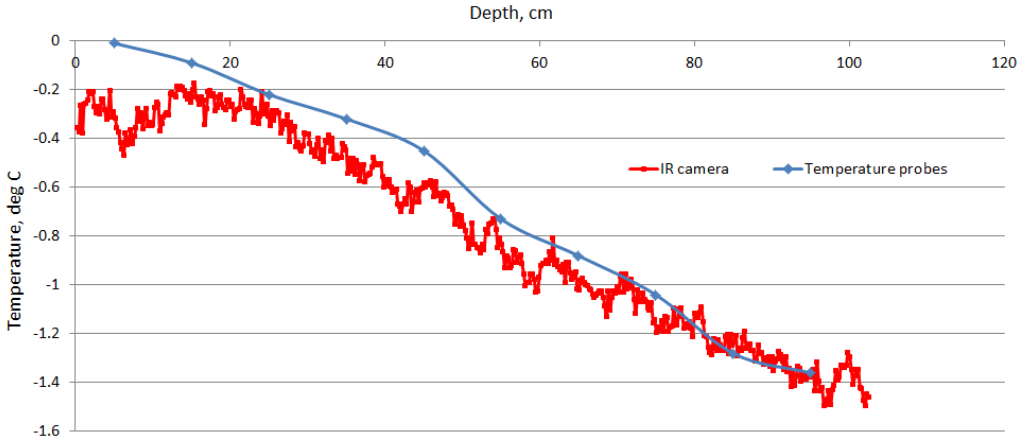

Figure 59. *Comparison between IR camera temperatures and temperature probe.*

An IR image contains raw data layer (integer counts) and temperature layer (raw data converted to temperatures). The temperature layer is calculated based on the settings. The most important setting is emissivity of the target in IR band.

4.7.5 Data Summary

IR photography is available at:

\SEA ICE\IR_PHOTO

Currently, raw IR data is converted to temperatures according to the default settings of the camera (emissivity of the target is 0.95, distance is 1 m., air temperature is 20 degrees). We assume that additional calibration is required. Based on the collected data, it is possible to obtain a calibration curve (raw counts versus temperature probe measurements) specifically for sea ice in the given temperature range (in our case this is -2 – 0 degrees).

4.8 Dielectric Hydraprobe Measurements

The summer multiyear ice cover is devoid of snow, though variations in the intensity of melt and the occurrence of liquid water which occurs at the ice surface can have a strong influence on observed microwave scattering signatures. In order to assess this, dielectric permittivity (ε′), dielectric loss (ε″), and electrical conductivity measurements of the ice surface were made at 1m horizontal intervals along a 10m line adjacent to the scatterometer scan region at different times at each of sites B1S1 and B1S2 (Figure 60). Measurements were made using the Stevens Water Monitoring Systems Hydra Probe (a.k.a. hydraprobe). The hydraprobe uses a tine assembly consisting of a central waveguide and three outer rods, each 4.5 cm in length and 3 mm wide, to measure the impedance of the sample at 50 MHz over a cylindrical area of 5.7 cm in length by 3 cm in diameter (Stevens, 2007). Samples were obtained by vertically inserting the probe tines into the surface ice layer, to their maximum depth and collecting a dielectric permittivity (ε′), dielectric loss (ε″), and electrical conductivity response, from which a surface wetness value can be estimated. This method was not always successful in generating a response, as either: the sensor tines were unable to physically penetrate the ice to its minimum required depth (the sensor is designed for snow or soil, which is typically much less solid); or the sensor was unable to read a strong enough response to generate output. Table 20 summarizes the hydraprobe data collected during ArcticNet 2A. Sensor bias and calibration data were measured using air samples (≈0°C and room temperature) and isopropyl alcohol for ε' and a saline solution of known conductivity for ε'', following Geldsetzer et al. (2009). Bias and calibration values have not been analyzed and applied, hence the data are currently in raw format.

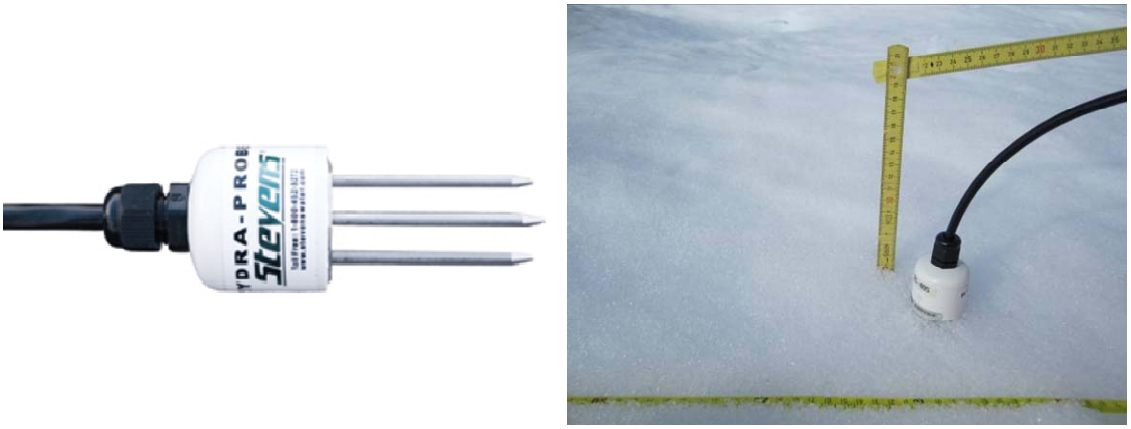

Figure 60. *The hydraprobe sensor (left), and the sensor inserted into the ice surface at B1S1 (right).*

Table 20. Dielectric hydraprobe data collected during ArcticNet Leg 2A. Times and dates are in UTC.

Site	*Session*	*Date (mm.dd)*	*Time (hh:mm)*	*Number of samples*

B1S1	PS1	08.15	15:33	10
B1S1	PS2	08.15	20:02	9
B1S1	PS3	08.16	02:50	6
B1S1	PS4	08.16	15:57	5
B1S1	n /a	08.17	20:52	4
B1S2	PS2	08.18	02:01	10
B1S2	PS4	08.18	21:40	4
CAL-air(room)	n /a	08.20	16:12	51
CAL-isopropyl	n /a	08.20	16:22	62
CAL-saline	n /a	08.20	16:38	82
CAL-air(≈0°C)	n/a	08.24	23:00	30

Though the ice cover was devoid of meteoric snow, a change in the ice surface from solid to disaggregated (granular) was observed during hydraprobe sampling. The character of the grains were documented ay B1S1 and B1S2 by photographing ice grains against a gridded plate (Figure 61) and by measuring the depth of the granular layer associated with each hydraprobe sample.

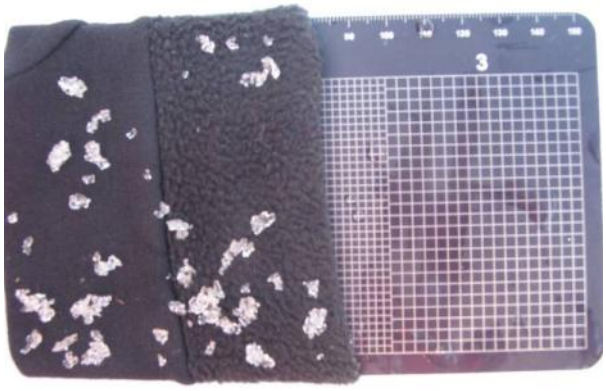

Figure 61*. Example surface granular layer photograph. Grains were placed on a felt insulator next to the grid as they would melt when placed directly on the metallic grid surface.*

4.9 Surface Roughness Profiles

A significant contribution to the intensity of microwave backscatter, as measured using the polarimetric radar scatterometer or via spaceborne synthetic aperture radar (SAR) such as RADARSAT-2, is determined by the magnitude of small-scale (radar-scale) surface roughness which is horizontally spaced on the order of the incident radar wavelength (i.e.,

mm- to cm-scale). In order to assess the radar-scale surface roughness contribution of sea ice and melt ponds to backscatter measured by the C-band polarimetric scatterometer, a scanning laser unit developed at Wood`s Hole Oceanorgraphic Institute was used to capture high-resolution, 1-D, scans of the surface roughness of small areas. The unit consists of a 905nm Hokuyo UTM-30LX scanning laser fixed to a survey tripod at a height of approximately 1m, or higher when suspended over a surface feature (Figure 62). The laser is powered using a 12V cell and controlled from a linux netbook using custom software. The complete unit remains stationary as the laser scans a 270° arc centred on NADIR (0°) at an angular resolution of 0.25°; the along-beam horizontal resolution is 0.02m at 4m. The resulting scan consists of range values (mm) in polar coordinates; values at angles <0° are discarded due to interference by the tripod.

During ArcticNet Leg 2A, 13 scans of surface features, primarily calm or ice lens capped melt ponds and multiyear ice surfaces, were collected (Table 21). Unfortunately, we were unable to collect a series of scans over a variety of melt ponds subject to wind-wave roughening (wave rippling) for various wind regimes. Dynamic surface roughness due to wind-wave roughening over melt ponds is known to cause ambiguity in the interpretation of microwave backscatter signatures of sea ice comprising melt ponds; as such this remains a priority for future summer sea ice and microwave remote sensing studies.

Figure 62. *The laser profilometer mounted over a melt pond.*

Table 21. Laser surface roughness profiles made during ArcticNet Leg 2A*. Times and dates in UTC format.*

Scan	*Site*	*Date (mm.dd)*	*Time (hh:mm)*	*Notes*

1	B1S1	08.15	21:55	Melt pond; smooth with slight rippling
2	B1S1	08.15	22:00	Repeat of 1
3	B1S1	08.16	19:41	Melt pond; 1 cm thick surface ice lens
4	B1S1	08.16	19:43	Repeat of 3
5	B1S1	08.16	21:50	Scatterometer footprint (perpendicular across); ice; LiDAR coincident
6	B1S1	08.16	21:53	Repeat of 5; new orientation; ice and melt pond
7	B1S1	08.16	21:58	Repeat of 5; new orientation; ice and melt pond
8	B1S2	08.18	20:54	Discard
9	B1S2	08.18	20:56	Discard
10	B1S2	08.18	20:58	Scatterometer footprint; perpendicular across; ice
11	B1S2	08.18	21:10	Frozen melt pond; 18.26m to opposite edge
12	B1S2	08.18	21:12	Frozen melt pond; 18.26m to opposite edge
13	B1S2	08.18	21:20	Ice patch; hydraprobe here

The surface roughness laser profile data is available in the database at :

\SEA ICE\Laser Profiler

4.10 Ice Dynamics

4.10.1 Introduction

Sea ice dynamics within this region are of particular interest due to the mix of old multiyear ice and first and second year ice which coexist and hence dynamically interact. This mix of old and young ice is attributable to the combination of the recirculation of ice through the Beaufort Gyre along with the thermodynamic growth of new sea ice within leads and areas of open water. Our group used the Skippy Boat to sample secondary sites near the primary site which was extensively sampled by the other participating groups. Our objectives were as follows:

- Deploy ice motion beacons on secondary flows to study ice motion and to track these flows for subsequent satellite imagery.
- Characterize the physical properties of these secondary flows by measuring ice thickness and ice cores of the top meter to understand the salinity and temperature profiles through the ice.
- Characterize local oceanographic conditions by performing several CTD casts at each site and deploying the MOBS buoy which provides us with surface roughness data on the open water.
- Deploy Up-TempO buoys for Dr. Mike Steele from the Applied Physics Laboratory at the University of Washington.

In total 6 remote sites were visited and sampled, 19 ice motion beacons were deployed, the MOBS buoy was deployed twice, 2 Up-TempO buoys were deployed and 8 CTD casts were completed by our team.

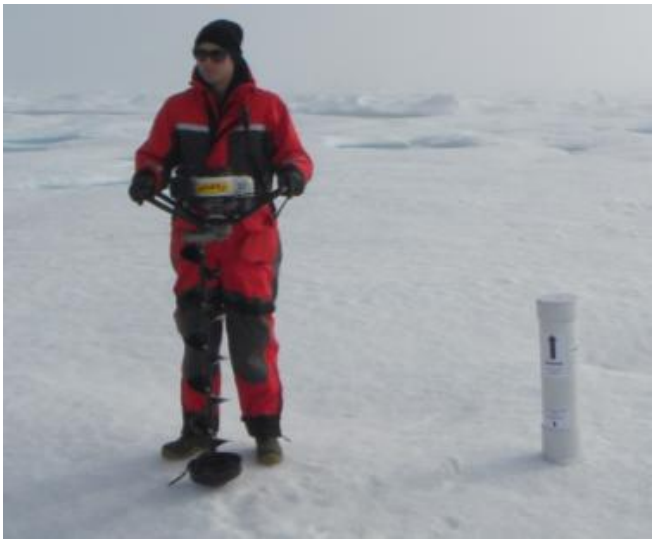

Figure 63. *Deploying a Canatech ice motion beacon.*

Note that sites were classified within the respective Box and Site but a subsequent Remote value was added, ex: the first remote site within Box 1 Site 1 was classified as Box 1 Site 1 Remote 1 (B1S1R1).

4.10.2 Methods and Data

4.10.2.1 Ice motion beacons

A total of 19 ice motion beacons were deployed over the course of Leg 2A. 3 of these were deployed on 3 ice islands by Dr. David Barber and Dr. Simon Prinsenberg on August 16th, while the remaining 16 were deployed on primary and secondary sites between August 16th and 18th. A combination of Canatec and Oceanetics ice tracking beacons were deployed. Canatec beacons were set to transmit location every 15 minutes while the Oceanetics beacons were programmed for every 1-2 hours.

Below is a preliminary drift map of the 10 Canatec beacons (Figure 64). Note the inertial loops within the yellow and pink tracks. From this data divergence events can be monitored, while overall motion can be related to atmospheric forcing fields. The true test of the ice motion beacons is how long they survive, ideally the beacons can last up to 1 year, however they rarely last this long.

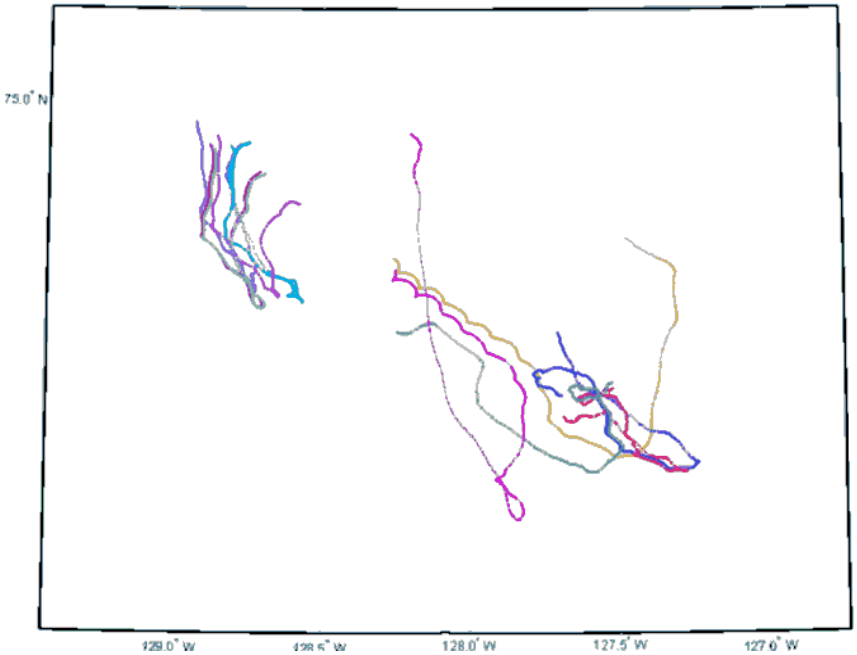

Figure 64. *Ice motion map from the 10 Canatec beacons deployed during Leg* 2A.

4.10.2.2 Physical Ice Properties

To classify the secondary flows several physical characteristics, such as ice thickness and temperature and salinity profiles were collected. In total 6 sites were sampled. Generally all sites were Multiyear ice with similar linearly decreasing temperature profile (1.0 - -1.5°C) and increasing salinity profiles (0 – 6.0 ppt). However a very old flow > 100 feet thick (B1S2R1) was sampled and while the temperature profile remained consistent with the others, the

salinity profile was very fresh with salinities between 0 – 0.5 ppt. Below find a sample of the typical ice temperature and salinity profiles and the profiles from site B1S2R1,

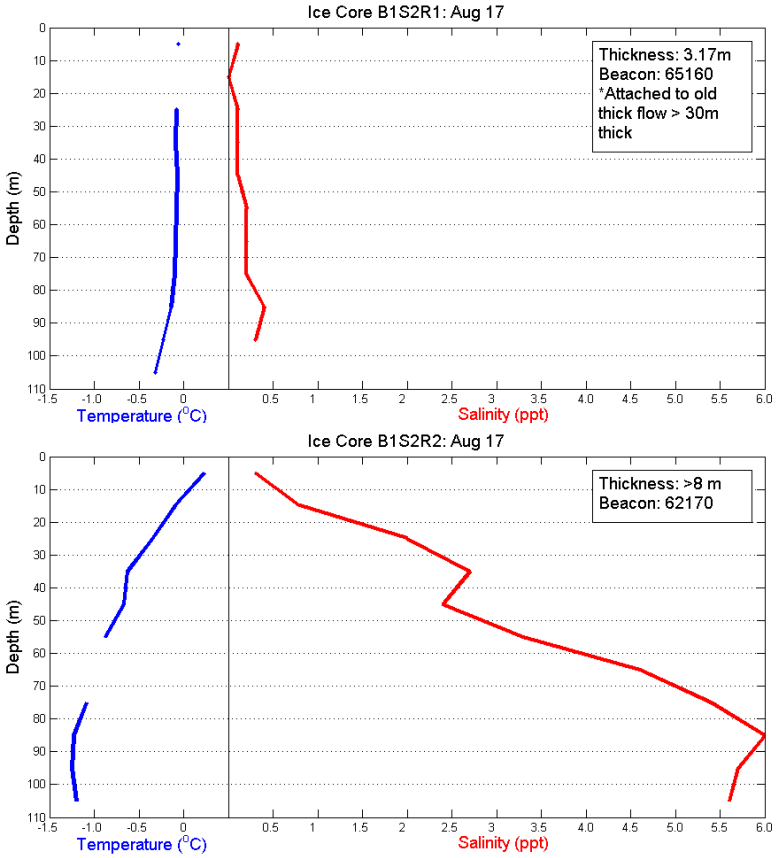

Figure 65. *Typical ice temperature and salinity profiles from site B1S2R1.*

4.10.3 Data Summary

15 ice drift beacons were deployed on mobile FY or MY ice during the 2011 field season.

Table 22: Beacons deployment summary :

Manufacturer	Beacon ID	Deployment Date	Deployed by :	Deployment Location
Canatec	115320	August 15th p.m.	Babb, J.B and D.B by Skippy	B1 S1 R1
Canatec	118310	August 18th am.	Babb, J.B and D.B by Skippy	B1 S2 (not at a full R station, Small drifting floe near B1 S2 R1)
Canatec	421340	August 16th a.m.	D.B. and S.P. by helicopter	Deployed on Large Ice island
Canatec	425340	August 18th p.m.	Babb, J.B and D.B by Skippy	B1 S2 (not at a full R station, Very Large ridge forward of the ship)
Canatec	425350	August 16th a.m.	D.B. and S.P. by helicopter	Deployed on Large Ice island
Canatec	426350	August 18th p.m.	Babb, J.B and D.B by Skippy	B1 S2 (not at a full R station, Flat piece of ice forward of the ship, Near 527940 and 425350)
Canatec	429340	August 18th p.m.	Babb, J.B and D.B by Skippy	B1 S2 Primary Site, 300 metres from the ship on a hummock. Floe broken night of August 18th
Canatec	429350	August 16th a.m.	D.B. and S.P. by helicopter	Deployed on Large Ice island
Canatec	520920	August 16th p.m.	Babb, J.B and D.B by Skippy	B1 S1 R3
Canatec	527940	August 18th p.m.	Babb, J.B and D.B by Skippy	B1 S2 (not at a full R station, Very Large ridge forward of the ship)
Oceanetics	280070	August 16th p.m.	Babb, J.B and D.B by Skippy	B1 S1 R4
Oceanetics	281060	August 16th p.m.	Babb, J.B and D.B by Skippy	B1 S1 R4 (Other side of lead from 280070 on primary floe)
Oceanetics	285060	August 15th p.m.	Babb, J.B and D.B by Skippy	B1 S1 R2
Oceanetics	65160	August 17th p.m.	Babb, J.B and D.B by Skippy	B1 S2 R1
Oceanetics	62170	August 17th p.m.	Babb, J.B and D.B by Skippy	B1 S2 R2

Drift buoy data files are currently being downloaded daily, and processed into an ASCII text file. The most recent quality-assured data is included as of 12 January 2011 at:

\SEA ICE\IDB

Data file header description is as follows:

Iridium modem ID
Unit Serial Number
Date: (dd/mm/yyyy)
Internal Variable
Latitude (decimal degrees)
Hemisphere (N/S)
Longitude (decimal degrees)
Hemisphere (E/W)
Altitude* (m)
Speed (m/s).
direction (degrees).

*GPS Altitude from these beacons is unreliable, and beacon altitude should be assumed to be within 2m of mean sea level.

4.11 Surface Temperature: Infrared Transducer

A downward-looking Infrared temperature sensor (Model Everest 4000.4ZL), mounted at 30° from the vertical, took surface temperature measurements at a 15 second sampling interval. The instrument is installed on the starboard gunwale on the foredeck, facing the ocean surface (Figure 66). It operates at 8 - 12 microns wavelength of the electromagnetic spectrum. The data collected from this instrument is typically used to characterize the surface temperature during C-Band scatterometer scans.

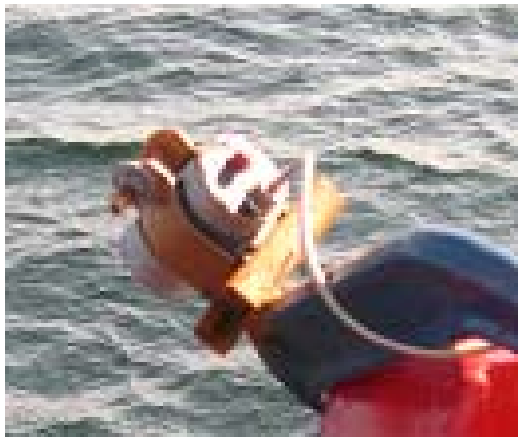

Figure 66. *Everest 4000.4ZL mounted on the starboard gunwale of the CCGS Amundsen at 30° from the vertical.*

The infrared transducer was deployed during 2011 as part of the micrometeorological tower and data is available in the daily processed MET files.

\ATMOS\TOWER\MET

SECTION 5: METEOROLOGICAL DATA

5.1 Micrometeorology Tower Program

5.1.1 Introduction

The motivation for this work stems from the general poor understanding of the processes that exchange nutrients, heat and momentum between the near ocean surface and atmosphere in the Arctic Ocean and peripheral seas. The group's focus is the exchange of CO2, heat and momentum, and in particular to achieve a better understanding of the role of sea ice (full and partial ice cover) and surface surfactants on the transport and exchange of the respective entities.

Specific objectives relate to the development of tools (observation, model, and remote sensing) to assist with regional budgeting of (primarily) heat, CO2, and momentum, and in the longer term, to develop the necessary process-level understanding of the exchange processes, to forecast how the ocean's response to climate change and variability will affect the atmosphere-ocean cycling of CO2.

Novel to our air-sea studies is the ship-based application of the eddy covariance technique for the direct measurement of heat, CO2 and momentum. Eddy covariance represents the lone local scale (100s m to km) direct micrometeorological measurement of the respective fluxes.

The surface meteorology and flux program of the CCGS *Amundsen* is designed to record basic meteorological and surface conditions, and to study exchanges of momentum, heat and mass across the atmosphere-sea ice-ocean interface in support of the objectives described above. Our group's 2011 ArcticNet monitoring and sampling program was designed to accommodate the monitoring requirement of IORVL within the the southern Beaufort Sea.

5.1.2 Methods

The micrometeorological tower located on the front deck of the CCGS *Amundsen* (Figure 67) provides continuous monitoring of meteorological variables and eddy covariance parameters. The tower consists of slow response sensors that record bulk meteorological conditions (air temperature, humidity, wind speed/direction, surface temperature) and fast response sensors that record the eddy covariance parameters (CO_2/H_2O concentration, 3D wind velocity, 3D ship motion, air temperature) (Table 23). In addition, radiation sensors (Figure 68, Table 23) were installed on the roof of the wheelhouse to provide information on incoming long-wave, short-wave, ultraviolet, and photosynthetically active radiation. All data was logged to Campbell Scientific dataloggers; a model CR3000 logger was used for the eddy covariance data, a CR1000 logger for the slow response met data, and a CR23X for the radiation data. All loggers were synchronized to UTC time using the ship's GPS system as a reference. Ship heading and location (lat., lon.) were measured to compensate measured apparent wind information for ship direction and motion.

The eddy covariance system on the tower makes use of two separate gas analyzers and a single 3D sonic anemometer. The dual gas analyzers system allows us to make use of both closed path and open path eddy covariance systems. The open path gas analyzer has the benefit of making measurements concurrently with the sonic anemometer, but the closed path gas analyzer is not as easily disturbed by adverse weather conditions.

In order to make sure that the two systems are comparable, careful calibrations are performed on both instruments. The closed path system is based on a LI-7000 gas analyzer which employs two optical cells, one of which was used to monitor the drift of the instrument by constantly passing a stream of ultra-high purity N_2. In addition, the sample cell of the instrument is calibrated daily using the ultra-high purity N_2 to zero the CO_2 and H_2O measurements, and a reference gas of known CO_2 to span the instrument. Occasionally, a span calibration of the H_2O sensor is performed using a dew point generator (model LI-610). The open path gas analyzer (LI-7500) cannot be calibrated as conveniently, and so it is calibrated approximately every three weeks. In general, we find that this is effective for this particular instrument, which does not drift significantly over time.

The ship motion correction necessary for the application of the eddy covariance technique requires accurate measurement of ship motion (3-axis measurement of angular acceleration and rate), heading and location. Rotational motion is monitored using a multi-axis inertial sensing system. Data related to heading and location is available from the ship's GPS and gyro. Using these data yaw, pitch and roll, in addition to translational motion is calculated, and collectively this information is used to correct our 3D wind measurements.

In addition to the eddy covariance solution to air-sea fluxes, data are collected for the more commonly used bulk approximation. Note however that the bulk approximation is unable to deal with ice in the flux footprint. This last point is a central research theme.

Figure 67: *Meteorology and flux program instrument setup. See Table 13 for description of instruments based on the numbers.*

Figure 68: *Meteorology and flux program instrument setup. See Table 13 for description of instruments based on the numbers.*

5.1.3 Dataset Details

Much of the flux tower was fully operational 11 - 25 August 2011. The slow sequence, largely meteorological variables, are scanned at 1s intervals and saved as 1 min averages. Data screening and ship motion correction to wind speed and direction is applied during post-processing. Wind data are screened for times when the apparent wind direction is forward of the ship's wheelhouse. Heavy rime will affect the measurement of wind speed and these periods are also removed from the data set.

The high frequency variables associated with the eddy covariance system are scanned at 0.1 s intervals and are stored as raw data and as 1-minute averages. The raw data are used to compute the fluxes (heat, mass and momentum) over time intervals that can range from 10 min. to 60 min. Frost, rime and aggressive sea spray affect our high frequency measurements of 3D wind and gas concentrations. Periods associated with these events are evident in the data, and need to be removed prior to processing. Fluxes are post-processing computed.

Table 23: Description of instruments shown in figure 67.

Figure 1	Sensor	Variables	Units	Ht from deck (r	Scan (s) / Ave (min)	Specs
1	wind monitor (RMYoung 05103)	ws-2D, wd-polar	m/s; º	8.11	1/1	±0.6 m/s ±3º deg
2	temperature/relative humidity probe (Vasailla HMP45C212)	Ta, RH	ºC; %	7.2	1/1	Humidity ±2% 0-90% @ 20ºC ±3% 90-100% @ 20ºC 0.05% RH/ºC Temperature ± 0.1 ºC
3	3D wind velocity (Gill Windmaster Pro ultra-sonic anemometer)	u,v,w, Ts	m/s; ºC	6.36	10 Hz	RMS noise <1% offset <0.01 m/s SOS < 0.5% accuracy
4	LI7500 open path gas analyzer	ρ_v /ρ_c	μmol/m^3 mmol/m	6.82	10 Hz	RMS noise ±0.1 μmol/mol zero drift 0.1 μmol/mol/ºC gain drift 0.1%/ºC
5 (inlet)	LI7000 closed path gas analyzer	ρ_v /ρ_c	μmol/mo mmol/m	inlet at 6.49	10 Hz	RMS noise ±0.1 μmol/mol zero drift 0.3 μmol/mol/ºC gain drift 0.2%/ºC
Not shown	multi-axis inertial sensor (MotionPak, Systron Donner)	rx,ry,rz accx,accy,ac	º/s; g	4.59	10 Hz	rate <0.004º/s acc <10 μg
6	pyranometer (Eppley, model PSP)	SW_in	W/m^2		2/1	~±5%
7	quantum sensor (Kipp & Zonen, PARLite)	PAR	μmol/m^2		2/1	~±5%
8	pyrgeometer (Eppley, model PIR)	LW_in	W/m^2		2/1	~±10%
Not shown	surface temperature (Apogee SI-111 precisio infrared radiometer)	Tsfc	ºC	1.6 m	1/1	±0.2 ºC accuracy @ -10 to 65 ºC ±0.5 ºC accuracy @ -40 to 70 ºC
Not shown	pressure transducer (RM Young, 61205V)	Patm	kPa		2/1	±0.5 hPa accuracy
9	UV radiation (Kipp & Zonen model UV-S-AB-T)	T_UV, UV_A UV_B	deg C W/m2		2/1	Daily uncertainty <5%
Not shown	GPS Receiver (Garmin GPS16X-HVS)	lat, lon, SOG COG	º,kts, º		1	Position: <15m, velocity, 0.1 kno
Not shown	Digital compass (Ocean Server OS5000)	H, pitch, roll	º		1	Precision: 0.5 deg (heading) <1 deg (roll/pitch)

The Micrometeorology datasets are available at:

\ATMOS\TOWER\MET

Where daily files are named using the following convention:

proc_MET_YYYY_JDXXX_MMDD.dat

Radiation datasets are available at:

\ATMOS\TOWER\RAD

Where daily files are named using the following convention:

proc_RAD_YYYY_JDXXX_MMDD.dat

For both MET and RAD files, the naming convention corresponds to date information:

YYYY = year
JDXXX = julian day of year
YYDD = month, day of year

Header information for the MET files is presented in Table 24, and the RAD files in Table 25.

Table 24: Header information for the MET files.

Header	Units	Description
Year		
Month		
Day		
Hour		-DATES/TIMES IN UTC
Min		
Sec		
ProgVer		Datalogger program version used (e.g. foredeck_met_2010_v1.1)
batt_volt_min	V	Minimum datalogger battery voltage, useful for identifying poor datalogger performance
panel_temp_avg	deg C	Temeprature of data logger, useful for identifying poor datalogger performance
batt_volt_std		Standard Deviation of battery voltage over 1 minute averaging period, useful for identifying poor datalogger performance
panel_temp_std	V	Panel temperature standard deviation over 1 minute averaging period, useful for identifying poor datalogger performance
t_hmp_avg	deg C	Atmospheric temperature, measurement height ~14m above sea level
rh_hmp_avg	%	Atmospheric relative humidty, measurement height ~14m above sea level
Tsrfc_avg	deg C	Surface skin temperature measured from infrared radiometer
Patm_avg	kPa	Atmospheric pressure
Raw_W_Vel	m/s	Raw wind velocity, uncorrected for ship motion
Raw_W_Dir	deg	Raw wind direction (0/360=wind blowing into front of ship)
Raw_W_std	deg	Raw wind direction standard deviation
t_hmp_std	deg C	Atmospheric T standard deviation over 1 minute averaging period
rh_hmp_std	%	Relative Humidity standard deviation over 1 minute averaging period
Tsrfc_std	deg C	Surface temperature standard deviation over 1 minute averaging period
Patm_std	kPa	Atmospheric pressure standard deviation over 1 minute averaging period
Lat	deg	Latitude of observation (obtained from Ship GPS system)
Long	deg	Longitude of observation (obtained from ship GPS system)
SOG	kts	Speed over ground of ship (obtained from ship GPS system)
COG	deg	Course over ground of ship (obtained from ship GPS system)
Heading	deg	Heading of vessel relative to true north (obtained from ship Gyro system)
SOG_std	kts	Speed over ground of ship standard deviation
COG_std	deg	Course over ground of ship standard deviation
True_W_Vel	m/s	True wind velocity corrected for ship motion, measurement height ~14m above sea level
True_W_Dir	deg	True wind direction relative to true north, measurement height ~14m above sea level
Diag		Diagnostic code word for data processing. If 'NaN', data is ok: 1=tower down, 2=faulty conventional anemometer, 3=faulty infrared radiometer, 4=faulty T/RH probe, 5=faulty P sensor
Pitch	deg	Pitch angle of the tower relative to sea surface (for diagnostic purposes)
Roll	deg	Roll angle of the tower relative to sea surface (for diagnostic purposes)

Table 25: Header information for the RAD files.

Variable	Units	Description
Year		
Month		
Day		
Hour		
Minute		
Second		
Batt_avg	V	Average battery voltage of datalogger (used for some diagnostics)
Panel_T_avg	deg C	Temperature of datalogger
Kdown_avg	W/m2	Incoming shortwave radiation
Thermopile_avg	W/m2	Thermopile measurement of long wave radiation sensor (intermediate value for calculating incoming LW)
Tcase_avg	K	Temperature value of long wave radiation sensor (intermediate value for calculating incoming LW)
Tdome_avg	K	Temperature value of long wave radiation sensor (intermediate value for calculating incoming LW)
LWin_avg	W/m2	Incoming longwave radiation
PARmd_avg	umol/m2/s	Incoming photosynthetically active radiation measured on top of wheelhouse
T_UV_avg	deg C	Temperature of UV radiation sensor
UV_B_avg	W/m2	Incoming UV-B radiation
UV_A_avg	W/m2	Incoming UV-A radiation
PARft_avg	umol/m2/s	Incoming photosynthetically active radiation measured on the flux tower
Batt_stdev	V	Standard deviation of battery voltage over 1 min averaging period
PanelT_stdev	deg C	Standard deviation of datalogger temperature over 1 min averaging period
Kdown_stdev	W/m2	Standard deviation of incoming shortwave radiation over 1 min averaging period
Thermopile_stdev	W/m2	Standard devaiation of Thermopile over 1 min averaging period
Tcase_stdev	deg C	Standard deviation of Tcase over 1 min averaging period
Tdome_stdev	deg C	Standard deviation of Tdome over 1 min averaging period
LWin_stdev	W/m2	Standard deviation of incoming longwave radiation over 1 min averaging period
PARmd_stdev	umol/m2/s	Standard deviation of incoming PAR measured on top of wheelhouse over 1 min averaging period
T_UV_stdev	deg C	Standard deviation of UV sensor temperature over 1 min averaging period
UV_B_stdev	W/m2	Standard deviation of incoming UV-B over 1 min averaging period
UV_A_stdev	W/m2	Standard deviation of incoming UV-A over 1 min averaging periiod
PARft_stdev	umol/m2/s	Standard deviation of incoming PAR measured on the flux tower over 1 min averaging period
Latitude	deg	Latitude at time of measurement (from ship GPS data)
Longitude	deg	Longitude at time of measurement (from ship GPS data)

5.2 Passive Microwave Temperature and Water Vapour Profiles

5.2.1 Microwave Profiling Radiometer

A Radiometrics temperature and water vapour 3000A profiling radiometer (TP/WVP3000A) is used to measure the temperature and water vapour within the atmosphere up to 10km using passive microwave radiometry at 22 – 29GHz, and 51 – 59GHz. The TP/WVP3000A is installed on a mount attached to the white container laboratory (the 'Met Shack') located directly behind the ship's wheelhouse, approximately 19m above sea level (figure 5). The instrument is suspended away from the roof of the shed to ensure that the field-of-view (approximately 15° above the horizon to the left and right to the zenith) is clear of any obstruction (figure 69).

Figure 69: *TP/WVP 3000A mounted on the roof of the CCGS Amundsen 'met shack.'*

The radiometer sequentially views atmospheric radiances from the zenith direction in 12 channels - seven in the oxygen band (51-59 GHz) provide information on the temperature profile, and 5 between 22-30 GHz provide information on the humidity profile. The instrument set-up included sensors for surface pressure, temperature and humidity, and a zenith-pointing infrared radiometer (9.6-11.5 μm), which provides cloud-base altitude. The radiometer system rejected periods when the profiles may be erroneous due to precipitation scattering, and/or due to emissions from moisture on the radome filter.

The instrument generates a vertical profile of upper-level air variables including temperature, water vapour density, relative humidity, and liquid water from the surface to an altitude of 10km (Figure 70). The resolution of the measurements varies with height. The resolution of the instrument is 50 m from the surface to an altitude of 500 m, then increases to 100 m from 500 m to 2 km altitude, and is 250 m for measurements from 2 km to 10 km. Note: the height given for 50 m is actually 69 m as the instrument assumes it's at sea level when it's mounted 19m above sea level. In addition, the instrument also measures concurrent basic surface meteorology variables, including pressure, relative humidity, and ambient temperature. A

skyward-looking infrared sensor measures the temperature of the sky. A rain-sensor detects the presence of any precipitation. It should be noted that the fog registered as precipitation during much of the field season. The instrument also calculates integrated column water vapour, and liquid water content. The sampling frequency for all data is approximately one complete profile per minute.

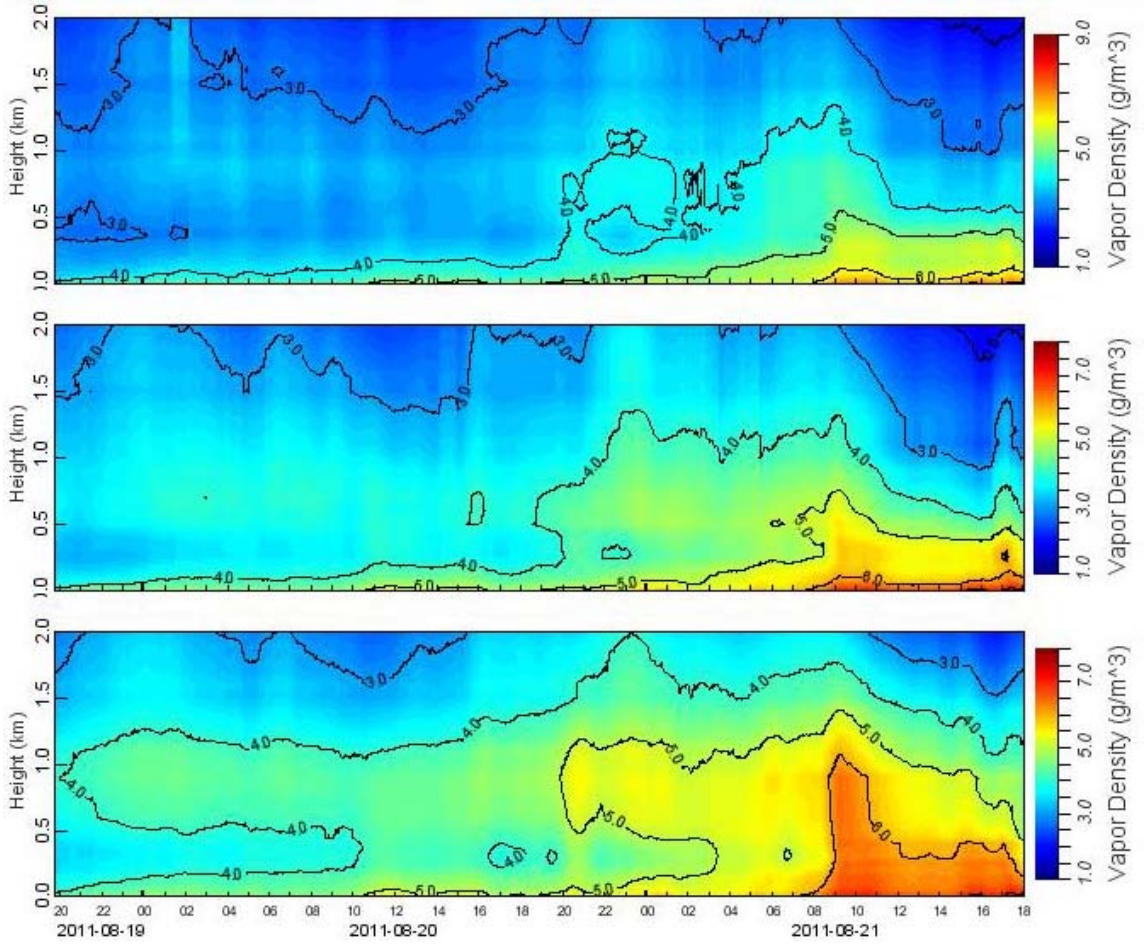

Figure 70. *Shows the off zenith angle scans, (top panel is starboard, middle panel is port) and the bottom panel shows the zenith scan from August 19th 2000 UTC to August 21st 1800 UTC.*

The calibration of the water vapour profiling process was continuously maintained by hourly tip curves. An external liquid-nitrogen-cooled blackbody was used to intermittently calibrate the temperature profiling process. All channels also viewed an internal black body target every 5 minutes for relative calibration. Temperature and humidity values (0 to 200 m at 50 meter intervals, 500 to 2000 m at 100 meter intervals, and 2000 to 10,000 m at 250 meter intervals) were derived from microwave brightness temperatures using the manufacturer's neutral network retrievals that had been trained using historical radiosonde measurements, and a radiative transfer model (Solheim et al., 1998). Historical radiosonde data from Inuvik N.W.T. was used to develop neural network coefficients for the Southern Beaufort Sea Region.

5.2.2 Data Summary

The TP/WVP 3000A was operational throughout the field season, July 11 to August 26. On July 12 the Barrow Alaska neural network was started. The neural network was problematic and the data from August 12th until August 19th will need to be post processed and will be made available when ready.

Typically, this data resides at:

\ATMOS\MWP

Datafiles follow the naming convention:

YYYY-MM-DD_HH-MM-SS_tip.csv
YYYY-MM-DD_HH-MM-SS_lv0.csv
YYYY-MM-DD_HH-MM-SS_lv1.csv
YYYY-MM-DD_HH-MM-SS_lv2.csv

Header information for these files is included in the first 6 lines of each data file.

Files with "*.Lv0, *.Lv1, and *.Lv2" are the raw, first-order processed, and second-order processed datafiles. The "*.tip" files are the daily TIP calibration files used by the radiometer, and are included for reference. The "Lv2" files are the files of interest to the end-user. Records marked 401 – 404 are the key records as they describe the vertical atmospheric profiles of temperature, water vapour density, liquid water, and relative humidity as post-processed by the TP/WVP3000A.

The variable abbreviations are described in table 26.

Table 26: Microwave Profiling Radiometer "Level 2" file header.

MWP File	Units	
Tamb	K	Surface Ambient air temperature
Rh	%	Surface relative humidity
Pres	Mb	Barometric pressure
Tir	K	Sky temperature (Infrared thermometer)
Rain	n/a	Rain sensor (1 or 0)
Vint	Cm	Vertically integrated water vapour (0 – 10km column total)
Lqint	Mm	Vertically integrated liquid wanter (0 – 10km column total)
Cldb	km	Cloud base height
Record 401	K	Atmospheric profile temperatures for 0 – 10km
Record 402	g/m^3	Atmospheric integrated vapour profile for 0 – 10km
Record 403	g/m^3	Atmospheric liquid water profile for 0 – 10km
Record 404	%	Atmospheric relative humidity profile for 0 – 10km

5.2.3 Problems and Recommendations

For the 2011 field season two new neural networks were purchased for the MWRP. These neural networks were purchased for the Baffin Bay region and Beaufort Sea. Both neural networks have the capability to profile in the zenith, to the port side of the ship (15 above

horizon) and to the starboard (15 degrees above horizon). The neural networks were not acquired prior to the departure of the *Amundsen* and as such much of the time on leg 1 was spent trouble shooting the new neural networks. During future field seasons this should no longer be a problem as the issues will have been resolved prior to the departure.

5.3 Weather Balloon Temperature and Water Vapour Profiles

Balloon launches can be used to profile low-pressure systems, cyclones, and periods of significant warm or cold-air advection aloft. During leg 2A radiosondes were launched on a regular schedule of every 6 hours. The radiosondes were being used to profile the atmosphere over the ice pack. As of Aug 19 all on-ice operations were halted; this caused the change in schedule for balloon launches. A total of 24 radiosondes were purchased during 2011 with 12 left as of Aug 19. Due to the limited number of new radiosondes the schedule then was changed to profile a large low-pressure system that moved up from the southwest into the region and interacted with a low-pressure system that was stalled in the northern Beaufort Sea. The 12 radiosondes were launched in 6 hour intervals to capture the changing upper atmosphere from Aug 21 0600 UTC until Aug 24 0000 UTC.

Vertical profiles of temperature, pressure, relative humidity, wind speed and wind direction were obtained using Vaisala RS92G GPS wind-finding radiosondes. The sonde was flown by 300 gm and 200 gm helium-filled balloons at a target ascent rate of 2 to 5 m/s to ensure a good vertical resolution through the boundary layer. An 8-channel uncoded GPS receiver in each sonde automatically detects all satellite signals in visible range. Raw wind vectors are transmitted to the ground station every 0.5 seconds during the flight via digital 1200 baud downlink. All wind computation is done within the ground equipment. Temperature is measured with a THERMOCAP® Capacitive bead, which has a +600C to -900C range, resolution of 0.10C and accuracy of 0.20C up to 50 hPa (most launches terminated before this level). The sensor also has a lag of less than 2.5 seconds in 6 m/s flow at 1000 mb. Pressure is measured with a BAROCAP® Capacitive aneroid. Its measuring range is 1060 mb to 3 mb with a resolution of 0.1 mb and accuracy of 0.5 mb. Humidity s measured with a HUMICAP® thin film capacitor. Its measuring range is from 0 to 100% relative humidity, with a resolution of 1% relative humidity and accuracy of 3%.

The sensor also has lag of 1 second in 6 m/s flow, 1000 mb pressure and +200C. The temperature, pressure and humidity sensors are collectively sampled at 7 times per 10 seconds. All raw data from the sonde are processed at the ground station through a DigiCORA/MARWIN processor. The DigiCORA is connected to a computer, where data can be viewed in real time throughout the launch and where the data is archived. PILOT and TEMP codes are also produced after the launch terminates. PILOT and TEMP codes, as well as raw and edited measurements were archived for each launch. The edited data is stored in a text file in delimited columns.

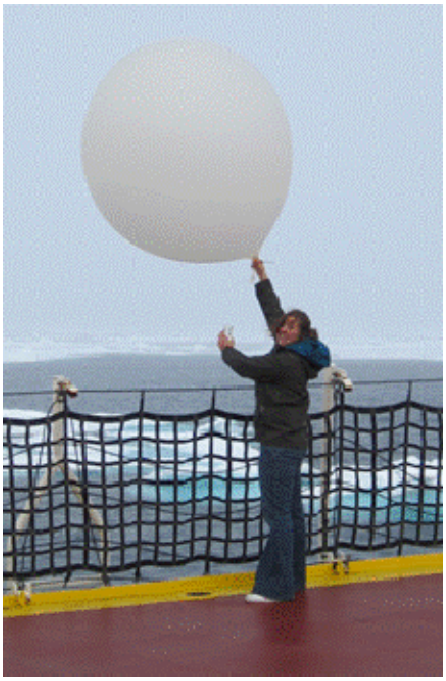

Figure 71. *A weather balloon with attached radiosonde, ready to be launched from the helicopter deck.*

Before launch, the radiosonde's temperature, pressure and humidity sensors are calibrated using the Vaisala ground station calibration unit. Surface meteorological observations are also noted and recorded for each launch. Starting meteorological conditions are input into the sounding including: sea level pressure, air temperature, relative humidity, and wind speed and direction.

Data is transmitted at a rate of one message per second via VHF radio (~400.00MHz). Each data message reports a value for pressure, temperature and humidity data (raw PTU data). GPS strings are also transmitted, and are used to calculate upper-level wind speed and direction. All raw PTU and GPS data is used to generate an ensemble of time series data (figure 72).

Record name:	Unit:	Data type:	Divisor:	Offset:
time	sec	float (4)	1	0
Pscl	ln	short (2)	1	0
T	K	short (2)	10	0
RH	%	short (2)	1	0
v	m/s	short (2)	-100	0
u	m/s	short (2)	-100	0
Height	m	short (2)	1	30000
P	hPa	short (2)	10	0
TD	K	short (2)	10	0
MR	g/kg	short (2)	100	0
DD	dgr	short (2)	1	0
FF	m/s	short (2)	10	0
AZ	dgr	short (2)	1	0
Range	m	short (2)	0.01	0
Lon	dgr	short (2)	100	0
Lat	dgr	short (2)	100	0
SpuKey	bitfield	unsigned short (2)	1	0
UsrKey	bitfield	unsigned short (2)	1	0
RadarH	m	short (2)	1	30000

Figure 72. *Variable denotation header found within radiosonde data files.*

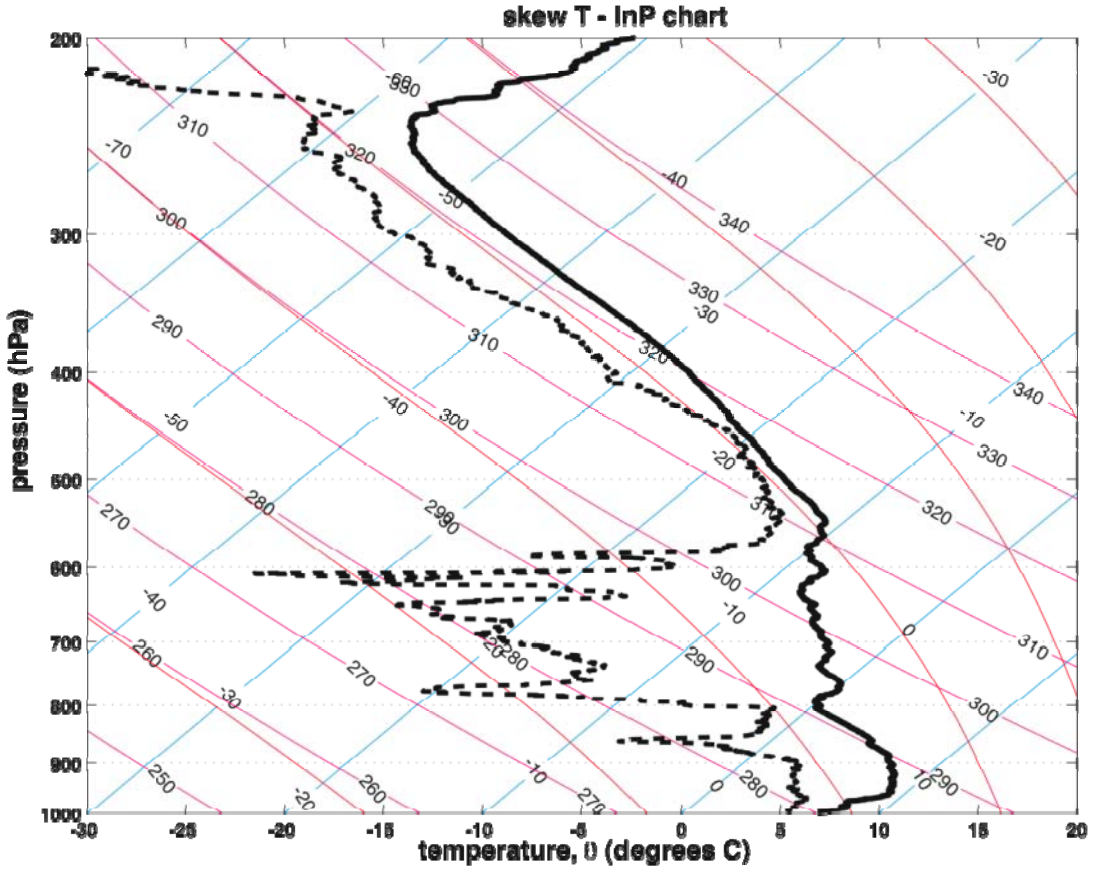

Figure 73. *The radiosonde launch from August 23 0000 UTC.*

Table 27. The radiosonde launch schedule.

Date	Time (UTC)	Lat	Lon	Radiosonde Purchase Year	Balloon Size
August 13	1810	72.48	-129.05	2011	350g
August 13	2330	72.52	-129.23	2008	350g
August 14	1810	74.52	-127.42	2011	200g
August 15	0010	74.51	-128.14	2008	350g
August 15	0620	74.52	-128.17	2011	200g
August 15	1200	74.51	-128.17	2008	350g
August 15	1740	74.51	-128.18	2011	200g
August 16	0000	74.50	-128.16	2008	350g
August 16	0420	74.50	-128.16	2011	200g
August 16	1200	74.50	-128.12	2008	350g
August 16	1750	74.49	-128.11	2011	200g
August 17	0000	74.49	-128.07	2008	350g
August 17	0610	74.48	-128.36	2011	200g
August 17	1200	75.00	-128.53	2008	350g
August 17	1800	75.01	-128.58	2011	200g
August 18	0000	75.01	-128.56	2008	350g
August 18	0600	75.00	-128.55	2011	200g
August 18	1200	74.59	-128.52	2008	350g
August 18	1800	74.58	-128.53	2011	200g
August 19	0000	74.57	-128.51	2008	200g
August 19	0600	74.55	-128.45	2011	200g
August 19	1200	74.46	-128.37	2008	350g
August 19	1820	74.49	-128.41	2011	200g
August 20	0000	74.52	-128.54	2008	350g
August 21	0600	74.54	-127.49	2011	200g
August 21	1200	74.26	-124.49	2011	200g
August 21	1800	74.28	-124.36	2011	200g
August 22	0000	74.30	-123.48	2011	200g
August 22	0600	74.27	-124.39	2011	200g
August 22	1200	74.26	-124.30	2011	200g
August 22	1800	74.26	-124.23	2011	200g
August 23	0000	74.26	-124.21	2011	200g
August 23	0600	74.37	-126.26	2011	200g
August 23	1200	74.50	-128.12	2011	200g
August 23	1800	74.53	-128.18	2011	200g
August 24	0000	74.51	-128.20	2011	200g

The radiosonde data is available in the database at:

\ATMOS\SONDES

5.4 Cloud Base Height

5.4.1 Vaisala CT25K Ceilometer

The Vaisala CT25K laser ceilometer measures cloud heights and vertical visibilities using pulsed diode laser LIDAR (Light Detection And Ranging) technology, where short powerful laser pulses are sent out in a vertical or near-vertical direction. The laser operates at a centre wavelength of 905 ± 5 nm, a pulse width of 100 ns, beamwidth of ±0.53 mrad edge, ±0.75 mrad diagonal and a peak power of 16 W. The manufacturer suggested measurement range is 0 – 25,000ft (0 – 7.5 km), however, it has been found that high, very visible cirrostratus cloud (~18-20 kft) are consistently undetected by the unit (Hanesiak, 1998). The vertical resolution of the measurements is 50 ft, but decreases to 100 ft after ASCII data file conversion. The reflection of light backscatter caused by haze, fog, mist, virga, precipitation, and clouds is measured as the laser pulses traverse the sky. The resulting backscatter profile (i.e., signal strength versus height) is stored, processed and the cloud bases are detected. Knowing the speed of light, the time delay between the launch of the laser pulse and the backscatter signal indicates the cloud base height. The CT25K is designed to detect three cloud layers simultaneously, given suitable conditions. Besides cloud layers, it detects whether there is precipitation or other obstruction to vision. No adjustments in the field are needed. Output files were created hourly by the system and are in ASCII format. The ceilometer measurements were made in conjunction with all-sky camera measurements throughout the entire observational period. Ceilometer data was collected continuously from 11 – 25 August 2011.

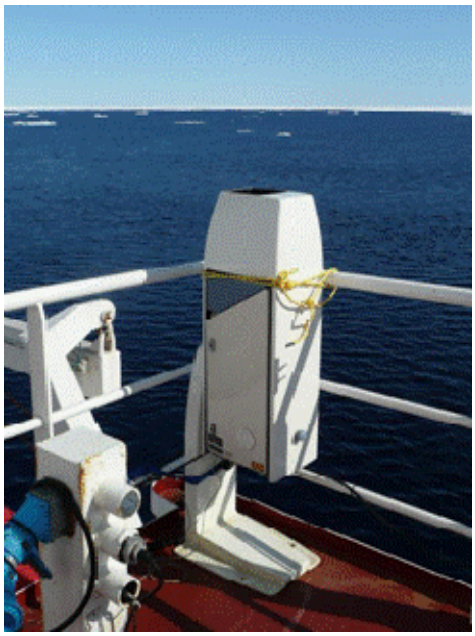

Figure 74. *Vaisala CT25K ceilometer mounted at 90° behind the wheelhouse.*

5.4.2 Data Summary

The ceilometer was running continuously from 11 – 25 August 2011, and daily data files are available for the entire period.

Ceilometer files are available in two forms: Raw daily logs and processed ASCII daily files.

The Processed files are available at

\ATMOS\CEIL\Processed

Daily filenames follow the naming convention:

CEIL_YYYY_MM_DD.csv

The file header information is defined in table 28:

*Table 28: Ceilometer *.CSV file header*

Header	Description	Units
J_day	Julian day of year	n/a
Year	Year	n/a
Month	Month	n/a
Day	Day	n/a
Hour	Hour	n/a
Min	Minute	n/a
Sec	Seconds	n/a
Lat	Latitude	decimal deg (DD.DDDDD)
Lon	Longitude	decimal deg (DDD.DDDDD)
SOG	Speed over ground	Nm / hr
COG	Course over ground	Degrees (°)
Layer1	Cloud layer base height 1	Ft
Layer2	Cloud layer base height 2	Ft
Layer3	Cloud layer base height 3	Ft

5.5 All-Sky Camera Imagery

5.5.1. Instrumentation

The all-sky camera system takes images of the sky and cloud cover. The system consists of a Nikon D-90 camera outfitted with fish-eye lenses with a viewing angle of 160 degrees, mounted in a heated weather-proof enclosure. The camera is programmed to take pictures using an external intervalometer set at 15-minute intervals, or 96 images per day. The system is mounted in a small 'crow's nest' immediately above the ship's wheelhouse (figure 75).

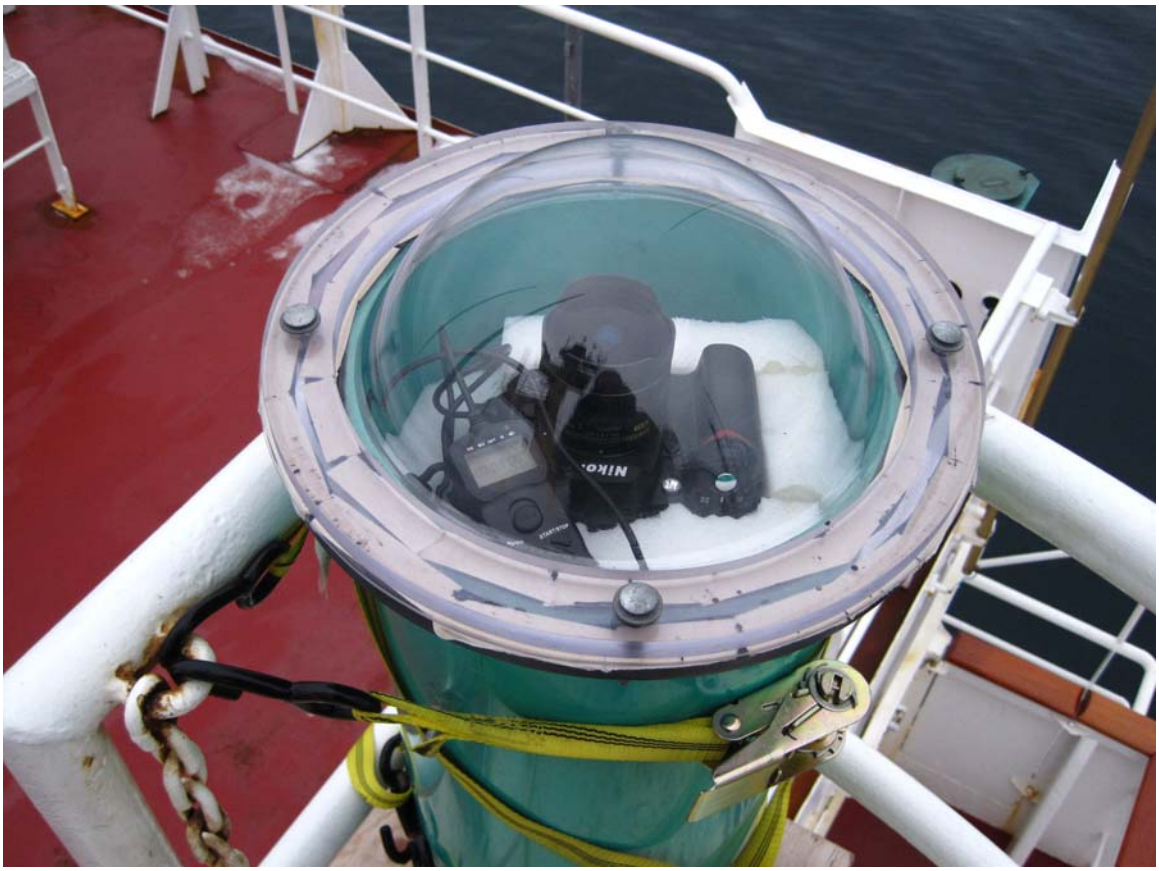

Figure 75. *Nikon D-90 Camera with fisheye lenses attached in a weatherproof enclosure.*

Imagery collection started on August 11th, and was continuous through to August 25th. Gaps in the data are due to routine maintenance and a power failure.

All All-sky images are available in the database at :

\ATMOS\ALLSKY

5.5.2 Data Visualization

A example all-sky image showing 6/8 broken cloud cover is shown in figure 76.

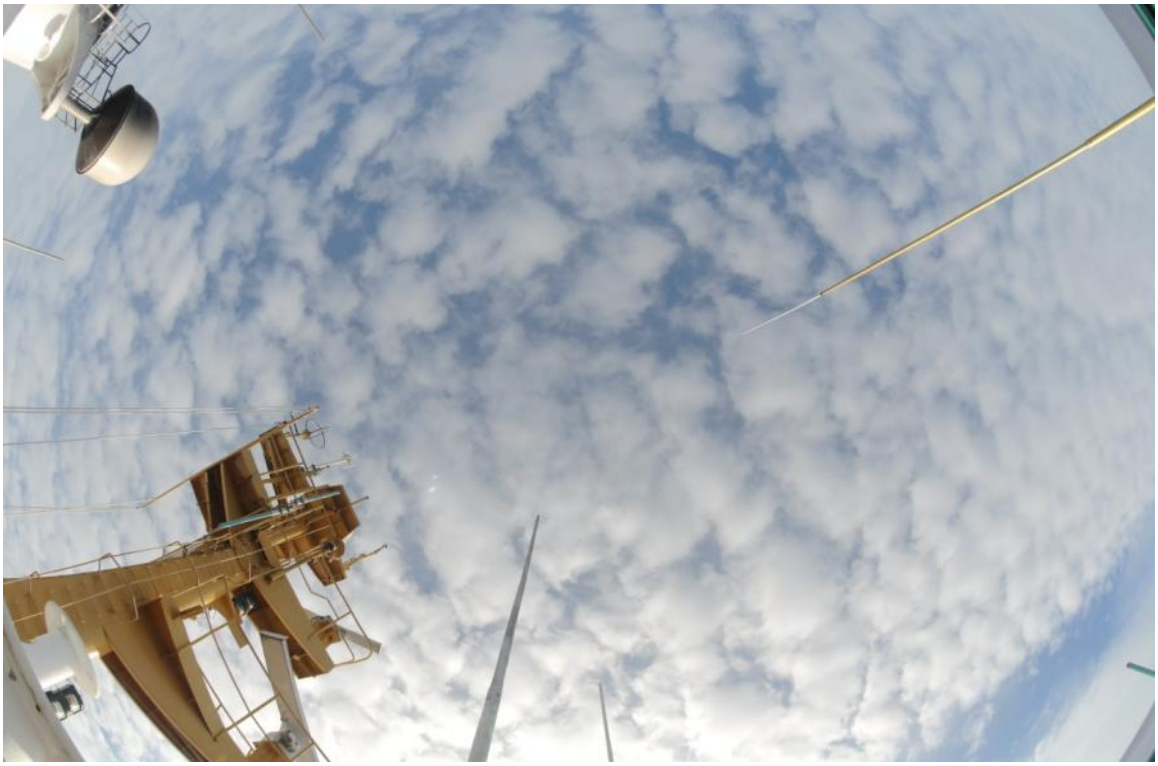

Figure 71. *An All-Sky image from Aug 17 1709 UTC.*

5.6 Manual Meteorological Observations

5.6.1 Instrumentation

Manual meteorological observations were conducted hourly throughout the entire leg, except for at night when observers were sleeping. Observations included current conditions with relation to precipitation type and intensity, visibility, cloud cover (octets), and sea ice coverage (tenths). Basic meteorological values were read and recorded from the onboard weather station, which is owned and operated by the Meteorological Service of Canada. Visibility, cloud octets, sea ice concentration, and precipitation type and intensity observations are subjective based on the observer. If the cloud coverage was not 100% it was not recorded at 8/8, similarly if the coverage has even 1% of clouds the cloud fraction was not recorded as 0/8.

The CCGS *Amundsen* is equipped with an AXYS Automated Voluntary Observation Ship (AVOS), with all sensors located on the roof of the wheelhouse. The AVOS is an interactive environmental reporting system that allows for the hourly transmission of current meteorological conditions to a central land station via Iridium satellite telemetry. Temperatures (air and sea surface), pressure, relative humidity (RH), wind speed, wind direction, and current GPS location are updated every ten minutes and displayed on a computer monitor located in the wheelhouse of the ship. The AVOS deploys a Rotronics MP 101A sensor for temperature and RH, with a resolution of 0.1ºC and an accuracy of ± 0.3ºC, and a 1% ± 1% accuracy for temperature and RH, respectively. Atmospheric pressure was obtained from a Vaisala PTB210 sensor with a 0.01mb resolution and an accuracy of ±0.15 mb. Wind speed and direction is collected from an RM Young 05103 anemometer, accurate to ±3º in direction and ±0.3 m/s.

5.6.2 Data Summary

Table 29: Parameters recorded by the observer.

Parameter	Units
Date	UTC
Time	UTC
Latitude	decimal degrees
Longitude	decimal degrees
Temperature	ºC
Relative Humidity	%
Wind Speed	kts
Wind Direction	º
Precipitation Type	snow, rain etc
Precipitation Intensity	Heavy, moderate, light etc.
Visibility	nm
Cloud Fraction	Octets
Sea Ice Concentration	Tenths

5.7 On-ice Micromet Tower

5.7.1 Instrumentation

The tower (an extendable tripod), 2.5 m high, will be set up on ice against the wind and away from ship to avoid tower and ship's obstructions. The tower had the following instruments (with height above ice surface where applicable):

- 3D sonic anemometer, Gill WindMaster Pro, 2.75 m
- Temperature and Relative Humidity Probe, Vaisala HMP, 2.15 m
- 4-component Net Radiometer, Kipp & Zonen CNR4, 1.35 m
- Surface Skin Temperature, Apogee SI-111 IR Radiometer, 1.35 m
- Barometric pressure, RM Young 61302V pressure transducer, 1.15 m
- GPS, Garmin GPS16X-HVS

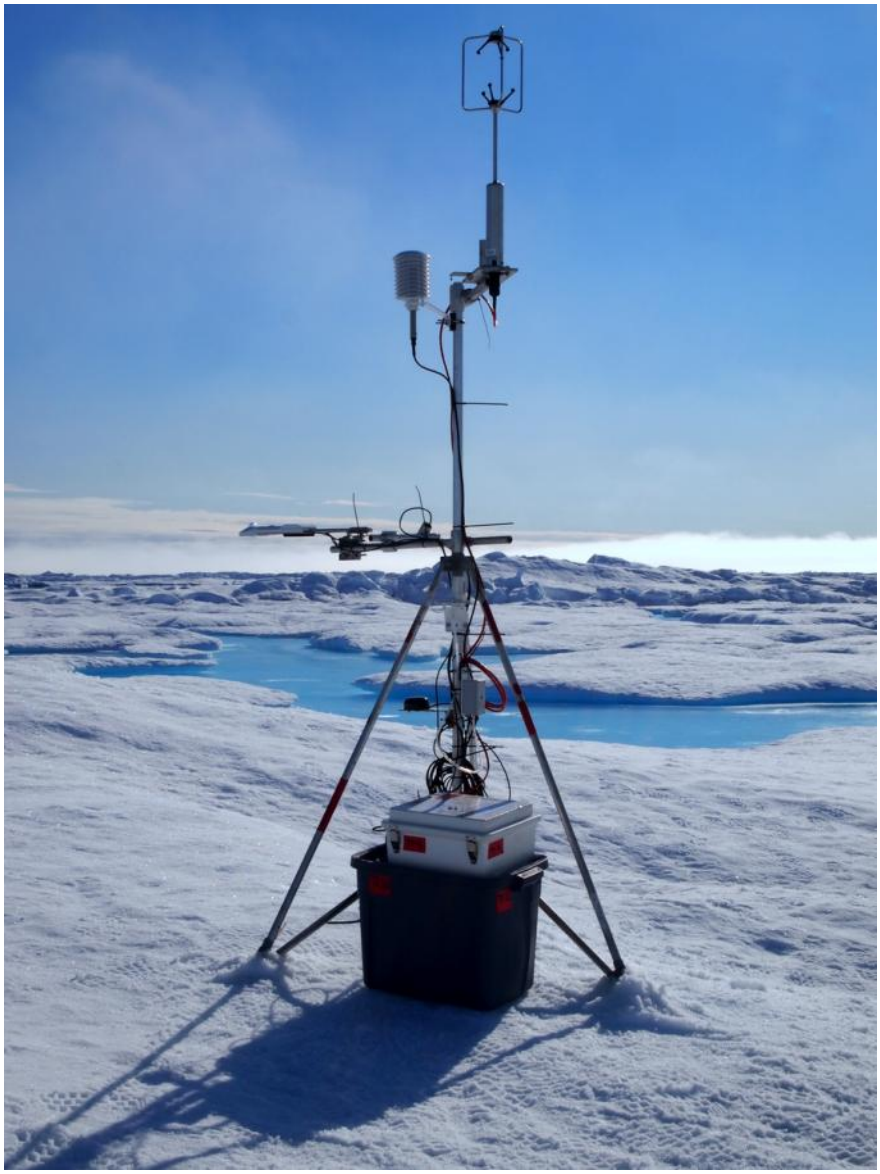

Figure 77. *The on ice tower deployed at Box 1 Site 2.*

The WindMaster Pro is an ultrasonic anemometer for measuring wind speed in three dimensions. It uses three pairs of non-orthogonally oriented transducers to sense the horizontal wind. Each pair of transducers transmits and receives the ultrasonic signal. The time of flight is directly related to the wind speed along the sonic transducer axis. The speed of sound is directly related of the air density, e.g. temperature and humidity. The WindMaster Pro can be used to measure average horizontal wind speed and direction or turbulent fluctuations of horizontal and vertical wind. The height of the anemometer is 2.75 m from the base of the tower. All data is recorded using CR3000 data logger and CFM storage module.

The HMP45C Temperature and Relative Humidity probe contains a Platinum Resistance Temperature detector (PRT) and a Vaisala HUMICAP® 180 capacitive relative humidity sensor. The instrument will be put on the same tower as the CSAT3 sonic anemometer on a different arm. The HMP45C must be housed inside a radiation shield when used in the field. The 41003-X Radiation Shield mounts to vertical or horizontal pipes up to 2 inches in diameter.

The CNR4 is a four component net radiometer is intended for the analysis of the radiation balance of solar and far infrared radiation. Solar radiation is measured by two pyranometers, one for measuring incoming solar radiation from the sky, and the other for measuring reflected solar radiation. Albedo can be determined from these two pyranometers. Far infrared radiation is measured by two pyrgeometers, one for measuring the far infrared radiation from the sky, and the other from the ice surface. The solar radiation spectral range is 0.3-2.8 µm, and the far infrared spectral range is 4.5-42 µm. An optional ventilation/heater unit can be utilized to minimize the formation of dew and melt frost.
The SI-111 is an infrared temperature sensor that provides a non-contact means of measuring the surface temperature of an object. It senses the infrared radiation being emitted by the target.

Variables recorded:

- Ux (m/s) : Orthogonal wind component (east-west)
- Uy (m/s) : Orthogonal wind component (north-south)
- Uz (m/s) : Orthogonal wind component (vertical)
- T_s (°C) :Sonic temperature
- Relative Humidity: RH (%)
- Air Temperature: T_a (°C)
- Incoming solar radiation: K_{in} (W m^{-2})
- Reflected solar radiation: K_{out} (W m^{-2})
- Incoming far infrared radiation: LW_{in} (W m^{-2})
- Outgoing far infrared radiation: LW_{out} (W m^{-2})
- Surface Skin Temperature: T_{srfc} (°C)
- Barometric Pressure: AtmP (kPa)
- Latitude and Longitude (degrees)

OUTPUTS: ux, uy, uz, and c (ux, uy, uz, are orthogonal wind components referenced to the anemometer head; c is the speed of sound)

SPEED OF SOUND: determined from 3 acoustic paths; corrected for crosswind effects

MEASUREMENT RATE: programmable from 1 to 60 Hz, instantaneous measurements; two oversampled modes are block averaged to either 20 Hz or 10 Hz

MEASUREMENT RESOLUTION: ux and uy are 1 mm/s rms; uz is 0.5 mm/s rms; c is 15 mm/s (0.025°C) with embedded code version 4 (standard) [c is 1 mm/s (0.002°C) with embedded code version 3]. Values are the standard deviations of instantaneous measurements made of a constant signal. The noise is unaffected by the sample rate.

OPERATING TEMPERATURE RANGE: -30° to 50°C (standard); -40° to 40°C (cold shifted)

ACCURACY (-30° to 50°C and -40° to 40°C operating range; wind speed < 30 m s-1; azimuth angles between ±170°):

Offset Error:

ux, uy: < ±4 cm/s
uz: < ±2 cm/s

Gain Error:

Wind vector within ±5° of horizontal < ±2 percent of reading
Wind vector within ±10° of horizontal < ±3 percent of reading
Wind vector within ±20° of horizontal < ±6 percent of reading

Physical Description

MEASUREMENT PATH LENGTH: 10.0 cm vertical; 5.8 cm horizontal

TRANSDUCER PATH ANGLE FROM HORIZONTAL: 60 degrees

TRANSDUCER: 0.64 cm (0.25 in) diameter

TRANSDUCER MOUNTING ARMS: 0.84 cm (0.33 in) diameter

SUPPORT ARMS: 1.59 cm (0.63 in) diameter

DIMENSIONS:

Anemometer Head: 47.3 cm (l) x 42.4 cm (h) (18.6 in x 16.7 in)
Electronics Box: 26 cm x 16 cm x 9 cm (10.2 in x 6.3 in x 3.5 in)
Carrying Case: 71.1 cm x 58.4 cm x 33 cm (28 in x 23 in 13 in)

WEIGHT:

Anemometer Head: 1.7 kg (3.7 lb)
Electronics Box: 2.8 kg (6.1 lb)
Shipping: 16.8 kg (37 lb)

Power Requirements

VOLTAGE SUPPLY: 10 to 16 Vdc
2.4 W @ 60 Hz measurement frequency
1.2 W @ 20 Hz measurement frequency

Description of deployment

The tower (an extendable tripod), 2.5 m high, was set up on ice (see site pictures) against the wind and away from ship to avoid tower and ship's obstructions. The height of the anemometer is 2.5 m from the base of the tower. Data is recorded using CR1000 data logger and CFM storage module.

5.7.2 Data Summary

File header information is as follows:

TIMESTAMP (TS) : Record timestamp DD/MM/YYYY HH :MM :SS.S
RECORD (RN) : Serial record number
Ux (m/s) : Orthoganal wind compent (east-west)
Uy (m/s) : Orthoganal wind compent (north-south)
Uz (m/s) : Orthoganal wind compent (vertical)
Ts (°C) : Surface temperature
Diag : Unitless, internal system use variable

The data are available in the database at:

\ATMOS\ON_ICE_MET

SECTION SIX: OTHER CRUISE DATA

6.1 Radarsat Inventory

An inventory of applicable ENVISAT-ASAR, TerraSAR-X and Radarsat-2 SAR imagery has been included in the dataset. The inventory includes all imagery collected from 11 – 25 August 2011 that provide coverage within the study region (lower-right extent 70°40.000'N 127°30.000'W, upper-left extent of 72°25.000'N 137°00.000'W).

the complete inventory is available in the database at:

\OTHER\SAR IMAGES DOC\IOL_2011_SAR.xlsx

6.2 GPS Position

NMEA RMC Strings collected by the CCGS *Amundsen's* DGPS system for the entire field season are processed into daily files, at minute and second intervals.

ASCII files (*.dat extension) are found in the database for 1 minute resolution at:

\OTHER\NAV\GPS_NMEA

Metadata can be found at:

\OTHER\NAV\GPS_NMEA\SYNCAPP

File naming convention is as follows for 1 minute resolution:

\1min_RMC_2011_JDxxx_MMDD.dat

Where: JDxxx corresponds to the julien day, and MMDD is month and day.

File header:

(Dates and times are in UTC).
Year:
Month:
Day:
Hour:
Min: Minute
Sec: Second
Lat: Latitude (decimal degrees)
Lon: Longitude (decimal degrees)
SOG: Speed over ground (nm / hr)
COG: Course over ground (degrees)
SOG_ST: (standard deviation of speed over ground
COG_ST: (standard deviation of course over ground

Note: Many of the GPS files were found to be corrupted during leg 2A. We were able to fill the missing gaps using data from the University of New Brunswick Ocean Mapping Group's GPS stream; however, we are presently negotiating rights of use with them and cannot release this data at this time.

6.3 Gyronometer

The CCGS *Amundsen's* Gyronometer provides ship heading.

ASCII files (*.dat extension) are found in the database at 1 minute resolution:

\OTHER\NAV\Ship_Heading

File naming convention is as follows for 1 minute resolution:

\1min_ GYRO _2011_JDxxx_MMDD.dat

Where: JDxxx corresponds to the julien day, and MMDD is month and day.

File header:

(Dates and times are in UTC).
Year:
Month:
Day:
Hour:
Min: Minute
Sec: Second
Heading: heading (degrees)

Note: Many of the GYRO files were found to be corrupted during leg 2A. We were able to fill the missing gaps using data from the University of New Brunswick Ocean Mapping Group's GPS stream; however, we are presently negotiating rights of use with them and cannot release this data at this time.

6.4 Science Log

The bridge staff of the CCGS *Amundsen* kept a written log of all science activities. For each science entry in the log, date (LST and GMT), geographic position (degree, decimal-minutes, and decimal degrees), depth, and basic meteorological variables including air temperature, relative humidity, wind speed and direction, and sea ice concentration are recorded.

These science logs are also available as digital files in the database at:

\OTHER\Science Logs

LITERATURE CITED:

Asplin, M.G. Barber, D.G. Galley, R. Prinsenberg, S. 2012. Dynamic and thermodynamic implications of storm swell induced fracturing of the summer perennial pack ice in the southern Beaufort Sea, September 2009. *Jour. Geophys. Res. In Review*

Barber, D.G., Galley, R., Asplin, M.G., De Abreu, R. Warner, K., Pucko, M., Gupta, M. Prinsenberg, S., Julien, S. 2009. The summer perennial pack ice in the southern Beaufort Sea was not as it appeared in the summer of 2009. *Submitted to Geophys. Res. Letters (Oct 2009), Manuscript 2009GL041434*

Gunn, R., and Kinzer, G.D., 1949, The terminal velocity of fall for water droplets in stagnant air, *J. of Meteorology*, Vol . 6, pp. 243–248).

Hanesiak, j., 1998: Ice camp meterological observations. *In:* NOW'98 Sea Ice/Climate Dynamic Subgroup Field Summary. Edited by Papakryriakou, T.N., CJ. Mundy, and D.G. Barber. Centre for Earth Observation Science, Geography Department, University of Manitoba, CEOS Tech 98-8-2, pp. 21-32.

Lalumiere, L. and S. Prinsenberg. 2009, "Integration of a Helicopter-Based Ground Penetrating Radar (GPR) with a Laser, Video and GPS System". In Proceedings of the Ninenteenth (2009) International Offshore and Polar Engineering Conference Osaka, Japan, June 21-26, 2009, Vol. I, pp. 658-665.

Peterson, I. K., S. J. Prinsenberg, and J. S. Holladay. 2003 "Sea ice thickness measurement: Recent experiments using helicopter-borne EM-Induction sensors". *Recent REs. Devel. Geophysics, 5 (2003)*, pp. 1-20.

Prinsenberg, S., I. Peterson and S. Holladay, 2008, Measuring the thicknesses of the freshwater-layer plume and sea ice in the land-fast ice region of the Mackenzie Delta using Helicopter-borne sensors,*Journal of Marine Systems*, 783-793

Solheim, F., J. R. Godwin, E. R. Westwater, Y. Han, S. J. Keihm, K. March, and R. Ware (1998), Radiometric profiling of temperature, water vapor, and cloud liquid water using various inversion methods, *Radio Science,* 33, 393 - 404.

APPENDIX A: SCIENCE LOG

LEG 2 B1S1													
14/08/2011	0921	74˚45.00N	127˚18.27W	220	ROSETTE ↓	377	040	19	2.5	8.3	1024	99	-
14/08/2011	0935	74˚44.90N	127˚18.27W	235	ROSETTE ↑	379	040	19	2.5	8.3	1024	99	-
15/08/2011	1031	74˚51.42N	128˚18.78W	310	ROSETTE ↓	388	060	6	-1.1	4.8	1025.1	99	6 - 10
15/08/2011	1048	74˚51.44N	128˚18.76W	310	ROSETTE ↑	388	060	6	-1.1	4.8	1025.1	99	6 - 10
15/08/2011	1550	74˚51.3N	128˚16.5W	310	ROSETTE ↓	389	030	7	-0.5	4.9	1025.3	99	8+/10
15/08/2011	1617	74˚51.3N	128˚16.5W	310	ROSETTE ↑	389	030	7	-0.5	4.9	1025.3	99	8+/10
15/08/2011	1908	74˚50.8N	128˚16.8W	311	ROSETTE ↓	389	040	6	0.0	4.9	1025.05	99	8+/10
15/08/2011	1923	74˚50.8N	128˚16.8W	310	ROSETTE ↑	389	030	6	-0.9	4.9	1024.98	99	8+/10
16/8/2011	1053	74˚49.91N	128˚11.92W	-	ROSETTE ↓	389	340	5	0.6	5.3	1021.9	99	7/10
16/8/2011	1114	74˚49.92N	128˚11.72W	-	ROSETTE ↑	387	340	5	0.6	5.3	1021.9	99	7/10
16/8/2011	1401	79˚49.9N	128˚09.4W	-	ROSETTE ↓	386	330	5	0.3	5.5	1021.2	97	7/10
16/8/2011	1424	79˚49.9N	128˚09.4W	-	ROSETTE ↑	386	330	5	0.3	5.5	1021.2	97	7/10
16/8/2011	1830	79˚49.31N	128˚09.21W	-	ROSETTE ↓	386	270	3	0.8	5.6	1020.00	95	7/10
16/8/2011	1849	79˚49.31N	128˚09.21W	-	ROSETTE ↑	386	270	3	0.8	5.6	1019.96	95	7/10
17/8/2011	1450	75˚01.06N	128˚58.04W	-	ROSETTE ↓	399	LEGER	LEGER	1.5	4.7	1015.5	96	7+/10
17/8/2011	1508	75˚01.06N	128˚58.04W	-	ROSETTE ↑	399	LEGER	LEGER	1.5	4.7	1015.5	96	7+/10
17/8/2011	1908	75˚01.07N	128˚56.61W	155	ROSETTE ↓	396	LEGER	LEGER	0.7	5.16	1014.6	98	8/10
17/8/2011	1925	75˚01.03N	128˚56.56W	155	ROSETTE ↑	395	LEGER	LEGER	0.8	5.20	1014.5	98	8+/10
17/8/2011	1935	75˚01.01N	128˚56.55W	155	EM SCAN	395	LEGER	LEGER	0.6	5.22	1014.5	99	8/10
17/8/2011	2115	75˚00.8N	128˚56.2W	155	EM SCAN	394	240	5	1	5.24	1013.9	91	7/10
18/8/2011	0845	74˚58.9N	128˚52.9W	158	EM SCAN START	394	W	8	0.6	5.24	1013	99	7/10
LEG 2 B1 S2													
18/8/2011	1000	74˚58.7N	128˚53W	158	ROSETTE ↓	396	W	4	0.7	5.25	1013	99	7/10
18/8/2011	1023	74˚58.7N	128˚53W	158	EM SCAN STOPPED	395	W	6	0.9	5.27	1013	99	7/10
18/8/2011	1020	74˚58.7N	128˚53W	158	ROSETTE ↑	395	W	6	0.9	5.27	1013	99	7/10
18/8/2011	1348	74˚58.3N	128˚52.7W	158	ROSETTE ↓	397	W	5	1.3	5.34	1012.9	96	7/10
18/8/2011	1411	74˚58.3N	128˚52.7W	158	ROSETTE ↑	397	W	5	1.3	5.34	1012.9	96	7/10
18/8/2011	1819	74˚52.57N	128˚51.32W	159	ROSETTE ↓	398	330	7	0.4	5.17	1013.30	95	7/10
18/8/2011	1839	74˚52.57N	128˚51.32W	159	ROSETTE ↑	398	330	7	0.4	5.20	1013.37	96	7/10

LEG 2 B1 S3													
19/8/2011	1995	74˚52N	128˚53.8W	315	ROSETTE ↓	397	240	5	-0.8	3.23	1010.2	94	6/10
19/8/2011	2009	74˚52.04N	128˚52.93W	312	ROSETTE ↑	398	240	5	-0.8	3.24	1010	95	6/10
20/8/2011	0834	74˚40.7N	127˚33.4W	178	ROSETTE ↓	367	240	10	0.9	4.54	1010	92	4/10
20/8/2011	0850	74˚40.6N	127˚33.3W	217	ROSETTE ↑	369	220	9	1.0	4.67	1019.8	90	4/10
20/8/2011	1255	74˚48.77N	128˚42.91W	082	ROSETTE ↓	391	190	6	0.1	3.16	1009.9	96	5+/10
20/8/2011	1307	74˚48.75N	128˚42.37W	097	ROSETTE ↑	392	200	3	0.6	3.13	1009.33	96	5+/10
20/8/2011	1838	74˚48.015N	128˚42.42W	020	ROSETTE ↓	393	150	1	2.3	2.24	1009.16	93	5+/10
20/8/2011	1856	74˚48.054N	128˚42.53W	041	ROSETTE ↑	393	150	3	2.8	2.21	1001.03	93	5+/10
LEG 2 B1 S5													
23/8/2011	0930	74˚53.2N	128˚05.9W	VAR	EM SCANS COMPLETES	376	100	15	0.4	3.3	1001.8	99	4/10
23/8/2011	1010	74˚53N	128˚05W	033	ROSETTE ↓	376	95	15	0.4	3.3	1001.8	99	4/10
23/8/2011	1041	74˚53.7N	128˚04.82W	35	ROSETTE ↑	376	95	15	0.4	3.3	1001.8	99	4/10
23/8/2011	1347	74˚53.3N	128˚16.06W	328	ROSETTE ↓	384	E	7	0.4	1.7	1002.9	99	7+/10
23/8/2011	1408	74˚53.3N	128˚16.06W	328	ROSETTE ↑	384	E	7	0.4	1.7	1002.9	99	7+/10
23/8/2011	2015	74˚39.99N	128˚13.05W	-	Bouy	367	NE	9	2.5	3.73	1003.9	99	0/10
23/8/2011	2039	74˚40.18N	128˚13.78W	316	ROSETTE ↓	371	70	8	2.5	3.74	1003.8	99	0/10
23/8/2011	2047	74˚40.18N	128˚13.89W	316	ROSETTE ↑	371	70	8	2.5	3.74	1003.8	99	-
23/8/2011	2050	74˚40.19N	128˚14.06W	303	ROSETTE ↓	371	70	8	2.5	3.74	1003.8	99	-
23/8/2011	0851	74˚40.17N	128˚14.66W	235	ROSETTE ↑		70	9	2.5	3.73	1003.8	99	-
24/8/2011	0855	73˚06.76N	130˚17.22W	231	ROSETTE ↓		50	11	2.3	1.0	1002.9	99	8/10
24/8/2011	0908	73˚06.77N	130˚17.38W	-	ROSETTE ↑		50	11	2.3	1.0	1002.9	99	8/10
24/8/2011	1528	73˚06.024N	130˚34.332W	325	ROSETTE ↓		60	7	3	1.3	1003.5	98	8/10
24/8/2011	1607	73˚06.013N	130˚34.69W	079	ROSETTE ↑		50	13	2.7	1.4	1003.5	99	8/10
25/8/2011	0951	71˚55.634N	125˚22.140W	267	SX -90 ↓		130	6	8.7	1.33	1002.52	97	ICE
27/8/2011	1853	71˚36.133N	133˚14.669W		SX -90 ↑		340	6	0.5	3.9	1016.3	99	ICE